THE UNIVERSITY OF OKLAHOMA

GRADUATE COLLEGE

ULTIMATE FRACTURE FAILURE ANALYSIS OF STRUCTURES USING INCREMENTAL PLASTICITY THEORY

A THESIS

SUBMITTED TO THE GRADUATE FACULTY

in partial fulfillment of the requirements for the

degree of

MASTER OF SCIENCE

By

MIR SHABBAR ALI

Norman, Oklahoma

1987

cop. 1

ULTIMATE FRACTURE FAILURE ANALYSIS OF STRUCTURES USING INCREMENTAL PLASTICITY THEORY

A THESIS

APPROVED FOR THE DEPARTMENT OF CIVIL ENGINEERING AND ENVIRONMENTAL SCIENCE

By [redacted]

God alternates night and daylight:
in that there lies a lesson
for those possessing insight.

(Al-Quran 24:44)

TO MY PARENTS

whose love, patience and encouragement gave me strength to carry out this study.

TABLE OF CONTENTS

TABLE OF CONTENTS (continued)

TABLE OF CONTENTS (continued)

TABLE OF CONTENTS (continued)

ACKNOWLEDGEMENTS

The author must contribute his humble thanks to Almighty Allah who has provided him with health and knowledge to pursue this study.

Sincere thanks and appreciation are expressed to Dr. Kukreti for his suggestions, supervision, help and invaluable guidance throughout the course of this study.

Thanks and appreciation are also extended to Drs. Zaman and Wallace for agreeing to serve on this M.S. thesis committee and also for their constructive criticism and advice.

Financial support from the Department of Civil Engineering and Environmental Science is gratefully acknowledged.

The author expresses his deepest gratitude to his parents, brother and sisters for their support, patience and endless love.

Many thanks are expressed to all friends for their sincere help, encouragement and understanding during the course of this study.

Special thanks and appreciation are expressed to Dr. Stan Neely for his experienced help and encouragement.

Finally, thanks are extended to Ms. Barbara Jones for doing an excellent job in typing this manuscript.

ABSTRACT

Two computer programs are developed for the finite element analysis of nonlinear elasto-plastic problems using constant strain-stress triangular elements. The first computer program predicts initiation and propagation of yielding, and the complete load-displacement history of the structure up to failure due to excessive yielding. The second computer program is an extension of the first one, and predicts initiation and propagation of yielding, crack initiation, stable and unstable crack growth, ultimate fracture failure load and the complete load-displacement history of the structure up to ultimate fracture failure. The Prandtl-Reuss incremental plasticity equations are used with the von Mises yield criterion in the analytical formulations describing the behavior in the plastic range. Small displacement theory is considered to be valid.

In the first computer program a small assumed load increment is applied and the strain and stress components are computed for each element. These are used to compute the load increment required to cause yielding of the most stressed elastic element, while the previously yielded

elements move along the nonlinear portion of the uniaxial stress-strain curve of the material based on isotropic hardening plasticity model. Once an element yields, it's elasto-plasticity matrix is used to formulate it's new stiffness matrix. Thus, the analysis is repeated, in cycles, with the application of incremental load in each load cycle and the computation of the updated system stiffness matrix which depends on the state of stresses and strain of the yielded elements corresponding to the loading acting. The analysis is continued until the incremental plastic strain becomes negative for any yielded element, and then the program execution is terminated and the final total load computed is defined as the failure load of the system.

In the second computer program the incremental elasto-plastic analysis is carried out until an element fractures. Before application of any further external load, the internal energy of the fractured element is redistributed to the remaining unfractured system by an "element nodal load release" method developed in this study. If another element fractures during the energy redistribution process of a fractured element, then unstable crack growth is said to occur. The total load at this stage is reported as the ultimate fracture failure load and the program execution is terminated.

A test V-notched tension specimen is considered as a

numerical example for verification of the first computer program and a center pre-cracked rectangular panel tension specimen is considered as a numerical example for verification of the second computer program. The results predicted by the two computer programs compare well with the results reported in the literature for similar numerical examples.

LIST OF TABLES

LIST OF TABLES (continued)

LIST OF FIGURES

LIST OF FIGURES (continued)

LIST OF FIGURES (continued)

CHAPTER I

INTRODUCTION

1.1 GENERAL

The demands imposed on today's design of structural components often extend to include plastic analysis in order to ensure their safety, reliability, and the most efficient use of the material. Also, defects in the manufacturing process or use over an extended period of time often lead to crack initiation and propagation when loads are applied, thus reducing the load carrying capacity of the structure and sometimes premature failure. The study of fracture mechanics is of critical importance in the design of aircraft, nuclear power plants, and drilling rigs, etc. Many theories have been developed to obtain better solutions for these problems. The finite element method is a computer oriented tool for analysis, which has enhanced research in the areas of plastic analysis and fracture mechanics. With easy access to more sophisticated computational devices, more extensive applications are developing in these areas. The present study is an attempt to apply the finite element method to

the analysis of elasto-plastic fracture mechanics problems using an incremental plasticity formulation.

1.2 LITERATURE REVIEW

1.2.1 Plastic Analysis

One of the most commonly used methods in plastic analysis is the incremental flow theory of plasticity, in which the yielding of the material is described by the following: (i) a work-hardening model, (ii) a yield surface, and (iii) a flow law. The earliest model used is the isotropic hardening model proposed by Hill [12]*, which assumes that equal hardening occurs in all directions. This model will be depicted in the stress space as expansion (for increasing loads) of initially congruent yield surfaces about their common origin. This model gives reasonably good results for monotonically increasing loads but does not account for the Bauschinger effect. To overcome this difficulty, Prager [29] suggested the kinematic hardening model, which was later modified by Zeigler [34]. Prager [29] considered a single yield surface and attempted to represent strain hardening by the rigid body translation of the yield surface in the stress space. The translation is assumed normal to the yield surface and in the direction of the

* Number in [] refers to reference number in Bibliography

incremental plastic strain vector. Zeigler [34] showed that Prager's model is not invariant with respect to the reduction in dimensions in the stress space, i.e., when one or more stress components vanish. He corrected this by assuming that the translation of the yield surface is in the direction of the vector joining the stress point on the yield surface to the center of the yield surface. Mróz [25,26] combined both the isotropic and the kinematic hardening models. In this model the uniaxial stress-strain curve of the material is represented by a number of linear segments and each stress point in this idealized curve is represented by a yield surface in the multi-axial stress space. In this model hardening is represented by the simultaneous expansion and translation of the yield surfaces.

The fourth model suggested for plasticity problems is the mechanical sublayer model proposed originally by Duwez [11] and developed in detail by Iwan [16]. In this model, again the uniaxial stress-strain curve of the material is idealized by linear segments and the material behavior is so modeled such that it is represented by a linear elastic elements connected in parallel to perfectly plastic elements with different yield stressses. The areas and values of the yield stresses of the layered elements are so chosen that they predict the input uniaxial stress-strain curve.

Dafalias and Popov [9] have proposed an alternative but conceptually similar model to that proposed by Mróz [25,26]. Instead of defining a series of yield surfaces, they have defined only two surfaces: a bounding or limiting surface and a loading surface. The parameters required to describe the elasto-plastic deformation process are obtained by defining expressions that, among other factors, depend on these two surfaces. As a result the model is considerably simplified as compared to the Mróz [25,26] model.

The aforementioned isotropic and kinematic hardening models have been tested by various researchers, including, Marcal and King [23], Yamada et al. [32], Armen et al. [1], Nayak and Zeinkiwicz [28] and Barsoum [2].

Marcal and King [23] used the tangent-modulus approach for the solution of elasto-plastic problems by the finite element method. For the stiffness analysis in their incremental load approach, they used partial stiffness coefficients which were obtained by partially differentiating the incremental stress-strain relationship, in one of the three dimensions. They assumed that the incremental strain components for the next load increment are equal to the incremental strain components obtained for the current load level as a first guess if the same load increment is applied. Otherwise, they have suggested to scale them based on the difference between the

current and the next load increment values taken. The strain increments for the next load cycle are needed to compute the mean partial stiffness coefficients. Thus, in this approach the total load is divided into incremental load steps, and incremental elasto-plastic analysis in each successive load step is conducted to compute the nodal displacements and element stresses until the full (known) load level is achieved. No failure criterion is suggested in this work to stop the analysis at any time.

Yamada et al. [32], made modifications in the work done by Marcal and King [23] so as to come up with a analytical technique in which the incremental load is so computed that the most stressed elastic element yields, while the previously yielded elements move along the non-linear (plastic) portion of the uniaxial stress-strain curve based on an isotropic hardening plasticity flow model. They used the Prandtl-Reuss equation for relating the plastic strain increments to the deviatoric strain components and the von Mises yield criterion as the failure law in the formulation of the elasto-plastic material law to be used to march along the nonlinear part of the uniaxial stress-strain curve of the material. They have presented explicit expressions for the elasto-plastic material matrix, $[D^{eP}]$, for a general three-dimensional problem and for a plane stress problem. A

small assumed load increment is applied and incremental strain and stress components of each element of the finite element mesh are computed. These are used to compute the incremental effective stress of each element, which in turn is used to find the most stressed elastic element. Then a load scaling factor is computed such that if the assumed incremental load is multiplied by this scaling factor the most stressed elastic element will yield. Then the element stiffness matrix of the yielded element is changed using the elasto-plastic material law, i.e., using the elasto-plastic material matrix $[D^{eP}]$. The scaling factor is also used to multiply the incremental strain and stress components computed for the assumed incremental load and the results are added to the strain and stress components computed at the end of the previous load cycle, to yield the current total strain and stress components of each element. In this manner, one element at a time is made to yield and the analysis proceeds. Failure is said to occur when the incremental plastic strain value, computed at the end of the present load cycle, becomes negative. This basically indicates that excessive yielding has occurred and the structure does not have sufficient stiffness left to resist any further increase in the loading. The load, when such a situation occurs, has been termed by Yamada et al. [32], as the 'collapse' load. They have reported

reasonable results for monotonically increasing loads and for materials which exhibit a well defined yield plateau.

Armen et al. [1], applied Zeigler's [34] model for the analysis of structures subjected to cyclic loads causing stress reversal into the plasticity range. They developed an analysis procedure which is capable of treating materials whose behavior can be categorized as elasto-plastic, linear, nonlinear strain hardening or limited strain hardening.

The mechanical sublayer model has been implemented by Nayak and Zeinkiwicz [28] and they have found that it predicts hysteresis loops better than the hardening models suggested by Prager [29] and Zeigler [34].

Barsoum [2] applied Prager's kinematic hardening rule for the solution of the elasto-plastic analysis of pressure vessels subjected to cyclic, mechanical and thermal loading.

1.2.2 Fracture Analysis

The study of fracture mechanics problems can be divided into two broad groups. First, it may be termed as the microscopic approach which deals with only localized behavior in certain selected most stressed regions, and the second may be termed as the macroscopic approach which deals with the effect of fracture growth on the load carrying capacity of the total structural system.

In the microscopic studies only certain regions of the structural system are considered to determine crack growth in the structure. The regions are selected based on the value of a factor called as stress intensity factor. This factor depends on the loading and the geometry of both the crack and the body. It is defined in terms of the stress distribution near the crack tip and is generally denoted as K_I, for mode I (opening mode) fracture. By definition, the crack growth is supposed to occur when

$$K_I = K_{IC} \tag{1.1}$$

where K_{IC} is a property of the material and does not depend on the geometry of the body or crack. In Eq. (1.1), K_{IC} is defined as the critical stress-intensity factor under conditions of plastic strain for slow loading and linear elastic behavior [30]. The value of K_{IC} is experimentally determined for a material. Other parameters considering the plastic deformations near the crack tip include an energy line-integral, called the J-integral, which is an average measure of the elasto-plastic stress-strain field ahead of a crack [30]; and the crack opening displacement (COD), which is a measure of the pre-fracture deformation at the tip of a sharp crack under conditions of inelastic behavior [30]. A crack propagation is assumed to occur when J attains a certain value,

J_{IC}, which can be given in terms of K_{IC}, Young's modulus of elasticity, E, and Poisson's ratio, v, as [30]

$$J_{IC} = \left(\frac{1 - v^2}{E}\right) K_{IC}^2 \qquad (1.2)$$

Concerning COD, it is assumed that the crack instability occurs when the computed value of COD reaches a critical value, denoted as δ_c, and given by [30]

$$\delta_c = E \frac{K_{IC}^2}{F_y} \qquad (1.3)$$

where F_y is the yield stress of the material.

The finite element method has been applied by various researchers for computations of the stress intensity factor and other related parameters for elasto-plastic problems. Lynn et al. [22], used quadratic isoparametric elements for the determination of the stress singularity near the crack tip. Hussain et al. [14], simulated the singularity in the stress field using the finite element method. The crack tip was modeled using special crack tip finite elements. They have been reported that the concepts presented in their study cannot be easily extended to three-dimensional cases without considering additional parameters.

Karabin and Sweldon [19], used the finite element method to determine path independence of the J- integral

using a model which employs a variable singularity at the crack tip that keeps track of changes in the material response during the loading process. They concluded two reasons for the path independence of J, i.e., non-proportionality of stress field local to the crack tip and relative resharpening of the crack in a manner peculiar to the overall geometry. Dodds et al. [10] carried out analytical studies using the finite element method to predict J- integral values in single-edge-notch tensile panels. They studied the effects of near-tip-stiffness on the results for elastic and fully plastic response at the predicted limit loads.

Numerous other researches have been reported in the area of numerical modeling to predict the behavior near the crack tip both under monotonic and cyclic loads. Most of these studies involve comparison of numerical results with experimental observations. A large volume of this literature has been published in the recent past. But, since this study does not deal solely with this area of research, so these works have not been reviewed here.

In the macroscopic approach the structural system is analyzed as a whole to predict the load-displacement history and the ultimate fracture failure load. Some pertinent references on the application of the finite element method for the elasto-plastic analysis of fracture mechanics problems are presented in the sub-

sequent paragraphs.

Miller et al. [24] performed an incremental elasto-plastic analysis of a center pre-cracked rectangular panel tension specimen subjected to a monotonically increasing applied stress. They used a tangent stiffness formulation for each load step. The finite element modeling consisted of constant stress-strain triangular elements. The von Mises yield criterion and Prandtl-Reuss incremental stress-strain equations were used for the solution of the nonlinear plasticity problems. Whenever any crack tip element fractures the crack tip needs to be extended. In the method suggested by them, the crack tip node, which would previously be constrained in the direction perpendicular to the crackline, is released and the crack tip is advanced to the next node on the crack line. A nodal release method is applied to redistribute the energy of the released node. This is done in two ways. In one method, the energy of the released node is dissipated to the system in one step, and in the other method, this process is done in ten equal steps. The ultimate failure stress for both of the above methods are compared to the experimental results, which were also conducted by them. The ultimate failure stress found by the first method was 28 ksi and by the second method 30 ksi as compared to the test panel failure stress 24 ksi. It is concluded that the discrepancy

between the experimental and analytical results may be attributed to the thickness effect of the test panel.

Belie [3] developed a finite element program to solve two-dimensional elasto-plastic fracture mechanics problems for the prediction of ultimate fracture failure loads. Only plane stress conditions and uniaxial loading were considered in the analysis. The nonlinear uniaxial material stress-strain curve was divided into various linear segments, with the modulus of elasticity and the Poisson's ratio defined for each segment in terms of the values of the stresses and strains at the end points of the segment. The equation suggested by Bert et al. [4], and Nadai [27] was used to compute the Poisson's ratio. The values of modulus of elasticity and the Poisson's ratio are updated for an element each time it enters a new segment. When an element fractures, the energy of the fractured element is redistributed to the remaining unfractured system by a method which is referred to as "zero-modulus-unload-reload" method. In this method the structure is artificially unloaded following the elastic response of the unfractured specimen. The fractured element is then made inert by setting its modulus of elasticity equal to zero and Poisson's ratio equal to 0.5. The structure is then reloaded back to its original load level. Further load is applied after reloading of structure is completed. Unstable crack growth is assumed

to occur if another element fractures before the full load level is achieved during the reloading phase of distributing the energy of the element. If unstable crack growth occurs then the structure is considered to have collapsed and the corresponding load level is referred to as the ultimate fracture failure load. Belie concluded that a very fine mesh is usually needed near the crack tip, as well as, along the expected crack path, in order to obtain stable crack growth. He used the three-noded constant stress-strain triangular elements and all the mesh layout was manually prepared.

Iranmanesh [15], developed a finite element fracture program using an automated mesh generator and the "zero-modulus-unload-reload" method to predict ultimate fracture failure load and the load-displacement history. A library of different two-dimensional elements was used, including three-noded triangular elements and four- and eight-noded isoparametric elements. The mesh processor program was able to generate these elements as desired by the user. He used the same approach as Belie [3] to approximate the nonlinear uniaxial material stress-strain curve and to redistribute the energy of the fractured element (i.e., the zero-modulus-unload-reload method). The program had the option so that both plane stress and plane strain problems could be analyzed. Both von Mises and St. Venant yield criteria were used to determine the

element yielding. It was observed that both yield criteria giveabout similar results for metallic structures. It was also concluded that the yield pattern is very much dependent on the type of mesh used. A finer mesh gives better results than a cruder one, especially if the mesh in the higher stress regions consists of very fine elements. Considering the use of the different types of two-dimensional elements, it was concluded that higher order elements give better results, but the computer time also increases significantly. The four-noded isoparametric quadrilateral element is suggested to be the best considering both accuracy and computational costs.

Kumar [20] applied the concepts presented by Belie [3] and Iranmanesh [15] to three-dimensional problems. The eight-noded isoparametric element developed by Levy [21] was used to model an elasto-plastic structural system. To represent the nonlinear uniaxial material stress-strain curve, two types of piece-wise linear approximations were presented using the tangent modulus and the secant modulus concepts. He had the option to use von Mises and St. Venant yield theories both in terms of stress computations and strain computations. The three-dimensional input mesh was prepared manually. It was found that the results of a crude three-dimensional mesh compares very well to the results from a very fine two-dimensional mesh for a plane stress problem. It is

reported that a three-dimensional finite element mesh using about 100 times larger elements than the two-dimensional finite element mesh gives the same degree of accuracy for the results.

Shammaa [31] used the concepts presented by Belie [3] and Iranmanesh [15] to develop a computer program which has an automated logic to refine the mesh gradually as one advances along the uniaxial stress-strain curve of the material in the plastic region. The input mesh consisted of three-noded constant stress-strain triangular elements. The points selected on the stress-strain curve, which were used to demarcate these segments, are called "yield points". A comprehensive mesh refinement scheme is included which refines the current mesh in the regions of high stress concentration. The refinement is done based on effective stress of the element compared to the stress at the corresponding yield points and the minimum area specified at each of the yield points. To confine the mesh refinement locally, special five-noded triangular elements are developed, which engulf the refined regions. The two extra nodes, which are created on the two adjacent sides to the refined elements, are considered to be the average of the original nodes, to avoid any incompatibility. Options for both von Mises and St. Venant yield criteria are used to predict yielding of elements. He concluded that the automated mesh refine-

ment significantly improves the results. In particular, the ultimate fracture fail load predicted is very accurate. Regarding the size of the elements he observed that as the area is decreased, the results converge towards the accurate solution. But after a certain limit, when the areas are smaller, the solution no longer converges because of significant round-off errors that occur during the solving of a very large number of linear simultaneous equations to obtain the incremental displacements during each load increment.

1.3 OBSERVATIONS

From the literature review presented in Sub-section 1.1.1 and 1.1.2 the following pertinent observations are summarized.

(1) The isotropic hardening model seems to give good results for structural systems subjected to only monotonically increasing loads and undergoing plastic deformations. Yamada et al. [32], have presented a systematic approach, which can be conveniently automated and which predicts the incremental load needed to yield the most stressed elastic element, one at a time, whereas, the yielded (i.e., plastic) element move along the nonlinear part of the uniaxial stress-strain curve using the isotropic

hardening incremental plasticity model. This method could be extended to analyze fracture problems also by simply redefining the mode of failure, which would be different than that suggested by Yamada et al. [32].

(2) Miller et al. [24], have presented a method to determine the response of a pre-cracked structural system using the Prandtl-Reuss incremental stress-strain plasticity equations, the von Mises yield criterion, and an isotropic work hardening model. To march along the non-linear portion of the uniaxial stress-strain curve, a tangential stiffness approach is used with a two-step Runge-Kutta integration scheme in each incremental load step. When the stress at the node of the crack tip exceeds the material fracture stress then that node is considered to be fractured. In this manner the crack tip is extended. Before the next load increment is applied and the new cracked node is treated as a free node for further analysis, it's reaction is put as an equal and opposite load on the system and a new stress analysis is performed. The new state of stresses of the elements are then taken as the initial stresses for the next load increment. In this manner

the energy of the fractured node is redistributed into the unfractured system. The main drawback of this approach, in which fracturing of a node is considered, is that the crack path is pre-fixed, which may not be correct for the problem analyzed, and, above all, may not be possible to be pre-determined for problems with complicated geometry and loading. This problem can be overcome if the fracturing of an element is considered instead of fracturing of a node. Of course, the premise being that the areas of the elements in the yield zone, which has an effective stress value close to the fracture stress value for the material, are of a reasonably small value in the finite element mesh used for the problem. Belie [3], has presented a technique in which fracturing of an element is considered. The nonlinear portion of the uni-axial stress-strain curve of the material is divided into linear segments and each segment is characterized by its own elastic Young's modulus of elasticity and Poisson's ratio. The element in each segment is considered as an elastic element. In this approach, an incremental load factor is so computed such that all the elements in a particu-

lar linear segment move along the stress-strain curve to an effective stress value equal to the yield stress value of the end-point of that segment. Thus, plastic deformation theory is not used in this formulation, but the element stiffness matrices are recomputed depending on which linear segment the element lies in. So in order to obtain accurate and realistic results for the yield patterns, the rate of yielding, and the load-displacement history up to fracture or failure, it is important to consider a large number of segments, so that the linearized stress-strain curve is close to the actual uniaxial stress-strain curve. So, one problem that one would always be confronted with this approach would be to decide on how many segments in the stress-strain curve one should consider to model the behavior accurately. This is of special concern since fracture analysis for even simple problems is a costly process even on today's fast computers.

(3) The unloading and reloading method used by Belie [3], and later by Iranmanesh [15], Kumar [20] and Shammaa [31], is actually an artificial unloading, since the actual specimen never experiences this. Also, it has been reported

by Kumar [20] and Shammaa [31], that after complete unloading of the fractured element still some small residual compressive stress remains in that element, which was ignored. This effect would accumulate if in any problem a large number of elements fracture successively during each stable crack growth cycle. This may cause localized buckling phenomenon to occur. Also, in this approach, it has been reported [3, 15, 20, 31] that a very fine mesh near the crack tip is needed in order to obtain stable crack growth. For the pre-cracked rectangular panel tension specimen previously analyzed by Miller [24], Belie [3] has reported that stable crack growth prediction was obtained for a minimum crack tip area of 0.01 sq. in., whereas, Kumar [20] and Shammaa [31] have reported that they did not obtain any stable crack growth for even a minimum crack tip area of 0.001 sq. in. for the same problem.

From the literature review, thus, it is concluded that there is a need to develop a better analysis procedure to predict crack initiation, its growth and behavior till ultimate fracture failure of a structural system. The formulation should be based on the well established incremental plasticity theories so that the actual

material uniaxial stress-strain curve is followed during the analysis. A more rationale procedure is needed to be encorporated to redistribute the energy of the fractured zone into the remaining unfractured part, before the fractured zone is removed from the analysis and the external loading acting on the system is increased further.

1.4 OBJECTIVES AND SCOPE OF THE PRESENT STUDY

The primary objective of this study is to develop an analytical procedure to predict fracture initiation and its growth till ultimate fracture failure of a two-dimensional structure occurs, if it is subjected to monotonically increasing loading which produces plastic deformations. To model the plastic behavior, it is proposed to use an isotropic hardening model with the von Mises yield criterion, and the solution algorithm suggested by Yamada et al. [32] to march along the uniaxial stress-strain curve of the material. The two-dimensional domain is discretized using finite element theory and the computer program is developed for only three-noded triangular elements. It is assumed that all deformations are such that small displacement theory is valid. Also, it is assumed that no local buckling and closure of cracks occur due to compression. If the effective stress of an element, computed using the von Mises yield criterion, becomes equal to or exceeds the

fracture stress obtained from the uniaxial test of the material, then that element is considered to have fractured. At this stage, the nodal loads of the fractured element are computed, which are later used to redistribute the internal energy of the fractured element into the remaining unfractured system. Then this element is made inert by taking its modulus of elasticity, E, equal to zero and Poisson's ratio, v, equal to 0.5 in computation of its element stiffness matrix. With no external loads acting and keeping the state of stresses of the remaining unfractured elements, as computed before, the negative of the nodal loads, computed for the fractured element are proposed to be iteratively applied in increments to redistribute the internal energy of the fractured element into the remaining unfractured plastic or elastic elements. The stresses in the elements in the vicinity of the fractured element will thus increase. This procedure, developed in this study, will be called as "element nodal load release" method. It is completely different than the "zero-modulus-unload-reload" method suggested by Belie [3] and the "nodal release" method suggested by Miller [24]. During the process of redistributing the internal energy of the fractured element, it may be found that (based on the numerical results predicted), some plastic elements get artificially unloaded. Thus, indicating that elastic stiffness matrix

should be used for such elements. It is proposed to iteratively model such a behavior, if it occurs, and make sure that element stresses do not decrease during the energy re-distribution phase. If during any energy re-distribution phase, before the fractured element's full nodal loads have been applied, another element fractures, then unstable crack growth would be said to have occurred and the analysis is proposed to be terminated. The total fracture load just prior to this phenomenon would be defined as the collapse or the ultimate fracture failure load of the structure.

To achieve the aforementioned objectives, the study is divided into the following two tasks:

1. Task I: Develop a plasticity computer program following the algorithm suggested by Yamada et al. [32] and possessing the following capabilities:
   - (i) Locate the initiation of yielding and the initial yield load.
   - (ii) Predict the yielding patterns of the structural system.
   - (iii) Predict the failure load based on the failure criterion suggested by Yamada et al. [32], in which failure is said to take place when excessive yielding occurs.
   - (iv) Predict the load-displacement history of the structure up to failure.

Verify and validate this computer program by comparing the results predicted for the V-notched tension specimen analyzed by Yamada et al. [32]. Since only three-noded triangular elements are proposed to be used in this study for fracture problems, a very fine finite element mesh will be needed in the region next to the tip of the crack to obtain accurate results. Also, it is well known that it is advantageous to use equilateral triangular elements to obtain faster convergence with mesh refinement. So, the plasticity computer program developed would be verified for the V-notched tension specimen example problem with regard to the following: (i) convergence of results due to mesh refinement; and (ii) effect on results predicted by changing the shape and the size of the elements in the expected yielded region.

3. Task II: Modify the plasticity computer program, developed in Task I, to possess the following additional capabilities:

   (i) Locate the crack initiation and predict the path of the crack propagation.

   (ii) Predict stable and unstable crack growth.

   (iii) Predict the load-displacement history up to collapse or fracture failure of the structure. It should be noted that the

mode of failure here is defined differently than that defined by Yamada et al. [32].

(iv) Directly predict the ultimate fracture failure load and the corresponding deflection of structures comprised of elasto-plastic materials.

Verify and validate the computer program by comparing the results predicted for the center pre-crack rectangular panel tension specimen analyzed by Miller [24], Belie [3], Kumar [20] and Shammaa [31]. Experimental results for this example problem have been reported by Miller [24] for only the ultimate fracture failure load.

CHAPTER II

THEORETICAL AND MODELING CONCEPTS USED

2.1 INTRODUCTION

In any structural mechanics problem one is generally interested in computing the variation of stresses due to external loads acting on the structure or due to secondary effects such as temperature change, prestrain, prestress, and prescribed boundary displacements. The stress variation can be computed if the variation of strain in the continuum and the material law describing the stress-strain relationship for the material used are known. The strain variation can be computed if the variation of displacement or deformation components along the global x-, y- and z-axis are known. Thus, the problem reduces to prediction of the displacement components at any point of the continuum. These can be computed by solving the governing differential equations for the problem so as to satisfy a given set of boundary conditions. If the geometry of the structure and its boundary conditions are complex, then it is often impossible to find closed-form solutions of the governing

differential equations for the problem. In such a situation one has to adopt a numerical solution procedure such as the finite difference or the finite element method to obtain the variation of displacements. In this study the finite element method is used since it has the flexibility of accommodating variation of material properties in the continuum, it can conveniently solve problems with irregular shaped boundaries, and, above all, it can be automated.

The first and the most important step in any finite element analysis is to discretize the structural continuum. To achieve this the structure is divided into a finite number of elements of various shapes (e.g., triangles, quadrilaterals, etc.), connected at discrete points called "nodes". The choice of the shape and the type of elements (i.e., the number of nodes it has) depends on the shape or geometry of the given structural continuum and also on the degree-of-accuracy desired. For planar problems these elements range from three-noded triangular shaped elements to four- and eight- noded isoparametric quadrilateral elements. In the present study only three-noded triangular elements are used, which are also referred to as constant stress and constant strain elements.

This chapter presents the theoretical concepts of the Finite Element Method (FEM) used in this study. In

Section 2.2, the finite element formulation for elastic problems and the nomenclature used are presented. In Section 2.3, the extension of these concepts to solve plasticity problems is presented. In this section the analysis procedures using the incremental "plastic flow law" are discussed. This is followed by Section 2.4, in which the application of the FEM, developed in Section 2.3 for plasticity problems, is extended to solve fracture mechanics problems.

2.2 FINITE ELEMENT MODELING FOR ELASTIC PROBLEMS

2.2.1 General Requirements

For linear elastic problems, any finite element formulation involves the following steps:

(1) Definition of the constitutive law or the stress-strain relationship used.

(2) Element formulation for a typical element (or elements) used to discretize the continuum. This gives element matrices describing its behavior.

(3) Assembly of the element matrices so as to satisfy compatibility and equilibrium at common nodes. This gives the stiffness equilibrium equation of the continuum, in which the displacements of the nodes (called "nodal displacements") are the unknowns.

(4) Solution of the system stiffness equilibrium equation for nodal displacements.

(5) Computation of strains and stresses for each element at the nodes and/or at any other selected points.

2.2.2 Choice of Stress-Strain Relationship

Before starting on the element formulation some stress-strain relationships have to be considered as they form the basis of the formulation. According to Hooke's law the uniaxial stress ,σ_x, and the uniaxial strain, ϵ_x, can be related as follows:

$$\sigma_x = E\,\epsilon_x \tag{2.1}$$

where E is the Young's modulus of elasticity of the material. For linear isotropic material, this can be extended to a general three-dimensional case by making use of another material property called as the Poisson's ratio and denoted by ν. These relationships are:

$$\begin{Bmatrix} \sigma_x \\ \sigma_y \\ \sigma_z \\ \tau_{xy} \\ \tau_{yz} \\ \tau_{zx} \end{Bmatrix} = \frac{E}{1+\nu} \begin{bmatrix} 1 & \frac{\nu}{1-2\nu} & \frac{\nu}{1-2\nu} & 0 & 0 & 0 \\ \frac{\nu}{1-2\nu} & 1 & \frac{\nu}{1-2\nu} & 0 & 0 & 0 \\ \frac{\nu}{1-2\nu} & \frac{\nu}{1-2\nu} & 1 & 0 & 0 & 0 \\ 0 & 0 & 0 & 1/2 & 0 & 0 \\ 0 & 0 & 0 & 0 & 1/2 & 0 \\ 0 & 0 & 0 & 0 & 0 & 1/2 \end{bmatrix} \begin{Bmatrix} \epsilon_x \\ \epsilon_y \\ \epsilon_z \\ \gamma_{xy} \\ \gamma_{yz} \\ \gamma_{zx} \end{Bmatrix} \tag{2.2}$$

or denoted as

$$\{\sigma\} = [D]\{\epsilon\} \tag{2.3}$$

in which the stress vector, $\{\sigma\}$, contains the normal stress components σ_x, σ_y and σ_z acting along the x-, y-, and z-directions, respectively, and the shear stress components τ_{xy}, τ_{yz} and τ_{zx} acting in the xy-, yz- and zx-planes, respectively. Similarly the strain vector, $\{\epsilon\}$, contains the three normal strain components ϵ_x, ϵ_y and ϵ_z acting in the x-, y-, and z-directions, respectively, and the three shear strain components γ_{xy}, γ_{yz} and γ_{zx} acting in the xy-, yz- and zx-planes, respectively. In Eq. (2.3), [D] is called as the elasticity material matrix for the three-dimensional problem.

In this study only two-dimensional problems are considered. These problems may be classified into two categories, namely, plane stress and plane strain problems. If the thickness of the elastic body (taken along z-axis) is constant and very small in comparison to the other lateral dimensions and the loading acts in the xy-plane only, then this problem is characterized as a plane stress problem. In this case the stress components related to the z-axis vanishes, which means that

$$\sigma_z = \tau_{yz} = \tau_{zx} = 0 \tag{2.4}$$

Substituting Eq. (2.4) into Eq. (2.2), gives

$$\begin{Bmatrix} \sigma_x \\ \sigma_y \\ \tau_{xy} \end{Bmatrix} = \frac{E}{1-\nu^2} \begin{bmatrix} 1 & \nu & 0 \\ \nu & 1 & 0 \\ 0 & 0 & \frac{1-\nu}{2} \end{bmatrix} \begin{Bmatrix} \epsilon_x \\ \epsilon_y \\ \tau_{xy} \end{Bmatrix} \tag{2.5}$$

or

$$\{\sigma\} = [D]\{\epsilon\} \tag{2.6}$$

where [D] is called as the elasticity material matrix for the plane stress problems and is given as

$$[D] = \frac{E}{1-\nu^2} \begin{bmatrix} 1 & \nu & 0 \\ \nu & 1 & 0 \\ 0 & 0 & \frac{1-\nu}{2} \end{bmatrix} \tag{2.7}$$

If the elastic body is very long (say along the z-axis) in comparison to its cross-sectional dimensions and the loading is constant along the z-axis, then this problem is characterized as a plane strain problem. In this case all the strains related to z-axis vanish, which means that

$$\epsilon_z = \gamma_{yz} = \gamma_{zx} = 0 \tag{2.8}$$

Substituting Eq. (2.8) into Eq. (2.2), gives

$$\begin{Bmatrix} \sigma_x \\ \sigma_y \\ \tau_{xy} \end{Bmatrix} = \frac{E}{(1+\nu)(1-2\nu)} \begin{bmatrix} 1-\nu & \nu & 0 \\ \nu & 1-\nu & 0 \\ 0 & 0 & \frac{1-2\nu}{2} \end{bmatrix} \begin{Bmatrix} \epsilon_x \\ \epsilon_y \\ \tau_{xy} \end{Bmatrix} \tag{2.9}$$

or

$$\{\sigma\} = [D]\{\epsilon\} \tag{2.10}$$

where [D] is called as the elasticity material matrix for plane strain problems and is given as

$$[D] = \frac{E}{(1+\nu)(1-2\nu)} \begin{bmatrix} 1-\nu & \nu & 0 \\ \nu & 1-\nu & 0 \\ 0 & 0 & \frac{1-2\nu}{2} \end{bmatrix} \tag{2.11}$$

2.2.3 Finite Element Formulation for a Three-Noded Triangular Element

Consider a planer triangular finite element which has three "nodes", i, j and k (also called as nodes 1, 2 and 3, respectively) and two degrees-of-freedom at each node, denoted as x-translation (u-displacement) and y-translation (v-displacement), as shown in Fig. 2.1. These degrees-of-freedom will be referred to as the nodal displacements. As shown in this figure, for convenience of the mathematical formulation the origin for the element coordinate system, (x,y), is taken to be at the element local node "i". Also, the element coordinate system, (x,y), is taken parallel to the global coordinate system, $(\bar{x},\bar{y})$, which is used to describe the geometry of the finite element mesh adopted to discretize the domain.

For the convergence of the finite element solution, the choice of functions giving the variation of the displacement components within the element has to satisfy

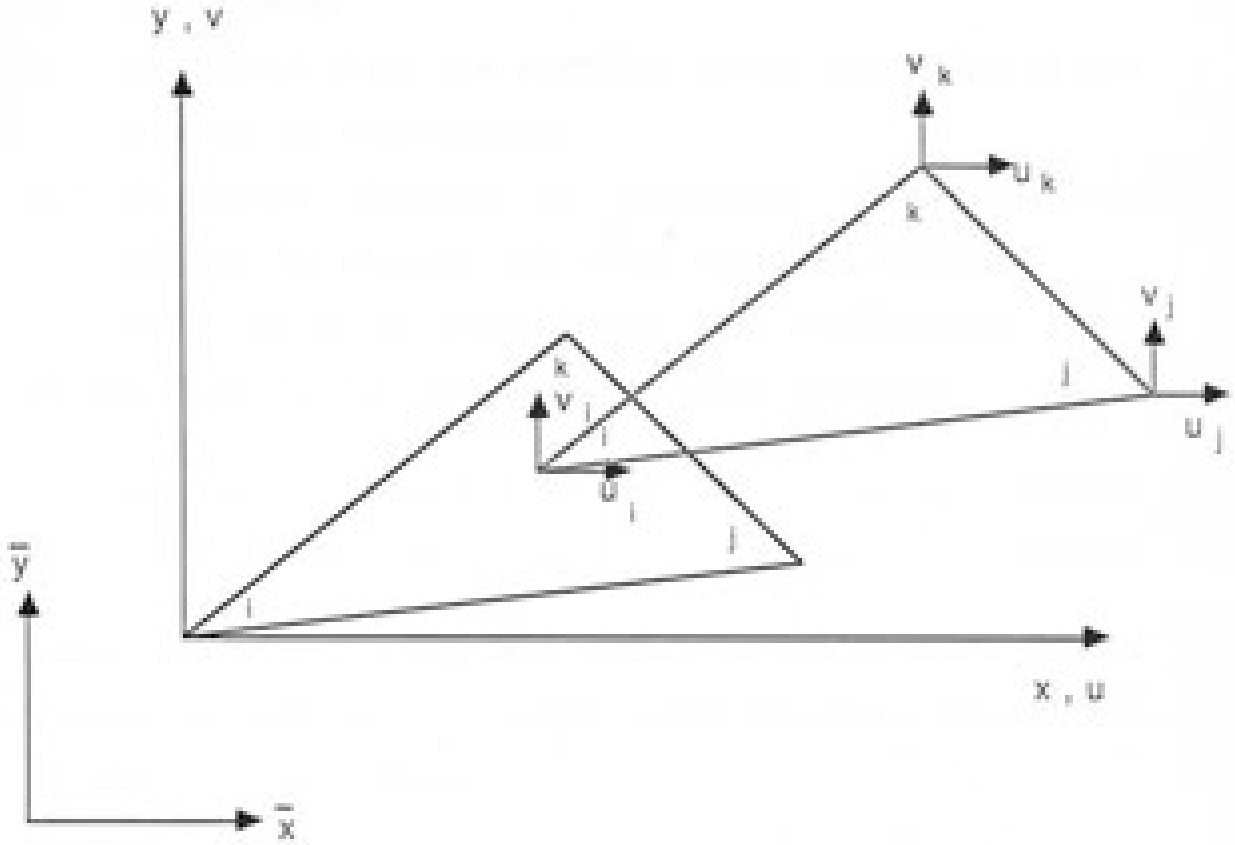

(x, y) : Element Coordinate System

($\bar{x}$, $\bar{y}$) : Global Coordinate system

——— : Initial Position

- - - - - - - - : Displaced Position

Fig. 2.1 Typical Three-Noded Triangular Finite Element

the following requirements, [6]:

1. It should consider the rigid body displacement of the element.
2. It should allow the constant strain condition of the element to be achieved.
3. It should consider the continuity of displacement within the element and among adjacent elements.

Based on these requirements, the displacement field at any point within the element can be taken as

$$u(x,y) = a_1 + a_2\, x + a_3\, y \tag{2.12a}$$

$$v(x,y) = a_4 + a_5\, x + a_6\, y \tag{2.12b}$$

where a_1, a_2, ..., a_6 are called as the element generalized coordinates. In matrix notation, Eqs. (2.12a) and (2.12b) can be written as

$$\begin{Bmatrix} u(x,y) \\ v(x,y) \end{Bmatrix} = \begin{bmatrix} 1 & x & y & 0 & 0 & 0 \\ 0 & 0 & 0 & 1 & x & y \end{bmatrix} \begin{Bmatrix} a_1 \\ a_2 \\ a_3 \\ a_4 \\ a_5 \\ a_6 \end{Bmatrix} \tag{2.13}$$

using subscript "n" to denote the quantities pertaining to a typical nth element, Eq. (2.13) is abbreviated as

$$\{\phi\}_n = [\bar{N}]_n \{a\}_n \tag{2.14}$$

where

$$\{\phi\}_n = \begin{Bmatrix} u(x,y) \\ v(x,y) \end{Bmatrix} \tag{2.15}$$

is the element displacement vector;

$$\{a\}_n = \begin{Bmatrix} a_1 \\ a_2 \\ a_3 \\ \cdot \\ \cdot \\ \cdot \\ \cdot \\ \cdot \\ a_n \end{Bmatrix} \tag{2.16}$$

is the element generalized coordinates vector; and

$$\underset{(2x6)}{[\bar{N}]_n} = \begin{bmatrix} 1 & x & y & 0 & 0 & 0 \\ 0 & 0 & 0 & 1 & x & y \end{bmatrix} \tag{2.17}$$

is the element shape function matrix with respect to the element generalized coordinates vector, $\{a\}$.

Substituting the coordinates of the nodes i, j and k from Fig. 2.1, a relationship can be developed between the element nodal displacements and the element generalized coordinates, as follows:

$$\begin{Bmatrix} u_i \\ v_i \\ u_j \\ v_j \\ u_k \\ v_k \end{Bmatrix} = \begin{bmatrix} 1 & 0 & 0 & 0 & 0 & 0 \\ 0 & 0 & 0 & 1 & 0 & 0 \\ 1 & x_j & y_j & 0 & 0 & 0 \\ 0 & 0 & 0 & 1 & x_j & y_j \\ 1 & x_k & y_k & 0 & 0 & 0 \\ 0 & 0 & 0 & 1 & x_k & y_k \end{bmatrix} \begin{Bmatrix} a_1 \\ a_2 \\ a_3 \\ a_4 \\ a_5 \\ a_6 \end{Bmatrix} \tag{2.18}$$

which can be denoted for an element "n", as follows:

$$\{\delta\}_n = [A]_n \{a\}_n \tag{2.19}$$

in which $\{\delta\}_n$ is called as the element nodal displacement vector, and its transpose is given as

$$\{\delta\}_n^T = < u_i \; v_i \; u_j \; v_j \; u_k \; v_k > \tag{2.20}$$

where symbol < > is used to denote a row matrix, and matrix $[A]_n$ is given as

$$[A]_n = \begin{bmatrix} 1 & 0 & 0 & 0 & 0 & 0 \\ 0 & 0 & 0 & 1 & 0 & 0 \\ 1 & x_j & y_j & 0 & 0 & 0 \\ 0 & 0 & 0 & 1 & x_j & y_j \\ 1 & x_k & y_k & 0 & 0 & 0 \\ 0 & 0 & 0 & 1 & x_k & y_k \end{bmatrix} \tag{2.21}$$

Inverting Eq. (2.19), gives

$$\{a\}_n = [A]_n^{-1} \{\delta\}_n \tag{2.22}$$

where, in view of Eq. (2.18)

$$[A]_n^{-1} = \begin{bmatrix} \Delta_n & 0 & 0 & 0 & 0 & 0 \\ y_{jk} & 0 & y_k & 0 & -y_j & 0 \\ x_{kj} & 0 & -x_k & 0 & x_j & 0 \\ 0 & \Delta_n & 0 & 0 & 0 & 0 \\ 0 & y_{jk} & 0 & y_k & 0 & -y_j \\ 0 & x_{kj} & 0 & -x_k & 0 & x_j \end{bmatrix} \tag{2.23}$$

in which

$$\Delta_n = 2 \text{ (area of the elemental triangle)} \tag{2.24a}$$

$$y_{jk} = y_j - y_k \tag{2.24b}$$

$$x_{kj} = x_k - x_j \tag{2.24c}$$

Substituting Eq. (2.22) into Eq. (2.14) gives the desired element displacement field vector in terms of the element nodal displacements, as follows:

$$\{\phi\}_n = [\bar{N}]_n [A]_n^{-1} \{\delta\}_n = [N]_n \{\delta\}_n \tag{2.25}$$

in which $[N]_n = [\bar{N}]_n [A]_n^{-1}$ is called as the element shape function matrix with respect to the element nodal displacement vector, $\{\delta\}_n$.

Using small displacement theory, the strain components for a two-dimensional elasticity problem are given by

$$\epsilon_x = \frac{\partial u}{\partial x} \tag{2.26a}$$

$$\epsilon_y = \frac{\partial v}{\partial y} \tag{2.26b}$$

$$\gamma_{xy} = \frac{\partial u}{\partial y} + \frac{\partial v}{\partial x} \tag{2.26c}$$

which can be written in matrix form for an element "n", as follows:

$$\begin{Bmatrix} \varepsilon_x \\ \varepsilon_y \\ \gamma_{xy} \end{Bmatrix} = \begin{bmatrix} \frac{\partial}{\partial x} & 0 \\ 0 & \frac{\partial}{\partial y} \\ \frac{\partial}{\partial y} & \frac{\partial}{\partial x} \end{bmatrix} \begin{Bmatrix} u(x,y) \\ v(x,y) \end{Bmatrix} \tag{2.27}$$

or

$$\{\varepsilon\}_n = \begin{bmatrix} \frac{\partial}{\partial x} & 0 \\ 0 & \frac{\partial}{\partial y} \\ \frac{\partial}{\partial y} & \frac{\partial}{\partial x} \end{bmatrix} \{\phi\}_n \tag{2.28}$$

in which

$$\{\varepsilon\}_n = \begin{Bmatrix} \varepsilon_x \\ \varepsilon_y \\ \gamma_{xy} \end{Bmatrix} \tag{2.29}$$

is called as the element strain vector. Substituting Eqs. (2.19) and (2.22) into Eq. (2.28) gives the element strain vector, $\{\varepsilon\}_n$, in terms of the element nodal displacement vector, $\{\delta\}_n$, as follows:

$$\{\varepsilon\}_n = [\bar{B}]_n [A]_n^{-1} \{\delta\}_n = [B]_n \{\delta\}_n \tag{2.30}$$

in which

$$[\bar{B}]_n = \begin{bmatrix} \frac{\partial}{\partial x} & 0 \\ 0 & \frac{\partial}{\partial y} \\ \frac{\partial}{\partial y} & \frac{\partial}{\partial x} \end{bmatrix} \quad [\bar{N}]_n = \begin{bmatrix} 0 & 1 & 0 & 0 & 0 & 0 \\ 0 & 0 & 0 & 0 & 0 & 1 \\ 0 & 0 & 1 & 0 & 1 & 0 \end{bmatrix} \tag{2.31}$$

is the element strain-displacement transformation matrix with respect to $\{a\}_n$, and

$$[B]_n = [\bar{B}]_n [A]_n^{-1} \tag{2.32}$$

is the element strain-displacement transformation matrix with respect to $\{\delta\}_n$.

Using either Eq. (2.6) or Eq. (2.10), the variation of stresses within the element "n" is given by

$$\{\sigma\}_n = [D]_n \{\varepsilon\}_n \tag{2.33}$$

Substituting Eq. (2.30) into Eq. (2.33), gives the element stress vector, $\{\sigma\}_n$, in terms of the element nodal displacement vector, $\{\delta\}_n$, as

$$\{\sigma\}_n = [D]_n [\bar{B}]_n [A]_n^{-1} \{\delta\}_n \tag{2.34}$$

Now, if the element is subjected to a set of body forces and surface tractions, the internal work done, W, by them will be given by the following expression:

$$W = \iiint_{V_n} (Xu + Yv)\, dV_n + \iint_{S_n} (R_x u + R_y v)\, dS_n \tag{2.35}$$

where X and Y are the body forces per unit volume along the x- and y-directions, respectively; R_x and R_y are the

surface tractions per unit area along the x- and y-directions, respectively; and S_n and V_n denote the element boundary surface areas and element volume, respectively. For an element "n", Eq. (2.35) can be written in terms of the element displacement field vector, $\{\phi\}_n$, as

$$W_n = \iiint_{V_n} \{\phi\}_n^T \{X\}_n \, dV_n + \iint_{S_n} \{\phi\}_n^T \{R\} \, dS_n \tag{2.36}$$

where

$$\{\phi\}_n = \begin{Bmatrix} u \\ v \end{Bmatrix} \tag{2.37a}$$

$$\{X\}_n = \begin{Bmatrix} X \\ Y \end{Bmatrix} \tag{2.37b}$$

$$\{R\}_n = \begin{Bmatrix} R_x \\ R_y \end{Bmatrix} \tag{2.37c}$$

Substituting Eq. (2.25) into Eq. (2.36), gives

$$W_n = \iiint_{V_n} \{\delta\}_n^T [N]_n^T \{X\}_n \, dV_n + \iint_{S_n} \{\delta\}_n^T [N]_n \{R\}_n \, dS_n \tag{2.38}$$

The internal work done, U_n, by the element stresses is given by the following expression:

$$U_n = \tfrac{1}{2} \iiint_{V_n} \{\epsilon\}_n^T \{\sigma\}_n \, dV_n \tag{2.39}$$

Substituting Eqs. (2.30) and (2.34) into Eq. (2.39) gives

$$U_n = \tfrac{1}{2} \iiint_{V_n} \{\delta\}_n^T [B]_n^T [D]_n [B]_n \{\delta\}_n \, dV_n \tag{2.40}$$

Since vector, $\{\delta\}_n$, contains scalar numbers, Eq. (2.40) can be rearranged to give

$$U_n = \frac{1}{2} \{\delta\}_n^T \left(\iiint_{V_n} [B]_n^T [D]_n [B]_n \, dV_n \right) \{\delta\}_n \qquad (2.41)$$

The total potential energy functional, π_n, for the element is given by

$$\pi_n = U_n - W_n \qquad (2.42)$$

Substituting Eqs. (2.38) and (2.41) into Eqs. (2.42), gives the potential energy functional in terms of the element nodal displacements, as follows:

$$\pi_n = \frac{1}{2} \{\delta\}_n^T \left(\iiint_{V_n} [B]_n^T [D]_n [B]_n \, dV_n \right) \{\delta\}_n - \{\delta\}_n^T \left(\iint_{S_n} [N]_n^T \{X\}_n \, dS_n + \iint_{S_n} [N]_n^T \{R\}_n \, dS_n \right) \qquad (2.43)$$

For equilibrium to be satisfied, the potential energy functional should be a minimum, which requires

$$\frac{d\pi_n}{d\{\delta\}_n} = 0 \qquad (2.44)$$

This reduces Eq. (2.43) to

$$\left(\iiint_{V_n} [B]_n^T [D]_n [B]_n \, dV_n \right) \{\delta\}_n = \iiint_{V_n} [N]_n^T \{X\}_n \, dV_n + \iint_{S_n} [N]_n^T \{R\}_n \, dS_n \qquad (2.45)$$

This can be written in abbreviated form as follows:

$$[K]_n \{\delta\}_n = \{F\}_n \qquad (2.46)$$

where $[K]_n$ is the element stiffness matrix, which is

given by

$$[K]_n = \iiint_{V_n} [B]_n^T [D]_n [B]_n \, dV_n \qquad (2.47)$$

and $\{F\}_n$ is the element nodal force vector, which is given by

$$\{F\}_n = \iiint_{V_n} [N]_n^T \{X\}_n \, dV_n + \iint_{S_n} [N]_n^T \{R\}_n \, dS_n \qquad (2.48)$$

2.2.4 Assembly of the Element Matrices

The system stiffness matrix, [K], is assembled using the element stiffness matrices $[K]_n$'s by the "direct stiffness method". This assembly procedure accounts for the fact that displacements of two adjacent elements sharing a node must be equal at that node. Each element stiffness matrix, $[K]_n$, is, therefore, assembled in the system stiffness matrix, [K], considering the element connectivity, which gives the relationship of element local nodes to the system degrees-of-freedom. In the same manner the system load vector, {F}, is formulated by assembling the element load vectors, $\{F\}_n$ in such a manner that equilibrium at nodes is satisfied.

An important characteristic of the system stiffness matrix is that it is always symmetric, and depending on the nodal numbering scheme adopted it is generally banded. Considering these characteristics, only the upper or the lower half band of the system stiffness matrix, [K],

needs to be assembled. This assembly procedure finally yields the system stiffness equilibrium equation, which relates

$$[K]\{\delta\} = \{F\} \tag{2.49}$$

where [K] is the system stiffness matrix, {F} is the system load vector and {δ} is the system nodal displacement vector.

2.2.5 Solution of the System Stiffness Equilibrium Equation

Equation (2.49) developed in the previous section is solved for the unknown system nodal displacement vector, {δ}, by either a direct elimination method or an iterative procedure. In this study, this equation is solved using the modified Gauss Elimination procedure. In this procedure the banded system stiffness matrix is modified to an upper triangular matrix. The solution vector, {δ}, which contains the unknown system displacements, is then computed by using a back substitution procedure. The element strain vector, $\{\epsilon\}_n$, and the element stress vector, $\{\sigma\}_n$, can then be computed using Eqs. (2.30) and (2.34), respectively.

2.3 FINITE ELEMENT MODELING FOR PLASTICITY PROBLEMS

2.3.1 Plasticity Equations Used in the Study

All the derivations in the previous section hold good only if the material stresses and strains are within

the elastic limit and small displacement theory is valid. Then if any one, or both, are not true the problem is said to be nonlinear. Thus, nonlinear problems can be characterized as the following three types:

1) material nonlinearity

2) geometric nonlinearity, and

3) combined material and geometric nonlinearity.

In the material nonlinearity problems, the material stress-strain relationship is nonlinear beyond the proportional or the elastic limit, and if the material is unloaded beyond the elastic limit then it is found that the stress-strain curve is not traced back, but a residual strain (called plastic strain) is left on complete unloading. In the geometric nonlinearity problems, the kinematic hardening of the material is considered due to large displacements. The combined effect of the two is considered in the third type of nonlinearity. In this study, only material nonlinearity is considered and small displacement theory is assumed to be valid in all the formulations.

For the material nonlinearity problems, still the displacement continuity and the equilibrium requirements have to be satisfied at all points. In this situation, the linear elastic constitutive law (Eq. 2.1) is replaced by a nonlinear relationship which gives a relation between the stress vector, $\{\sigma\}$, and the strain vector, $\{\varepsilon\}$,

at any point. This relationship can be expressed as a function R, as follows:

$$R(\{\sigma\}, \{\epsilon\}) = 0 \tag{2.50}$$

This is called as the "plastic flow law". This form of the plastic flow law assumes that the material hardening is isotropic, i.e., equal hardening occurs in all directions.

Contrary to the linear analysis, one important characteristic of the nonlinear problems is that the solution is not unique. Thus, a small-step incremental approach is essential to arrive to the solution. In this study, the mathematical formulations first suggested by von Mises [12], defining the plastic strain increment in relation to the yield surface, and later extended by Prandtl and Reuss [12], are used.

Prandtl and Reuss assumed that the principal direction of the plastic strain components coincide with the principal direction of the current state of stresses. This condition gives the following relationship [12]:

$$\frac{d\epsilon_x^P}{S_x} = \frac{d\epsilon_y^P}{S_y} = \frac{d\epsilon_{xy}^P}{\tau_{xy}} = d\lambda > 0 \tag{2.51}$$

in which $d\epsilon_x^P$ and $d\epsilon_y^P$ are the normal plastic strain increment components, in the x- and y-directions, respectively; $d\epsilon_{xy}^P$ is the engineering plastic shear strain increment in the xy-plane (note: $d\epsilon_{xy}^P = 2d\gamma_{xy}^P$); S_x and S_y

are the deviatoric stress components along the x- and y-directions, respectively; τ_{xy} is shear stress in the xy-plane; and $d\lambda$ is a constant.

The total strain energy of a material can be divided into two components. One is called as the hydrostatic component, which accounts for volume change only, and the other is called as the deviatoric component, which accounts for distortion energy only. So while considering the deviatoric stress components, the volume change is considered as zero. For a planer problem the deviatoric stress components, S_x, and S_y, are expressed in terms of the normal stress components, σ_x and σ_y, as follows:

$$S_x = \frac{1}{3}(2\sigma_x - \sigma_y) \tag{2.52a}$$

$$S_y = \frac{1}{3}(2\sigma_y - \sigma_x) \tag{2.52b}$$

Substituting Eqs. (2.52a) and (2.52b) into Eq. (2.51), the plastic strain increment components are given by

$$d\varepsilon_x^p = S_x\, d\lambda = \frac{2\sigma_x - \sigma_y}{3}\, d\lambda \tag{2.53a}$$

$$d\varepsilon_y^p = S_y\, d\lambda = \frac{2\sigma_y - \sigma_x}{3}\, d\lambda \tag{2.53b}$$

$$d\varepsilon^{P}_{xy} = \tau_{xy}\, d\lambda \qquad (2.53c)$$

According to von Mises, yielding occurs when the effective stress, $\bar{\sigma}$, becomes equal to the material yield stress, or

$$\bar{\sigma} = F_y \qquad (2.54)$$

where F_y is the material yield stress, and $\bar{\sigma}$ for a planar problem is defined as

$$\bar{\sigma} = \left[\sigma_1^2 + \sigma_2^2 - \sigma_1 \sigma_2 \right]^{1/2} \qquad (2.55)$$

in which σ_1 and σ_2 are the major and minor principal stresses, respectively, which are related to the cartesian stress components, σ_x, σ_y and τ_{xy}, by the following expression:

$$\sigma_{1,2} = \frac{\sigma_x + \sigma_y}{2} \pm \left[\left(\frac{\sigma_x - \sigma_y}{2} \right)^2 + \tau_{xy}^2 \right]^{1/2} \qquad (2.56)$$

Substituting Eq. (2.56) into Eq. (2.55), the effective stress, $\bar{\sigma}$, can be expressed in terms of the cartesian stress components, σ_x, σ_y and τ_{xy}, as follows:

$$\bar{\sigma} = \left[\sigma_x^2 - \sigma_x\sigma_y + \sigma_y^2 + 3\tau_{xy}^2 \right]^{1/2} \qquad (2.57)$$

Using Eq. (2.6) or Eq. (2.10), the cartesian stress components, σ_x, σ_y and τ_{xy} can be related to the strain components ε_x, ε_y and γ_{xy}, in the xy- plane by the following general equation:

$$\sigma_x = D_{11}\,\epsilon_x + D_{12}\,\epsilon_y \tag{2.58a}$$

$$\sigma_y = D_{12}\,\epsilon_x + D_{22}\,\epsilon_y \tag{2.58b}$$

$$\tau_{xy} = D_{33}\,\gamma_{xy} \tag{2.58c}$$

where D_{11}, D_{12} and D_{33} are material constants. Substituting these equations into Eq. (2.57), the total effective stress, $\bar{\sigma}$, can be expressed as

$$\begin{aligned}\bar{\sigma}^2 = {} & (D_{11}^2 + D_{12}^2 - D_{11}\,D_{12})\,\epsilon_x^2 \\ & + (D_{12}^2 + D_{22}^2 - D_{12}\,D_{22})\,\epsilon_y^2 \\ & + (2D_{11}\,D_{12} + 2D_{12}\,D_{22} - D_{11}\,D_{22} \\ & - D_{12}^2)\,\epsilon_x\,\epsilon_y + 3D_{33}^2\,\gamma_{xy}^2\end{aligned} \tag{2.59}$$

For a plane stress problem, in view of Eq. (2.7), the coefficients D_{11}, D_{12} and D_{33} are given by

$$D_{11} = \frac{E}{1-\nu^2} = D_{22} \tag{2.60a}$$

$$D_{12} = \frac{E\,\nu}{1-\nu^2} \tag{2.60b}$$

$$D_{33} = \left(\frac{E}{1-\nu^2}\right)\left(\frac{1-\nu}{2}\right) \tag{2.60c}$$

Substituting Eqs. (2.60a) to (2.60c) into Eq. (2.59), gives

$$\bar{\sigma}^2 = \frac{E^2}{(1-\nu^2)^2} \left[(1-\nu+\nu^2)\ (\epsilon_x^2 + \epsilon_y^2) \right.$$

$$\left. + (4\nu - \nu^2 - 1)\ \epsilon_x\ \epsilon_y + 3(1-\nu)^2\ \epsilon_{xy}^2 \right] \qquad (2.61)$$

where ϵ_{xy} is the engineering shear strain, which is related to the shear strain, γ_{xy}, by the following relationship:

$$\epsilon_{xy} = \frac{\gamma_{xy}}{2} \qquad (2.62)$$

In view of this, and dividing throughout Eq. (2.61) by E^2, gives

$$\bar{\epsilon}^2 = \frac{1}{(1-\nu^2)^2} \left[(1-\nu+\nu^2)\ (\epsilon_x^2 + \epsilon_y^2) \right.$$

$$\left. + (4\nu - \nu^2 - 1)\ \epsilon_x\ \epsilon_y + 3(1-\nu^2)\ \epsilon_{xy}^2 \right] \qquad (2.63)$$

where $\bar{\epsilon}$ is called as the total effective strain, which is given by

$$\bar{\epsilon} = \frac{\bar{\sigma}}{E} \qquad (2.64)$$

The incremental (differential increment) form of Eq. (2.63) can be written as

$$d\bar{\epsilon}^2 = \frac{1}{(1-\nu^2)^2} \left[(1-\nu+\nu^2)\ (d\epsilon_x^2 + d\epsilon_y^2) \right.$$

$$\left. + (4\nu - \nu^2 - 1)\ d\epsilon_x\ d\epsilon_y + 3(1-\nu^2)^2\ d\epsilon_{xy}^2 \right] \qquad (2.65)$$

where $d\bar{\varepsilon}$ is the effective strain increment and $d\varepsilon_x$, $d\varepsilon_y$, and $d\varepsilon_{xy}$ are the cartesian strain increments in the xy-plane.

In the plastic range since the material is incompressible, so taking $\nu = \frac{1}{2}$ in Eq. (2.65), gives the effective plastic strain increment, $d\bar{\varepsilon}^P$, as follows:

$$d\bar{\varepsilon}^P = \frac{2}{3} \left[d\varepsilon_x^{P^2} + d\varepsilon_y^{P^2} + d\varepsilon_x^P \, d\varepsilon_y^P + d\varepsilon_{xy}^{P^2} \right] \qquad (2.66)$$

where $d\varepsilon_x^P$, $d\varepsilon_y^P$ and $d\varepsilon_{xy}^P$ are the plastic strain increment components in the xy-plane. Now substituting Eqs. (2.53a) to (2.53c) into Eq. (2.66), gives the effective plastic strain increment, $d\bar{\varepsilon}^P$, in terms of the cartesian stress components, σ_x, σ_y and τ_{xy} as follows:

$$d\bar{\varepsilon}^P = \frac{2}{3} \left[\sigma_x^2 - \sigma_x \sigma_y + \sigma_y^2 + 3\tau_{xy}^2 \right]^{1/2} d\lambda \qquad (2.67)$$

which, in view of Eq. (2.57), can be simplified to

$$d\bar{\varepsilon}^P = \frac{2}{3} \bar{\sigma} \, d\lambda \qquad (2.68)$$

Computing the scalar $d\lambda$ from this equation, gives

$$d\lambda = \frac{3}{2} \frac{d\bar{\varepsilon}^P}{\bar{\sigma}} \qquad (2.69)$$

The incremental (differential increment) form of Eq. (2.57) can be written as

$$(d\bar{\sigma})^2 = d\sigma_x^2 - d\sigma_x\, d\sigma_y + d\sigma_y^2 + 3d\tau_{xy}^2 \qquad (2.70)$$

where $d\bar{\sigma}$ is the effective stress increment, and $d\sigma_x$, $d\sigma_y$ and $d\tau_{xy}$ are the cartesian stress increment components in the xy-plane.

For the material under consideration, a curve can be drawn for cumulative effective plastic strain, $\bar{\varepsilon}^p$, versus the effective stress, $\bar{\sigma}$. The slope, H', of this curve, which is expressed by

$$H' = \frac{d\bar{\sigma}}{d\bar{\varepsilon}^p} \qquad (2.71)$$

is called as the Heils' function. An approximation of H' at any state of stress can be taken as $\frac{2}{3}$ times the plastic slope of the uniaxial stress-strain curve, at that state, determined from the experimental data [18]. This gives

$$H' = \frac{2}{3}\left(\frac{E_t\, E}{E - E_t}\right) \qquad (2.72)$$

where E is the slope of the elastic region of the uniaxial stress-strain curve, defined as the Young's modulus of elasticity, and E_t is the slope of the tangent to the uniaxial stress-strain curve taken in the plastic region

(beyond the elastic limit). E_t is also referred to as the tangent modulus of elasticity. Thus, using Eq. (2.71), the effective stress increment, $d\bar{\sigma}$, can be expressed in terms of the equivalent plastic strain increment, $d\bar{\varepsilon}^P$, as follows:

$$d\bar{\varepsilon}^P = \frac{d\bar{\sigma}}{H'} \tag{2.73}$$

Substituting Eq. (2.73) into Eq. (2.69), reduces it to

$$d\lambda = \frac{3}{2} \frac{d\bar{\sigma}}{\bar{\sigma} H'} \tag{2.74}$$

It should be noted that this equation is applicable for both plane stress and plane strain problems.

The total strain increment vector, $\{d\varepsilon\}$, is equal to the summation of the elastic strain-increment-vector, $\{d\varepsilon^e\}$, and the plastic strain increment vector, $\{d\varepsilon^P\}$, i.e.,

$$\{d\varepsilon\} = \{d\varepsilon^e\} + \{d\varepsilon^P\} \tag{2.75}$$

From Hooke's Law the total increment stress vector, $\{d\sigma\}$, can be related to the elastic strain increment vector, $\{d\varepsilon^e\}$, as follows:

$$\{d\sigma\} = [D^e] \{d\varepsilon^e\} \tag{2.76}$$

where $[D^e]$ is the elasticity material matrix, which is given by Eq. (2.7) for a plane stress problem and by Eq. (2.11) for a plane strain problem. Substituting Eq.

(2.75) for $\{d\varepsilon^e\}$ into Eq. (2.76), gives

$$\{d\sigma\} = [D^e]\ (\{d\varepsilon\} - \{d\varepsilon^P\}) \tag{2.77}$$

The plastic strain increment vector, $\{d\varepsilon^P\}$, according to the Prandtl-Reuss equation, Eq. (2.51), can be written as

$$\{d\varepsilon^P\} = \begin{Bmatrix} d\varepsilon_x^P \\ d\varepsilon_y^P \\ d\gamma_{xy}^P \end{Bmatrix} = \begin{Bmatrix} S_x \\ S_y \\ 2\tau_{xy} \end{Bmatrix} d\lambda \tag{2.78}$$

Substituting Eq. (2.69), for $d\lambda$, into Eq. (2.78), gives the components of the plastic strain increment vector, $\{d\varepsilon^P\}$, in terms of the effective plastic strain increment, $d\bar{\varepsilon}^P$, as follows

$$\{d\varepsilon^P\} = \{A\}\, d\bar{\varepsilon}^P \tag{2.79}$$

where

$$\{A\} = \frac{3}{2\bar{\sigma}} \begin{Bmatrix} S_x \\ S_y \\ 2\tau_{xy} \end{Bmatrix} \tag{2.80}$$

Substituting Eq. (2.79) into Eq. (2.77), gives

$$\{d\sigma\} = [D^e]\ (\{d\varepsilon\} - \{A\}d\bar{\varepsilon}^P) \tag{2.81}$$

In order to use this equation to develop the incremental stress-strain relationship in the plastic range, the effective plastic strain increment, $d\bar{\varepsilon}^P$, has to be related to the strain increment vector, $\{d\varepsilon\}$.

The effective stress, $\bar{\sigma}$, is a function of the stress components σ_x, σ_y and τ_{xy}, i.e., $\bar{\sigma} = f(\sigma_x, \sigma_y, \tau_{xy})$. Thus, from calculus $d\bar{\sigma}$ can be written as

$$d\bar{\sigma} = \frac{\partial \bar{\sigma}}{\partial \sigma_x} d\sigma_x + \frac{\partial \bar{\sigma}}{\partial \sigma_y} dy + \frac{\partial \bar{\sigma}}{\partial \tau_{xy}} d\tau_{xy} \tag{2.82}$$

in which, substituting Eq. (2.57) for $\bar{\sigma}$ to evaluate the partial derivatives, gives

$$d\bar{\sigma} = \frac{1}{2\bar{\sigma}} [(2\sigma_x - \sigma_y)\, d\sigma_x + (2\sigma_y - \sigma_x)\, d\sigma_y + (6\tau_{xy})\, d\tau_{xy}] \tag{2.83}$$

In view of Eqs. (2.52a) and (2.52b), this equation can be simplified and written in matrix form as follows:

$$d\bar{\sigma} = \frac{3}{2\bar{\sigma}} \langle S_x \quad S_y \quad 2\tau_{xy} \rangle \begin{Bmatrix} d\sigma_x \\ d\sigma_y \\ d\tau_{xy} \end{Bmatrix} \tag{2.84}$$

In view of the definition of $\{A\}$ by Eq. (2.80), Eq. (2.84) can be expressed as

$$d\bar{\sigma} = \{A\}^T \{d\sigma\} \tag{2.85}$$

where

$$\{d\sigma\} = \begin{Bmatrix} d\sigma_x \\ d\sigma_y \\ d\tau_{xy} \end{Bmatrix} \tag{2.86}$$

is the stress increment vector.

Substituting Eq. (2.73) for $d\bar{\sigma}$, and Eq. (2.81) for $\{d\sigma\}$ into Eq. (2.85), gives the desired relationship relating $d\bar{\epsilon}^P$ to $\{d\epsilon\}$, as

$$d\bar{\epsilon}^P = \frac{\{A\}^T [D^e]}{H' + \{A\}^T [D^e] \{A\}} \{d\epsilon\} \tag{2.87}$$

or

$$d\bar{\epsilon}^P = [W] \{d\epsilon\} \tag{2.88}$$

where

$$[W] = \frac{\{A\}^T [D^e]}{H' + \{A\}^T [D^e] \{A\}} \tag{2.89}$$

For a plane stress problem, substituting Eq. (2.7) for $[D^e]$ and Eq. (2.80) for $\{A\}$ into Eq. (2.89), gives $[W]$ as

$$\underset{(1\times3)}{[W]} = \frac{1}{a} < (S_x + \nu S_y) \quad (\nu S_x + S_y) \quad (1-\nu)\tau_{xy} > \tag{2.90}$$

where

$$a = \frac{3}{2\bar{\sigma}} \left[\frac{4H'(1-\nu^2)}{9E} \bar{\sigma}^2 + S_x^2 + 2\nu S_x S_y \right.$$

$$\left. + S_y^2 + 2(1-\nu)\tau_{xy}^2 \right] \tag{2.91}$$

For a plane strain problem, substituting Eq. (2.11) for $[D^e]$ and Eq. (2.80) for $\{A\}$ into Eq. (2.89), gives $[W]$ as

$$\underset{(1x3)}{[W]} = \frac{1}{s} < [(1-\nu)S_x + \nu S_y] \quad [(1-\nu)S_y + \nu S_x] \quad (1-2\nu)\tau_{xy} > \tag{2.92}$$

where

$$s = \frac{3}{2\bar{\sigma}} \left[\frac{4H'(1+\nu)(1-2\nu)}{9E} \bar{\sigma}^2 + S_x^2 + 2\nu S_x S_y + S_y^2 - \nu(S_x^2 + S_y^2) + 2(1-2\nu)\tau_{xy}^2 \right] \tag{2.93}$$

Finally, substituting Eq. (2.88) into Eq. (2.81), gives the desired incremental stress-strain law in the plastic range, as follows:

$$\{d\sigma\} = [D^e] (\{d\varepsilon\} - \{A\} [W] \{d\varepsilon\})$$

$$= ([D^e] - [D^e] \{A\} [W])\{d\varepsilon\} \tag{2.94}$$

or

$$\{d\sigma\} = [D^{eP}] \{d\varepsilon\} \tag{2.95}$$

where $[D^{eP}]$ is called as the elasto-plasticity material matrix, which is given by

$$[D^{eP}] = [D^e] - [D^e] \{A\} [W] \tag{2.96}$$

Substituting Eqs. (2.7), (2.80) and (2.90) for $[D^e]$, $\{A\}$ and $[W]$, respectively, into Eq. (2.96), gives the elasto-plasticity material matrix, $[D^{eP}]$, for a plane stress

problem, as

$$[D^{eP}] = \frac{E}{Q}\begin{bmatrix} S_y^2 + 2P & \text{Symmetrical} & \\ -S_xS_y + 2vP & S_x^2 + 2P & \\ -\frac{S_x + vS_y}{1+v}\tau_{xy} & \frac{-S_y + vS_x}{1+v}\tau_{xy} & \frac{R}{2(1+v)} + \frac{2H'}{9E}(1-v)\bar{\sigma}^2 \end{bmatrix} \tag{2.97}$$

where

$$P = \frac{2H'}{9E}\bar{\sigma}^2 + \frac{\tau_{xy}^2}{1+v} \tag{2.98a}$$

$$Q = R + 2(1-v^2)P \tag{2.98b}$$

$$R = S_x^2 + 2vS_xS_y + S_y^2 \tag{2.98c}$$

Similarly, substituting Eqs. (2.11), (2.8) and (2.92) for $[D^e]$, $\{A\}$ and $[W]$, respectively, into Eq. (2.96) gives the elasto-plasticity material matrix, $[D^{eP}]$, for the plane strain problem, as

$$[D^{eP}] = \frac{E}{(1+v)A}\begin{bmatrix} S_y^2 + 2(1-v^2)P & \text{Symmetrical} & \\ -S_xS_y + 2v(1+v)P & S_x^2 + 2(1-v^2)P & \\ -\tau_{xy}[(1-v)S_x + vS_y] & -\tau_{xy}[(1-v)S_y + vS_x] & \frac{R}{2} + \frac{2H'}{9E}(1+v)(1-2v)\bar{\sigma}^2 \end{bmatrix} \tag{2.99}$$

where

$$A = B + 2(1+\nu)(1-2\nu)P \tag{2.100a}$$

$$B = (1-\nu)S_x^2 + 2\nu S_x S_y + (1-\nu)S_y^2 \tag{2.100b}$$

and P is given by Eq. (2.98a).

Making use of either the elastic material matrix, $[D^e]$, or the elasto-plastic material matrix, $[D^{eP}]$, in Eq. (2.42), the elastic element stiffness matrix, $[K^e]_n$ can be obtained from

$$[K^e]_n = \iiint_{V_n} [B]_n^T [D^e]_n [B]_n \, dV_n \tag{2.101}$$

or the elasto-plastic element stiffness matrix, $[K^{eP}]_n$, can be obtained from

$$[K^{eP}]_n = \iiint_{V_n} [B]_n^T [D^{eP}]_n [B]_n \, dV_n \tag{2.102}$$

In the subsequent paragraphs few additional plasticity relationships are presented which are used in the analysis steps described in the subsequent Subsection 2.3.2. In the analysis procedure described in this subsection an incremental load (i.e., a finite load increment) is predicted such that the most stressed elastic element yields. During this finite (but small) load increment, the incremental stress components, the incremental effective stress and the incremental plastic strain

are computed for each element. Since all these quantities computed are finite, they will now be denoted by the symbol "Δ", instead of the symbol "d" used to denote a differential increment in the preceding analytical formulation presented. Thus, $\Delta\bar{\sigma}$ means the incremental effective stress produced due to the incremental load acting on the system. The additional relationships are given as follows:

(1) Using Eqs. (2.57) and (2.70), an incremental relationship can be formed relating an element's total effective stress, $\bar{\sigma}'$, produced after the application of the previous load increment to the incremental effective stress, $\Delta\bar{\sigma}$, produced due to the current load increment. The total effective stress produced after the application of the current load increment is

$$(\bar{\sigma}' + \Delta\bar{\sigma})^2 = (\sigma_x' + \Delta\sigma_x)^2 - (\sigma_x' + \Delta\sigma_x)(\sigma_y' + \Delta\sigma_y) + (\sigma_y' + \Delta\sigma_y)^2 + 3(\tau_{xy} + \Delta\tau_{xy})^2 \tag{2.103}$$

where σ_x', σ_y' and τ_{xy}' are the cartesian components of the total stress produced in the element after the application of the previous load increment, and $\Delta\sigma_x$, $\Delta\sigma_y$ and $\Delta\tau_{xy}$ are the cartesian incremental stress components produced due to the application of the current load increment. Solving for $\Delta\bar{\sigma}$, from Eq.

(2.99), gives

$$\Delta\bar{\sigma} = [(\sigma'_x + \Delta\sigma_x)^2 + (\sigma'_x + \Delta\sigma_x)(\sigma'_y + \Delta\sigma_y) + (\sigma'_y + \Delta\sigma_y)^2 + 3(\tau_{xy} + \Delta\tau'_{xy})]^{1/2} - \bar{\sigma}' \quad (2.104)$$

(2) In order to predict the load required to yield the most stressed elastic element, a factor r is computed for each elastic element such that

$$\bar{\sigma}' + r\ \Delta\bar{\sigma} = F_y \quad (2.105)$$

where $\bar{\sigma}'$ is the total effective stress produced in the element after the application of the previous load increment, $\Delta\bar{\sigma}$ is the incremental effective stress produced in the element by the current applied load increment, and F_y is the yield stress (proportional limit stress) of the material. Thus, the minimum value of r for all the elastic elements gives the scaling factor which is used to multiply the present load increment so as to predict the new yield load. To develop the expression for r, refer to Fig. 2.2, which shows for an element the following failure (yielding) envelopes obtained using the von Mises yield criterion: (i) after the application of the previous load increment (the innermost ellipse), (ii) at the initial yield (the in-between

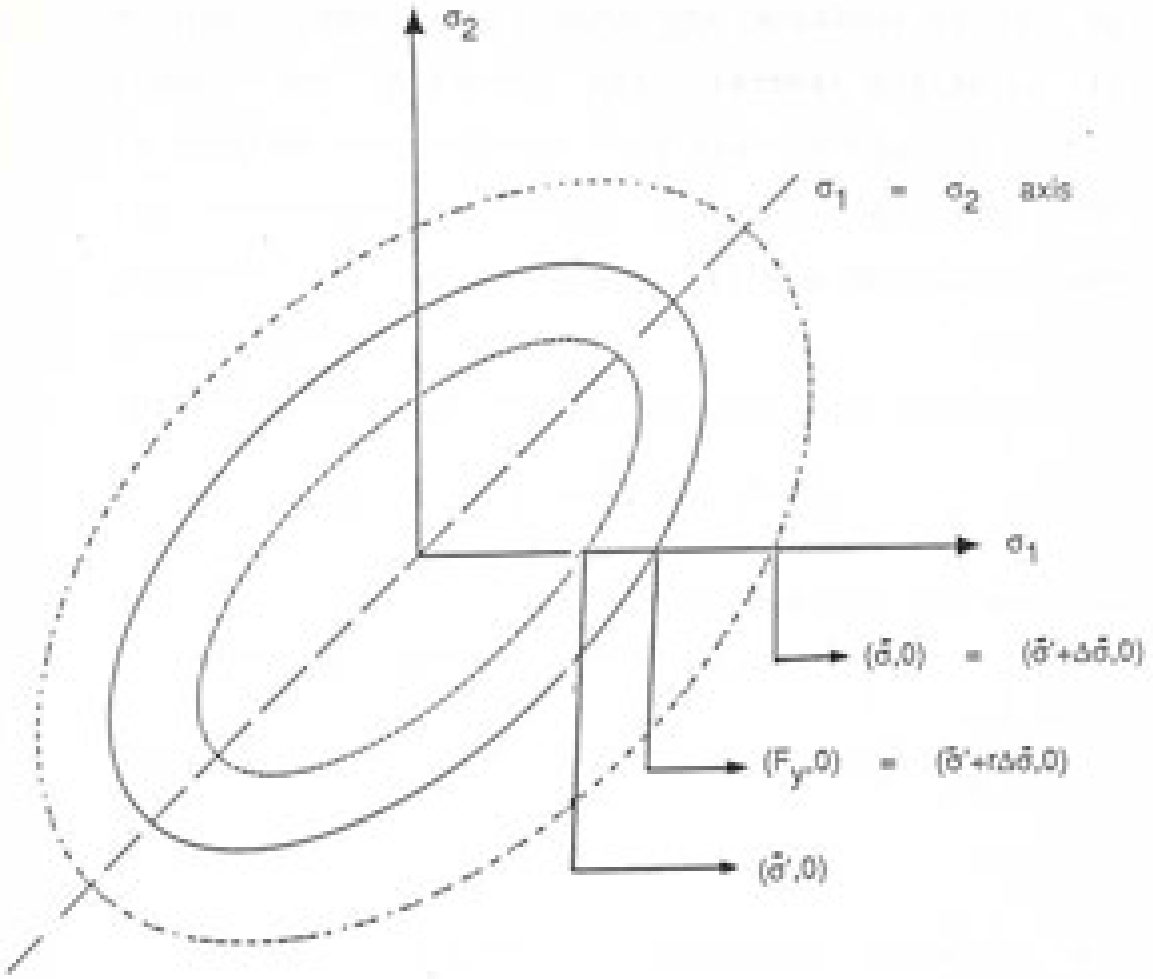

Legend:
- Failure envelope after the application of the previous load increment
- Failure envelope at initial yield
- Failure envelope after the application of the current load increment

Fig. 2.2 Failure Envelopes Obtained for an Element on von Mises Yield Criterion at Different Stages of Loading

ellipse), and (iii) after the application of the current load increment (the outermost ellipse). It is desired to predict r such that the failure envelope corresponding to (ii) and (iii) coincide. The equations for these three failure envelopes are given below:

(i) After application of previous load increment:

$$\sigma_x'^2 + \sigma_y'^2 - \sigma_x' \sigma_y' + 3\tau_{xy}'^2 = \bar{\sigma}' \qquad (2.106)$$

(ii) At initial yield or after scaling the applied load increment by the factor r:

$$(\sigma_x' + r\Delta\sigma_x)^2 + (\sigma_y' + r\Delta\sigma_y)^2 - (\sigma_x' + r\Delta\sigma_x)(\sigma_y' + r\Delta\sigma_y) + 3(\tau_{xy}' + r\Delta\tau_{xy})^2 = F_y^2 \qquad (2.107)$$

which on expansion, regrouping of terms, and substitution of Eq. (2.106), reduces to

$$\Delta\bar{\sigma}''^2 r^2 + [(2\sigma_x' - \sigma_y')\,\Delta\sigma_x + (2\sigma_y' - \sigma_x')\,\Delta\sigma_y + 6\tau_{xy}'\,\Delta\tau_{xy}]\, r + \bar{\sigma}' - F_y^2 = 0 \qquad (2.108)$$

where

$$\Delta\bar{\sigma}'' = [\,\Delta\sigma_x^2 + \Delta\sigma_y^2 - \Delta\sigma_x\,\Delta\sigma_y + 3\Delta\tau_{xy}^2\,]^{1/2} \qquad (2.109)$$

(iii) After application of the current applied load increment:

$$(\sigma'_x + \Delta\sigma_x)^2 + (\sigma'_y + \Delta\sigma_y)^2 - (\sigma'_x + \Delta\sigma_x)(\sigma'_y + \Delta\sigma_y)$$

$$+ 3(\tau'_{xy} + \Delta\tau_{xy})^2 = (\bar{\sigma}' + \Delta\bar{\sigma})^2 \qquad (2.110)$$

which on expansion, regrouping of terms, and substitution of Eqs. (2.106) and (2.109), reduces to

$$\bar{\sigma}'^2 + \Delta\bar{\sigma}''^2 + (2\sigma'_x - \sigma'_y)\,\Delta\sigma_x$$

$$+ (2\sigma'_y - \sigma'_x)\,\Delta\sigma_y + 6\tau'_{xy}\,\Delta\tau_{xy} = (\bar{\sigma}' + \Delta\bar{\sigma})^2 \qquad (2.111)$$

This operation gives

$$(2\sigma'_x - \sigma'_y)\,\Delta\sigma_x + (2\sigma'_y - \sigma'_x)\,\Delta\sigma_y$$

$$+ 6\tau'_{xy}\,\Delta\tau_{xy} = -\gamma \qquad (2.112)$$

where

$$\gamma = \Delta\bar{\sigma}''^2 - 2\bar{\sigma}\,\Delta\bar{\sigma} - \Delta\bar{\sigma}^2 \qquad (2.113)$$

Substituting Eq. (2.113) into Eq. (2.108) gives a quadratic equation in r, as follows:

$$\Delta\bar{\sigma}''^2\, r^2 - \gamma r - (F_y^2 - \bar{\sigma}'^2) = 0 \qquad (2.114)$$

which on substituting for r, gives

$$r = \frac{\gamma + \left[\,\gamma^2 + 4(\Delta\bar{\sigma}''^2)(F_y^2 - \bar{\sigma}'^2)\,\right]^{1/2}}{2(\Delta\bar{\sigma}''^2)} \qquad (2.115)$$

It should be noted that only the positive sign

outside the square root quantity has been considered, since the negative sign would give a negative value of r, which is not possible for monotonically increasing loads.

(3) In order to compute the value of incremental effective plastic strain, $\Delta\bar{\varepsilon}^{P}$, Eq. (2.88) can be used. Substituting Eq. (2.90) for [W] into Eq. (2.88), the incremental effective plastic strain, $\Delta\bar{\varepsilon}^{P}$, for a plane stress problem is obtained as

$$\Delta\bar{\varepsilon}^{P} = \frac{2}{3}\frac{\bar{\sigma}}{Q}\left[(S_x + \nu S_y)\,\Delta\varepsilon_x + (S_y + \nu S_x)\,\Delta\varepsilon_y + (1-\nu)\tau_{xy}\,\Delta\gamma_{xy}\right] \tag{2.116}$$

And substituting Eq. (2.92) for [W] into Eq. (2.88), the incremental effective plastic strain, $\Delta\bar{\varepsilon}^{P}$, for a plane strain problem is obtained as

$$\Delta\bar{\varepsilon}^{P} = \frac{2}{3}\frac{\bar{\sigma}}{A}\left[\left[(1-\nu)S_x + \nu S_y\right]\Delta\varepsilon_x + \left[(1-\nu)S_y + \nu S_x\right]\Delta\varepsilon_y + (1-2\nu)\tau_{xy}\,\Delta\gamma_{xy}\right] \tag{2.117}$$

In Eqs. (2.116) and (2.117) S_x and S_y are the deviatoric stress components along the x- and y-axis, respectively; τ_{xy} is the shear stress; $\Delta\varepsilon_x$, $\Delta\varepsilon_y$ and $\Delta\gamma_{xy}$ are the incremental strain components in the x-y plane; Q

is given by Eq. (2.98b), and A is given by Eq. (2.100a).

2.3.2 Analysis Steps to Find Failure Load Using the Plastic Flow Law

Based on the mathematical formulations, presented in Section 2.2 and Subsection 2.3.1, the steps for finding the failure load [5] due to excessive yielding are as follows:

(1) Apply a unit load to the system and solve the elastic system stiffness equilibrium equation, Eq. (2.46), to compute the system nodal displacement vector, $\{\delta\}$.

(2) Using the connectivity indices for each element, extract the element nodal displacement vector, $\{\delta\}_n$, from the system nodal displacement vector, $\{\delta\}$, and compute the element strain vector, $\{\epsilon\}_n$, and the element stress vector, $\{\sigma\}_n$, using Eqs. (2.30) and (2.34), respectively. From the element stress vector, $\{\sigma\}_n$, compute the effective stress, $\bar{\sigma}_n$, for each element using Eq. (2.57). Since all stresses are in the elastic range, this effective stress is called as elastic effective stress and is denoted as $\bar{\sigma}^e_n$.

(3) For each element compute the factor r^e given as

$$r^e = \frac{F_y}{\bar{\sigma}^e_n} \tag{2.118}$$

where F_y is the yield stress (proportional limit stress) of the material. Compute the minimum of all the r^e's computed for the elements in the input finite element mesh. As F_y is a constant, the minimum r^e will occur for that element for which the elastic effective stress, $\bar{\sigma}^e_n$, is a maximum value. This maximum value is denoted as $(\bar{\sigma}^e_n)_{max}$, and the element having this stress is the most stressed element for this load cycle.

(4) Scale-up the stresses of all the elements so that the most stressed element is made to yield by setting its effective stress, $\bar{\sigma}^e$, equal to yield stress, F_y. As a unit load was applied at this load cycle, so r^e is the load required to cause the initial yield to occur. Store this value as the total load {L} at this stage. Denote the total stress vector and the effective stress of each element corresponding to this load as $\{\sigma'\}_n$ and $\bar{\sigma}'_n$, respectively.

(5) Compute $[D^{eP}]$ for the yielded element(s) using the total stresses at this stage and Eq. (2.97). For each yielded element compute its new elasto-plastic stiffness matrix, $[K^{eP}]_n$, using Eq. (2.102) and assemble the new system stiffness matrix, [K].

(6) Apply an incremental load, say {ΔL}, to the system. Solve the system stiffness equilibrium equation, Eq.

(2.46), to compute the incremental system nodal displacement vector, $\{\Delta\delta\}$.

(7) Using the connectivity indices, for each element, extract the element nodal displacement vector, $\{\Delta\sigma\}_n$, from the system nodal displacement vector, $\{\Delta\delta\}$, and compute the incremental element strain vector, $\{\Delta\varepsilon\}_n$, and the incremental stress vector, $\{\Delta\sigma\}_n$, by substituting these nodal displacement values into Eqs. (2.30) and (2.34), respectively.

(8) For all the elastic elements compute the factor r using Eq. (2.111).

(9) Compute the minimum value, r_{min}, of the factor r for all the elastic elements. The element having this value is the most stressed elastic element, and $r_{min}\{\Delta L\}$ is the value of the incremental load required to just cause yielding of this element.

(10) For all the elements, multiply the incremental element strain vector, $\{\Delta\varepsilon\}_n$, and the incremental element stress components vector, $\{\Delta\sigma\}_n$, as obtained in Step (7), by r_{min}. Compute the total element strain vector, $\{\varepsilon\}_n$, and the total element stress vector, $\{\sigma\}_n$, by adding the incremental value computed to the corresponding value predicted at the end of the previous load cycle, i.e.,

$$\{\varepsilon\}_n = \{\varepsilon'\}_n + r_{min}\{\Delta\varepsilon\}_n \qquad (2.119)$$

$$\{\sigma\}_n = \{\sigma'\}_n + r_{min}\{\Delta\sigma\}_n \tag{2.120}$$

(11) Compute the total effective stress, $\bar{\sigma}_n$, for each element by subtituting $\{\sigma\}_n$ obtained from Step (10) into Eq. (2.57). The effective stress in the element with r_{min} (which was found in Step (9)) will be equal to F_y.

(12) Compute the total load by adding $r_{min}\{\Delta L\}$ to the previous load level, i.e.,

$$\{L\} = \{L'\} + r_{min}\{\Delta L\} \tag{2.121}$$

where $\{L'\}$ is the total load applied at the end of the previous load increment.

(13) For all the yielded elements, compute the equivalent plastic strain increment, $\Delta\bar{\varepsilon}^P$, using Eq. (2.112).

(14) If for any yielded element, $\Delta\bar{\varepsilon}^P$ is negative, then failure is said to occur. Then the analysis is terminated and the total load is printed as the failure load of the specimen. If $\Delta\bar{\varepsilon}^P$ for all the yielded elements is positive, then denote the total stress vector and the effective stress for each element as $\{\sigma'_n\}$ and $\bar{\sigma}'_n$, respectively, and return to Step (5).

It should be noted that after the execution of Step (11), whereas, the element with r_{min} will have its effective stress equal to the yield stress, F_y, there may be

a few more elastic elements (their number increases as the specimen is near its failure) whose effective stress is very close to F_y. Yielding them one by one in later cycles will only increase the computational cost at the expense of a small increase in the total load. Therefore, it was decided to modify Step (11) so as to find all the elastic elements having the effective stress, $\bar{\sigma}_n$, greater than or equal to $0.995F_y$ and yield all these elements together by setting their respective total effective stress equal to F_y.

2.4 FINITE ELEMENT MODELING FOR FRACTURE MECHANICS PROBLEMS

In this study it is proposed to use the analysis steps presented in Section 2.3.2 to march along the uniaxial stress-strain curve of the material up to the fracture stress value. This can be done by eliminating Step (13) and also modifying Step (14) (which now becomes Step (13)) to read as follows in the procedure suggested:

"(13) On the basis of Step (11) find the most stressed element, i.e., the element having maximum value of total effective stress, $(\bar{\sigma}_n)$, and check the following: (a) If the maximum value of this stress is greater than the fracture stress of the material as obtained from the uniaxial stress-strain curve, then discard this run and repeat Steps (6) to (13) by decreasing the incremental load $\{\Delta L\}$, in Step (6)

to 1/2 {ΔL}. Otherwise, proceed to (b), which follows. (b) If the value of the effective stress $(\bar{\sigma}_n)_{max}$ is within a preset allowable tolerance limit (± 0.5%) of the fracture stress, as obtained from the material uniaxial stress-strain curve, then this most stressed element is said to have fractured."

At the stage of loading, when the first element fractures, the structure as a whole may still be capable of withstanding some additional load. So the load predicted at first fracture cannot be called as the failure load. Definitely the element which has fractured is not capable of withstanding any more loads. This effect is proposed to be modeled by not assembling the element stiffness matrix of the fractured element into the system stiffness matrix for further analysis. In addition to this, the strain energy of the fractured element is proposed to be redistributed to the remaining unfractured elements in the system before any further load increment is applied to the system.

In this study, the redistribution of the load carried by the fractured element to the remaining unfractured system is proposed to be done by a method called as "element nodal load release" method. In this method the strain energy of the fractured element is proposed to be redistributed to the remaining unfractured

elements in the following steps:

(1) The nodal forces, $\{F^f\}_n$, of the fractured element are computed from

$$\{F^f\}_n = \iiint_{V_n} [B]_n^T \{\sigma^f\}_n \, dV_n \qquad (2.122)$$

where $\{\sigma^f\}_n$ denotes the stress components vector of the fractured element; $[B]_n$ is its strain-displacement transformation matrix, which is given as Eq. (2.32); and V_n is the volume of this element. For the constant stress-strain triangular element, since the element strain-displacement transformation matrix, $[B]_n$, and the element stress vector, $\{\sigma^f\}_n$, are constants, so Eq. (2.109) reduces to

$$\{F^f\}_n = (h * A_n) * [B]_n^T \{\sigma^f\}_n \qquad (2.123)$$

where h is the thickness of the element and A_n is the area of the element.

(2) Negative of these nodal forces are applied at the system nodes belonging to the fractured element, as follows:

(i) The vector containing the negative nodal forces is first normalized with respect to the maximum value (absolute) appearing in this vector. Say this maximum value is denoted as PNMAX.

(ii) The system load vector is assembled by applying

these normalized nodal loads acting at the system degrees-of-freedom related to the fractured element. Note that no other external loads are taken to be acting.

(iii) A small increment of PNMAX, say α(PNMAX), is applied to the system, where α is a very small number (say 10%).

(iv) The system stiffness matrix, [K], is assembled, such that the fractured element is not considered in the assembly, and the other element stiffness matrices are the same as computed in the end of the previous load cycle.

(v) The system stiffness equilibrium equation, Eq. (2.49), is solved for the system nodal displacements vector, $\{\Delta\delta\}$.

(vi) Using the connectivity indices, extract the element nodal displacement vector, $\{\Delta\delta\}_n$, for each element from the system nodal displacement vector, $\{\Delta\delta\}$, and compute the incremental element strain vector, $\{\Delta\varepsilon\}_n$, and the element incremental stress vector, $\{\Delta\sigma\}_n$, by substituting these nodal displacement values into Eqs. (2.30) and (2.34), respectively.

(vii) For each element, compute the total element stress vector, $\{\sigma\}_n$ by adding the incremental value computed in the preceding step to the

corresponding value predicted at the end of the previous redistribution load cycle, and compute total effective stress, $\bar{\sigma}_n$, using Eq. (2.57).

(viii) All yielded elements whose total effective stress, $\bar{\sigma}_n$, computed in Step (vii) is lesser than their total effective stress, $\bar{\sigma}'_n$, at the end of the previous redistribution load cycle, are called unloading yield elements. For these elements the elastic element stiffness matrix, $[K^e]_n$, has to be used (Eq. (2.97)) instead of the elasto-plastic element stiffness matrix, $[K^{eP}]_n$, (Eq. (2.98)).

(ix) In Step (viii) if any unloading yielded element is present, then this redistribution cycle has to be discarded and Steps (iv) and (viii) are repeated in cycles until this element again starts loading. It is reported by Miller [24] that these elements again start reloading in two cycles. Therefore, in this study it was decided to put a limit of four cycles to examine whether the unloading yielded elements start again loading. If at the end of the first four redistribution cycles, there are any unloading elements present, they are treated like all the other (loading) yielded elements and the analysis is continued.

(x) The total load achieved for the fractured element is computed as

$$P_f = P_f + \alpha \, PNMAX \qquad (2.124)$$

where P_f is set equal to zero during the first load cycle used to redistribute the energy of the fractured element.

(xi) Steps (i) to (x) are repeated until P_f becomes equal to PNMAX within a tolerance limit of ± 0.005%. When this load has been achieved, then it is considered that the strain energy of the fractured element has been dissipated into the unfractured system.

(3) If any other element fractures before the strain energy of the fractured element is completely dissipated, then this state is known as the state of "unstable crack growth". In that case the analysis is terminated and the ultimate fracture failure of the structure is said to occur. The total load at this stage is called as the ultimate fracture failure load of the structure.

After the redistribution of the strain energy of the first fractured element has been completed, then a further external incremental load is applied to the system and analysis Steps (6) to (12) of Section 2.2 and (13) of Section (2.3) are repeated until another element frac-

tures. Then the strain energy of this new fractured element is dissipated into the unfractured system using Steps (1) to (3) of the preceding paragraph of this section. This process of application of incremental external loads and the dissipation of the energy of the fractured element is continued until unstable crack growth is achieved.

It has to be noted that if all the elements surrounding any node fracture, then the system stiffness matrix becomes singular. But, this may not indicate that the ultimate fracture failure of the structure has occurred, i.e., the unfractured elements may still be capable of resisting additional external loads acting on the system. To activate the analysis further, in order to see whether such a situation is possible, this node is constrained and the analysis is continued until another element fractures.

CHAPTER III

DESCRIPTION OF THE COMPUTER PROGRAM DEVELOPED

3.1 INTRODUCTION

In the present study two computer programs are developed. They are written in Fortran 77 for the University of Oklahoma's IBM 3081 computer. The first program, called "PLAST", uses an isotropic plasticity hardening model to march along the nonlinear material stress-strain curve and predicts failure load due to excessive yielding. It uses the plastic flow concepts presented by Yamada et al. [32], as described in the previous chapter. In this model failure is said to occur when during an applied load increment the incremental plastic strain becomes less than zero (i.e., negative). The second program, called "CRACK", is the extension of the first program to predict crack initiation and ultimate fracture failure load. The same isotropic plasticity hardening model is used to march along the stress-strain curve until fracture occurs in one element. The strain energy of the fractured element is then released into the system by an "element nodal load release" method and then

it is made inert. In this manner this computer program redistributes the strain energy of the fractured element as each successive element fractures. Unstable crack growth or ultimate fracture failure of the specimen analyzed is said to occur if another element fractures during the process of releasing of the energy of the last fractured element. Both the programs predict a complete load-displacement history and the yield patterns for structural systems subjected to monotonically increasing loads.

The general features of the computer program PLAST are presented in Section 3.2. The flow charts of the main program and the important subroutines of this computer program are presented in Section 3.3. Section 3.4 contains the general features of the computer program CRACK. The flow charts of the main program and the subroutines of this computer program are presented in Section 3.5.

3.2 GENERAL FEATURES OF THE COMPUTER PROGRAM PLAST

The computer program PLAST is divided into six main stages, as shown in Fig. 3.1. The functions of each of these stages are described in the subsequent subsections.

3.2.1 Stage I: Input and Setting Up

The finite element mesh data, which is either gen-

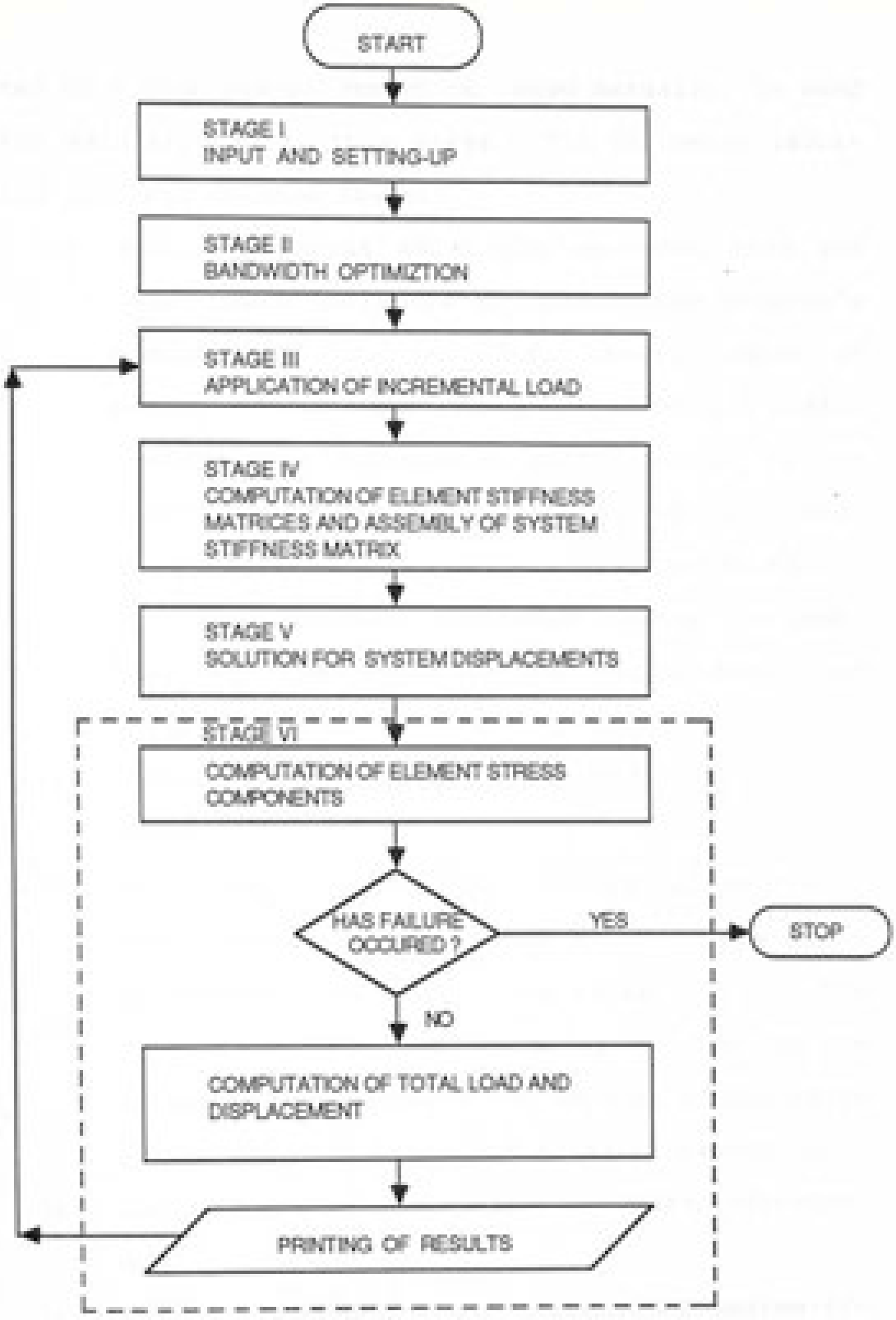

Fig. 3.1 Main Stages of the Computer Program PLAST

erated by a mesh pre-processor or coded manually, is read by the main program in this stage. The following information is input in this stage:

(1) Main information about the generated mesh and other input variables to control the program's execution. This includes: total number of nodes, NUMNP; total number of elements, NUMEL; maximum node difference, IDIFF; a flag to indicate the type of analysis to be performed, NCODE (NCODE = 0 for plane strain and NCODE = 1 for plane stress); thickness of the specimen, THM; and the value of the incremental load applied, ALFA.

(2) Nodal coordinates, X(I), Y(I), I = 1, 2, ..., NUMNP.

(3) The element connectivity indices for each element (which are the system nodes belonging to an element) are read in an array NI(I,J), I = 1, 2, ..., NUMEL and J = 1, 2, 3. The ith row of this array contains the indices of the three system nodes that the ith element belongs to.

(4) Total number of constrained degrees-of-freedom, NCD.

(5) An array containing the constrained degree-of-freedom numbers, NCONS(I), I = 1, 2, ..., NCD.

With the aforementioned input data two arrays are

generated by the computer program, which are:

(1) Array IDOF(I,J), I = 1, 2, ..., NUMNP, and J = 1, 2; which stores the two degree-of-freedom numbers for each system node. It's Ith row contains the x- degree-of-freedom number in the first column and the y- degree-of-freedom number in the second column for the Ith system node.

(2) Array IBF(I), I = 1, 2, ..., 2 * NUMNP, the Ith row of which represents the boundary condition for the Ith system degree-of-freedom. A value of +1 is stored to denote a constrained degree-of-freedom and a value of -1 is stored to denote a free degree-of-freedom.

3.2.2 Stage II: Band Width Optimization

As the system stiffness matrix is symmetric and banded, only either the upper half band or the lower half band needs to be stored in a rectangular array. Thus, in order to reduce the dimensions of this array (i.e., reduce the number of columns in this array), a bandwidth optimization feature is kept in the program so as to increase its computational efficiency. In this stage, the input nodal degree-of-freedom numbers are rearranged so as to yield the minimum half bandwidth for the system stiffness matrix. It calls subroutines JSET, SETUP and

OPTNUM. These subroutines are described in the subsequent paragraphs.

Subroutine JSET: This subroutine computes the half bandwidth for the nodal numbering schemes of the input mesh. Specifically it performs the following functions:

(1) Forms an array, JT(I), I = 1, 2, ..., (5 * NUMEL) containing five rows for each element, in which it stores the element node numbers. The computer program has provisions to analyze a mesh containing three-noded and five-noded triangular elements. For three-noded elements in the vector (JT) zeros are inserted in the fourth and the fifth rows.

(2) Finds the difference between the highest and the lowest node numbers for each element using the above array, and then finds the maximum value of this node difference, IDIFF, for the whole mesh. The value of IDIFF is the optimum value of the half bandwidth for the input finite element mesh.

Subroutine SETUP: This subroutine formulates the arrays (JMEM) and (MEMJT), which are used in the subroutine OPTNUM. Specifically it performs the following functions:

(1) Initializes the arrays JMEM(J), J = 1, 2, ..., NUMNP, and MEMJT(I), I = 1, 2, ..., (12 *

NUMNP) to contain zeros.

(2) Starts the do loop for the elements.

(3) Finds the number of element edges coming to each system node and forms a vector (JMEM), in which the Jth row contains the number of element edges coming into the Jth system node.

(4) Forms a vector (MEMJT) which has 12 rows for each system node. In this program the maximum number of edges that can come into a node is considered to be 12. The elements of the vector (MEMJT) are generated as follows:

For any system node J it first reads the number in the Jth row of the vector (JMEM). Say this number is K. Then it reserves K rows, starting from (12 * (J-1) + 1) to (12 * (J-1) + K), and stores the node numbers of these K nodes associated to the Jth system node in the vector (MEMJT). If K < 12, then the remaining rows reserved for the Jth system node, i.e., (12 * (J-1) + K + 1)th to (12 * J)th rows are filled with zeros.

(5) Steps (3) and (4) are repeated till all the elements are covered.

Subroutine OPTNUM: This subroutine makes use of the bandwidth reduction procedure presented by Collins [8] to obtain the nodal numbering scheme which gives the minimum

half bandwidth for the input finite element mesh. Specifically it performs the following steps:

(1) Starts the do loop for all the nodes.

(2) Takes the node number 1 of the existing numbering system and numbers it as new node number 1.

(3) Using the vector (JMEM) it first finds the number of nodes coming to this system node (say it is K) and then gets these node numbers from the vector (MEMJT). These nodes are renumbered starting from 2 to (K + 1).

(4) It computes the half bandwidth, IBD, of this new numbering scheme from the following expression:

$$IBD = 2 * (IDIFF + 1) \qquad (3.1)$$

(5) If the half bandwidth with this numbering system is less than the previous half bandwidth, then all the nodes connected to the next higher node are renumbered. The process is continued with the next node in Step (2), and Steps (2) to (5) are repeated. But, if this half bandwidth is greater than the previous (for the old numbering), then this numbering scheme is abandoned and the analysis goes to Step (2), and Steps (2) to (5) are repeated for the next node.

(6) Steps (2) to (5) are repeated so that all the nodes are covered, and NUMNP nodal numbering schemes are obtained.

(7) The program then stores the nodal numbering scheme giving the minimum half bandwidth in an array JNT(I), I = 1, 2, ..., NUMNP, so that its Ith row denotes the new node numbers for the Ith node of the original numbering scheme.

3.2.2 Stage III: Application of the Incremental Load

In this stage subroutine LODING is called by the main program to assemble the system load vector. In the present version of the program, this stage is written to analyze a tension specimen subjected to uniformly distributed load acting on two opposite edges of the specimen. As only the quarter panel is considered, there is only one edge where the load is applied. In the present version of the program the loaded edge is the right side vertical edge, as shown in Fig. 4.2 of Chapter IV.

The subroutine LODING involves the following steps:

(1) Total number of loaded nodes, NNC, is computed, which includes all the nodes on the loaded edge.

(2) Total number of loaded element edges is computed as (NNC-1).

(3) Length of these loaded element edges are stored

in an array YL(I), I = 1, 2, ..., (NNC-1) using the following equation:

$$YL(I) = Y(IB) - Y(IA) \qquad (3.2)$$

where Y(IB) and Y(IA) are the y-coordinates of the first and the second node, respectively, belonging to the loaded edge.

(4) The rows of the total load, PL(I), I = 1, 2, ..., (NNC-1), belonging to the degrees-of-freedom of the nodes lying on the loaded edge I is computed as

$$PL(I) = ALFA * YL(I)/2 \qquad (3.3)$$

where ALFA is the increment of the total load applied, which is read as an input variable. To apply a unit load in the first cycle ALFA is set equal to 1 for this cycle.

(5) Using vector {PL} the nodal load "P", applied at a loaded node I, is computed as follows:

$$P = PL(I), \text{ for the first and the last node} \qquad (3.4)$$

$$P = PL(I) + PL(I-1), \text{ for all the other nodes} \qquad (3.5)$$

(6) The degrees-of-freedom along which these loads are are applied are extracted using the vectors {JNT} and {IDOF}, which have been described

earlier.

(7) Using this information the system load vector BF(I), I = 1, 2, ..., NDOF is assembled, where NDOF is total number of degrees-of-freedom, which is computed as

$$NDOF = 2 * NUMNP \qquad (3.6)$$

The Ith row of the vector {BF} denotes the load applied at the Ith system degree-of-freedom.

In case the applied loading consists of concentrated loads acting at some nodes, then the following changes have to be made:

(1) All the loads are normalized with respect to the largest concentrated nodal load (denoted as PNMAX) acting on the system. The normalized concentrated nodal loads are stored in an array PNOD(I), I = 1, 2, ..., NNC, where NNC is the total number of loaded nodes.

(2) The system load vector {BF} is assembled by applying these normalized concentrated nodal loads at their respective system degrees-of-freedom such that at the Jth degree-of-freedom, belonging to Ith loaded node, the load applied is given by

$$BF(J) = ALFA * PNMAX * PNOD(I) \qquad (3.7)$$

where ALFA is the load increment, as described earlier (ALFA = 1 for the first load cycle).

3.2.4 Stage IV: Computation of the Element Stiffness Matrices and Assembly of the System Stiffness Matrix

This stage calls subroutines CYCLE, CYCLE1 and TRIAN3. It involves the following steps:

(1) It first finds the total number of degrees-of-freedom, MDF, for each element and then constructs a vector MID(I), I = 1, 2, ..., MDF, which contains the indices of these degree-of-freedom numbers. This step is accomplished in subroutine CYCLE or CYCLE1 in the first load analysis cycle and in subroutine EDOF in the later load analysis cycles.

(2) The element stiffness matrix, [EK], is then computed by calling subroutine TRIAN3 for each element.

(3) The system stiffness matrix, [A], is finally assembled. This step is accomplished in subroutine CYCLE or CYCLE1.

The subroutines involved in this stage are described in the subsequent paragraphs.

Subroutine CYCLE1: The main function of this subroutine is to assemble the system stiffness matrix. Specifically, it performs the following steps:

(1) It formulates the vector {MID} containing the indices of the nodal degree-of-freedom numbers for each element. For the first load cycle it writes the contents of this vector on the direct access file IO1, and in later load cycles it reads it from this direct access file.

(2) It next formulates the element stiffness matrix for each element. In the first load cycle the element stiffness matrices are computed by calling the subroutine TRIAN3 and are written on the direct access file IO1 and in later load cycles it reads them from this direct access file.

(3) The system stiffness matrix, [A], is assembled using the element stiffness matrices, [EK]'s, and the element degrees-of-freedom vector, {MID}.

Subroutine TRIAN3: This subroutine computes the following elemental quantities:

(1) The element elasticity material matrix, $[D^{e}]$, using Eqs. (2.7) and (2.11) of Chapter II for plane stress and plane strain problems, respectively, if the element is an elastic element, or the element elasto-plasticity material matrix, $[D^{eP}]$, using Eqs. (2.97) and (2.99) of

Chapter II, for plane stress and plane strain problems, respectively, if the element has yielded.

(2) The element stiffness matrix, EK(I,J), I = 1, 2, ..., MDF; J = 1, 2, ..., MDF, using the results of Eqs. (2.101) and (2.102) of Chapter II for elastic and yielded elements, respectively.

(3) The element strain-displacement transformation matrix, [BB], as given by Eq. (2.32) of Chapter II.

(4) The element stress-displacement transformation matrix, [DB], which is computed as

$$[DB] = [D]\,[BB] \tag{3.8}$$

where [D] and [BB] are computed in Steps (1) and (3), respectively.

After the execution of this subroutine four records are formed on the direct access file IO1, which are in the following order:

(1) MM, MDF, MID(I), I = 1, 2, ..., MDF, where MM is the element number and other variables have been defined earlier.

(2) EK(I,J), I = 1, 2, ..., MDF and J = 1, 2, ... MDF.

(3) DB(I,J), I = 1, 2, 3 and J = 1, 2, ..., MDF.

(4) BB(I,J), I = 1, 2, 3 and J = 1, 2, ..., MDF.

Subroutine CYCLE: This subroutine performs the same function as subroutine CYCLE1, but it is called by the main program when the total degrees-of-freedom are greater than 2000 and/or when NBD is greater than 200, where

$$NBD = 3 * (IDIFF + 1) \tag{3.9}$$

It uses an out-of-core storage to increase the computer efficiency. Specifically, it performs the following steps:

(1) It divides the system stiffness matrix into a number of blocks. Each block is a square matrix of size (NBD x NBD). The total number of blocks, NBL, is computed from

$$NBL = 1 + (NDOF - 1)/NBD \tag{3.10}$$

(2) As the system stiffness matrix is originally banded and symmetric, therefore, only 2 * NBD equations (i.e., two blocks) are needed at one time in the main computer core memory to perform the Gauss elimination procedure for one block. Also, some of the element stiffness matrices will be assembled into the rows and columns belonging to two consecutive blocks. Thus, at any instance two blocks are needed to be in-core, both during the assembly and the

solution phases. The first block would contain elements having degree-of-freedom numbers any where between 1 to NBD, and the second block would contain elements having degree-of-freedom numbers from (NBD + 1) to (2 * NBD).

(3) As soon as all the element stiffness matrices belonging to the first block have been assembled, then that block is stored in a sequential file IO2, and the second block is brought up in the place of the first block. Subsequently, the place of the second block is filled by bringing-up the next block in line.

(4) This procedure is repeated until all the blocks have been covered.

3.2.5 Step V: Solution for System Displacements

This stage calls either the subroutine SOLVE or the subroutine SOLVE1, depending on the total number of degrees-of-freedom and the value of NBD. The functions of these subroutines are described next.

Subroutine SOLVE1: This subroutine is called when the computer in-core storage memory is used. Its purpose is to solve the system stiffness equilibrium equation, Eq. (2.49) of Chapter II. Specifically, it performs the following steps:

(1) It modifies the symmetric and banded system

stiffness equilibrium equation to an upper triangular form using the Gauss elimination procedure.

(2) It then computes the unknown displacement vector, B(I), I = 1, 2, ..., NDOF by back substitution procedure.

Subroutine SOLVE: This subroutine is called when the total degrees-of-freedom of the system are greater than 2000 and/or the value of NBD is greater than 200. It uses the system stiffness matrix formulated by the subroutine CYCLE to solve the system stiffness equilibrium equations. Specifically, it performs the following functions:

(1) It uses two blocks of equations at a time by bring them in-core, and then triangularizes them to an upper triangular form using the Gauss elimination procedure.

(2) After the first block has been completely triangularized it is written back to the out-of-core file. Then the second block is made to take the position of the first block and the next block is read-in in its place.

(3) Steps (1) to (2) are repeated until all the blocks are triangularized.

(4) Nodal displacements (the solution vector) are computed by back substitution procedure by

bringing in the last two blocks in-core and first solving for all the nodal displacements belonging to the last block. Then the second-last block is shifted up to occupy the place of the first block and the third-last block is brought in-core as the second block. The procedure is continued till all nodal displacements have been computed.

3.2.6 Stage VI: Computation of Element Stress Components, Total Load and Checking for Failure

Subroutine PLASFL is called by the main program to compute the element stress components. This subroutine calls subroutines STRES and subroutine CHECK. Specifically, the subroutine PLASFL performs the following steps:

(1) It reads the element degree-of-freedom numbers from the direct access file IO1 and using these the element nodal displacement vector, EF(I), I = 1, 2, ..., MDF, is extracted out from the system displacement vector, {B}.

(2) It then calls subroutine STRES to compute the element incremental strain components vector, {STRANE}, and the element stress components vector, {SIGMA}, using the following equations, respectively:

$$\{STRANE\} = [BB]\{EF\} \qquad (3.11)$$

$$\{SIGMA\} = [DB]\{EF\} \qquad (3.12)$$

where [BB] is the element strain-displacement transformation matrix and [DB] is the element stress-displacement transformation matrix. These have been read from the direct access file IO1 in Step (1).

(3) The incremental stresses are computed and stored in an array SEL(I,J), I = 1, 2, ..., NUMEL and J = 1, 2, 3, 4. In this array the element incremental stress components, $\Delta\sigma_x$, $\Delta\sigma_y$ and $\Delta\tau_{xy}$ for the element I are stored in its first three columns, respectively, whereas, in the fourth column the incremental stress, $\Delta\bar{\sigma}''$, of the element is stored, which is computed using Eq. (2.109) of Chapter II.

(4) (a) For the first load cycle the factor YLOAD is computed using the following expression:

$$YLOAD = \frac{SO}{SEL(N,4)} \qquad (3.13)$$

where SO is the material yield stress (denoted as F_y in Chapter II, but denoted as SO in the computer program) and N is the element number.

(b) Steps (1) to (4) are repeated for all the elements and the minimum value of YLOAD for the finite element mesh is computed and stored as XLOAD. The element number having this value of the load is also stored as NYEL. So, XLOAD is the incremental load for the first cycle, which causes the element number NYEL to yield.

(c) All the element stresses are scaled by multiplying the element stress components, computed in Step (3) by XLOAD. The stress components of each element are stored in an array ST(N,I), N = 1, 2, ..., NUMEL, and I = 1, 2, 3, 4. The configuration of this array is the same as the array {SEL}, defined earlier. Thus, matrix [ST] contains the total (cumulative) stress components for all the elements and also their effective stress in the last column.

(d) Now the most stressed element (number = NYEL) is made to yield by making its effective stress, ST(NYEL, 4), equal to the material yield stress, SO, and its number is stored in an array NPL(J), J = 1, 2, ..., NYE, where NYE is total number of yielded elements. So, the vector {NPL}

contains the element numbers of the yielded elements.

(e) The incremental load which causes the most stressed element of the previous step to yield is now computed. As the load applied for the first load cycle is unity, so XLOAD is the incremental load, XP, i.e.,

$$XP = XLOAD \tag{3.14}$$

(f) The total load, PLOAD, is computed at the end of the current load cycle from

$$PLOAD = PLOAD + XP \tag{3.15}$$

where PLOAD is set equal to zero at the start of the program.

(g) The value of the total load, PLOAD, is printed and the program execution returns back to the main program.

(5) For later load cycles Steps (1) to (3) are repeated for all the elements. Then the program execution proceeds to the next step.

(6) For all the elastic elements the value of RMIN is computed by using Eq. (2.115) of Chapter II. The variable 'r' of this equation is called as RMIN in the computer program.

(7) The minimum of all the RMIN values is found for the finite element mesh and is stored as XLOAD. The element number of the element having this value of the load is also stored as NYEL, the most-stressed element.

(8) The element incremental stress components (computed in Step (3)) for this load cycle are multiplied by XLOAD and the results added to the appropriate rows of the previously computed total stress matrix, [ST].

(9) The total effective stress for each element, $\bar{\sigma}$, is computed by substituting the total stress components computed in Step (8), into Eq. (2.57) of Chapter II. This value is stored in the appropriate row of the fourth column of the matrix [ST].

(10) The most stressed element found in Step (7) is made to yield by setting its effective stress equal to the material yield stress, SO. The element number of this element is also stored (or added) in the vector (NPL). Also based on values of the element effective stress computed in Step (9), all elastic elements whose effective stress is greater than or equal to 0.995 * SO are made to yield together by setting their respective effective stresses equal to the ma-

terial yield stress, SO.

(11) The incremental load, which had caused the most stressed element in Step (7) to yield in this load cycle, is next computed from the following equation:

$$XP = XLOAD * ALFA \tag{3.16}$$

where ALFA is the applied load increment, which has been read-in as input (see Section 3.2.1). Finally, the total load at the end of the current load cycle is computed by updating PLOAD in Eq. (3.15).

(12) To check whether failure has occurred or not, subroutine CHECK is called to compute the value of $\Delta\bar{\varepsilon}_p$ for all the yielded elements (given by Eqs. (2.116) and (2.117) of Chapter II for plane stress and plane strain problems, respectively). The variable $\Delta\bar{\varepsilon}_p$ is coded as 'EP' in the computer program. If, for any element the value of EP is negative then the value of PLOAD is printed as the "failure load" and the execution of the program is stopped. If EP is positive then the execution of the program returns to the main program for the application of the next load increment, ALFA, and the whole analysis is repeated for the next incremental load.

3.3 FLOWCHARTS OF THE MAIN PROGRAM AND THE SUBROUTINES FOR PROGRAM PLASFL

In this section the flowcharts of the main program and some of the important subroutines are presented. The flowchart of the main program is shown in Fig. 3.2. The flowcharts of the subroutines PLASFL, TRIAN3, CYCLE1 and LODING are shown in Figs. 3.3, 3.4, 3.5 and 3.6, respectively. These and other subroutines have been described earlier in Section 3.2.

3.4 GENERAL FEATURES OF THE PROGRAM CRACK

As mentioned in Section 3.1, the computer program CRACK is an extension of the first computer program, PLAST, so as to solve fracture mechanics problems for ultimate fracture failure load. It is divided into six main stages, as shown in Fig. 3.7. These stages are described in the subsequent sub-sections.

3.4.1 Stage I: Input and Setting-Up

This stage is the same as Stage I of the computer program PLAST as far as reading of the input mesh information is concerned. After reading of the data, in addition to the information set-up, as described in Section 3.2.1, the following variables are also generated:

(1) IRANGE: This is a flag which is initially set equal to zero for all the elements. Later as the total effective stress for any yielded ele-

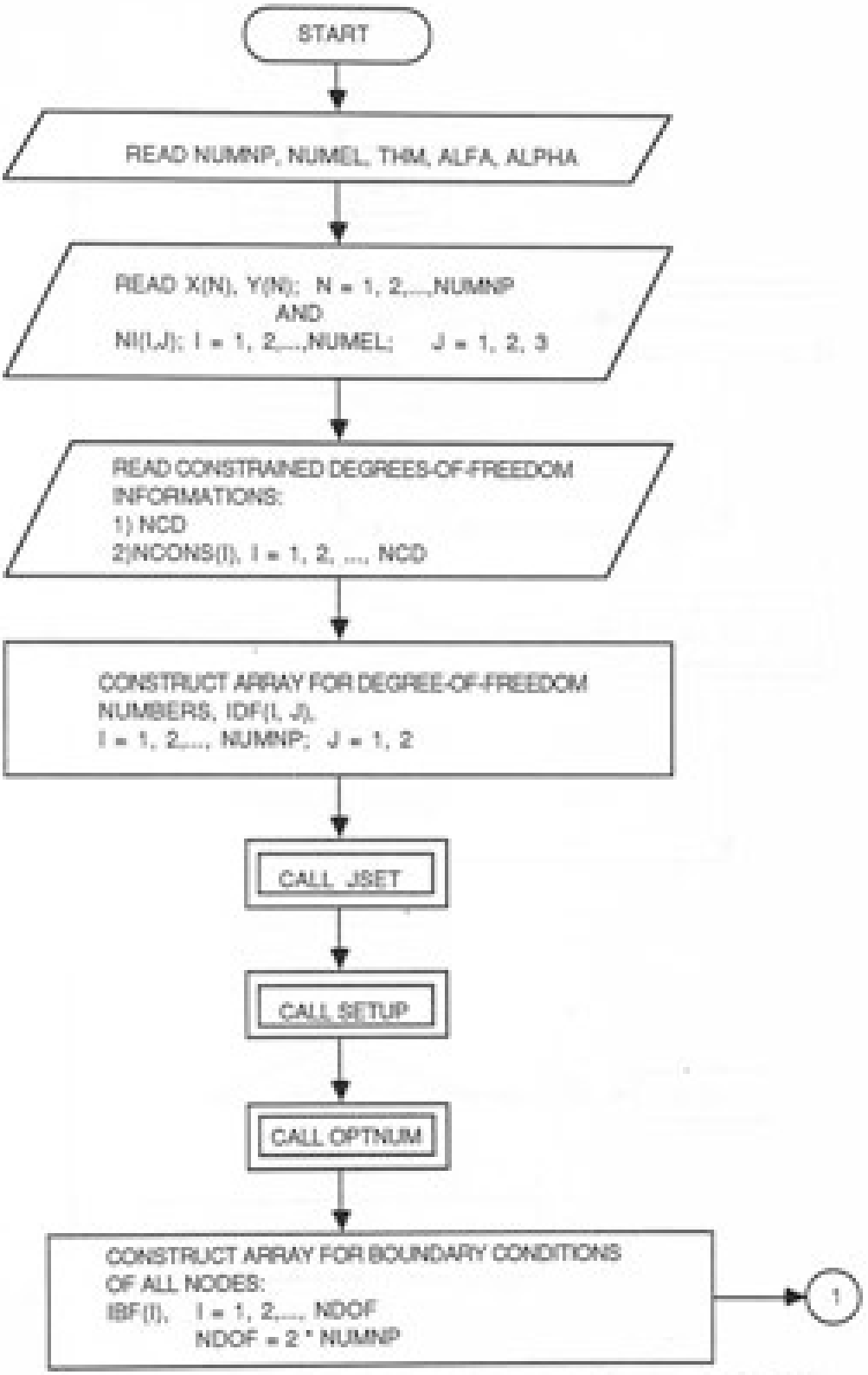

Fig. 3.2 Flowchart of the Main Program PLAST

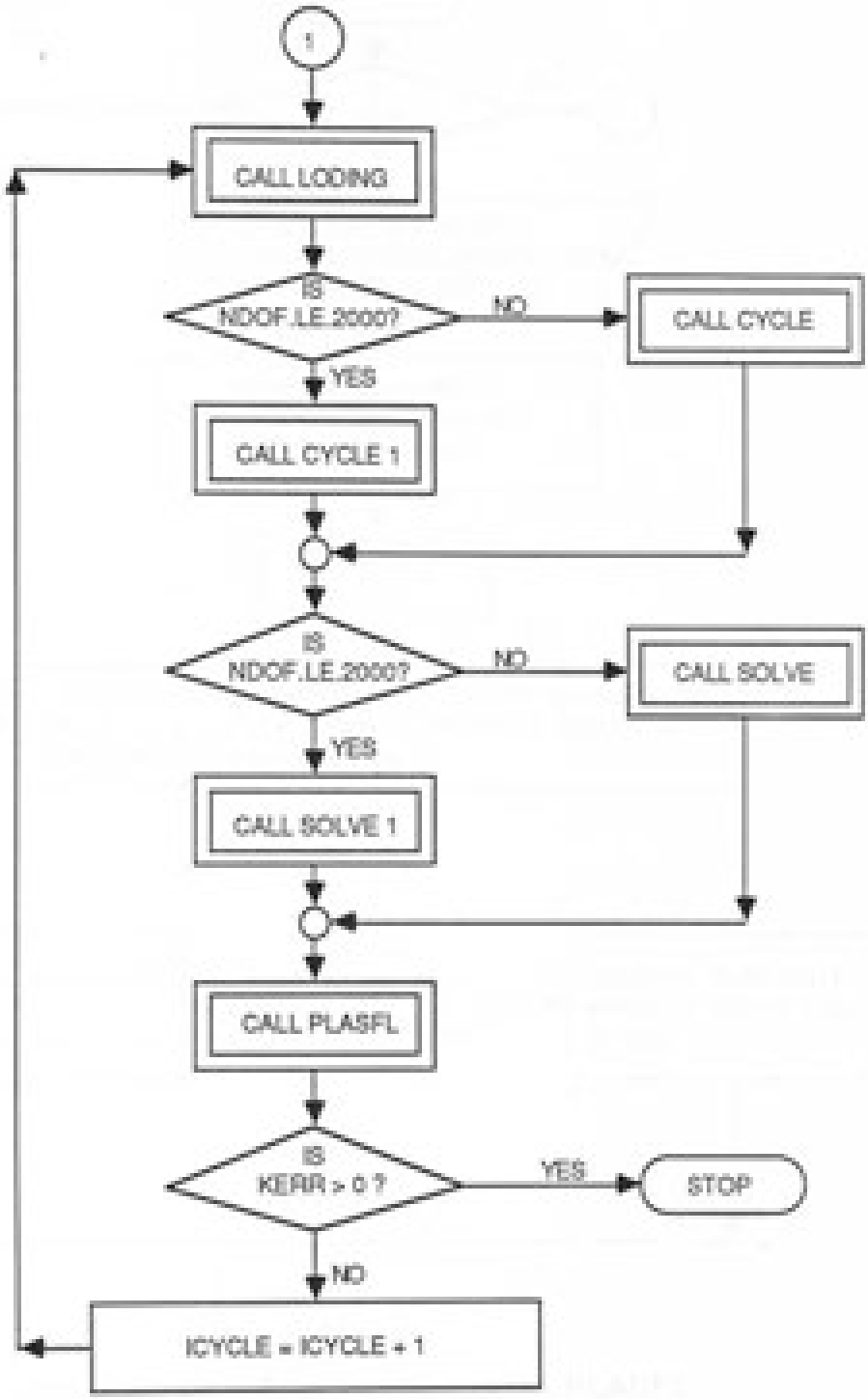

Fig. 3.2 (Cont'd) Flowchart of the Main Program PLAST

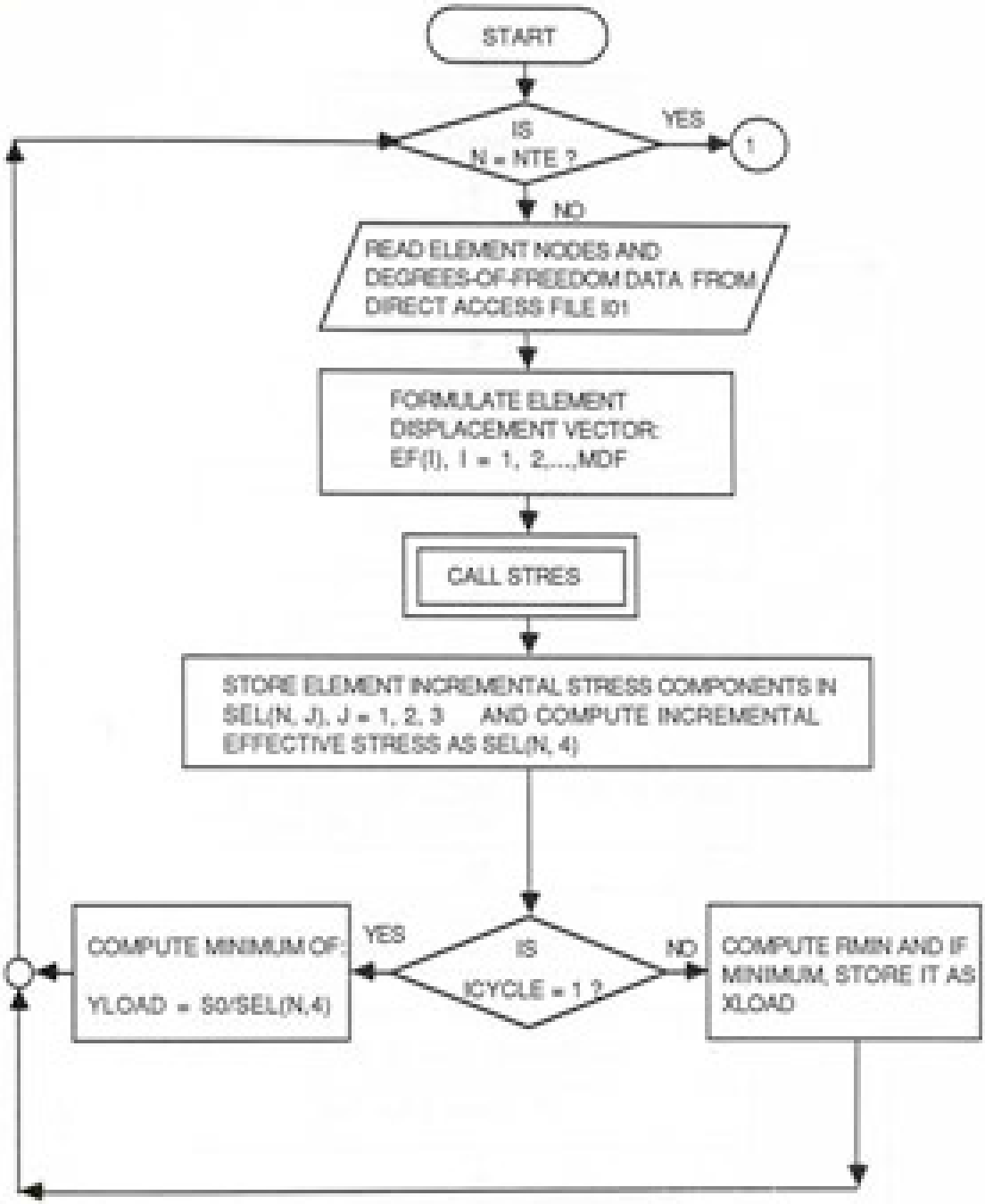

Fig. 3.3 Flowchart of Subroutine PLASFL

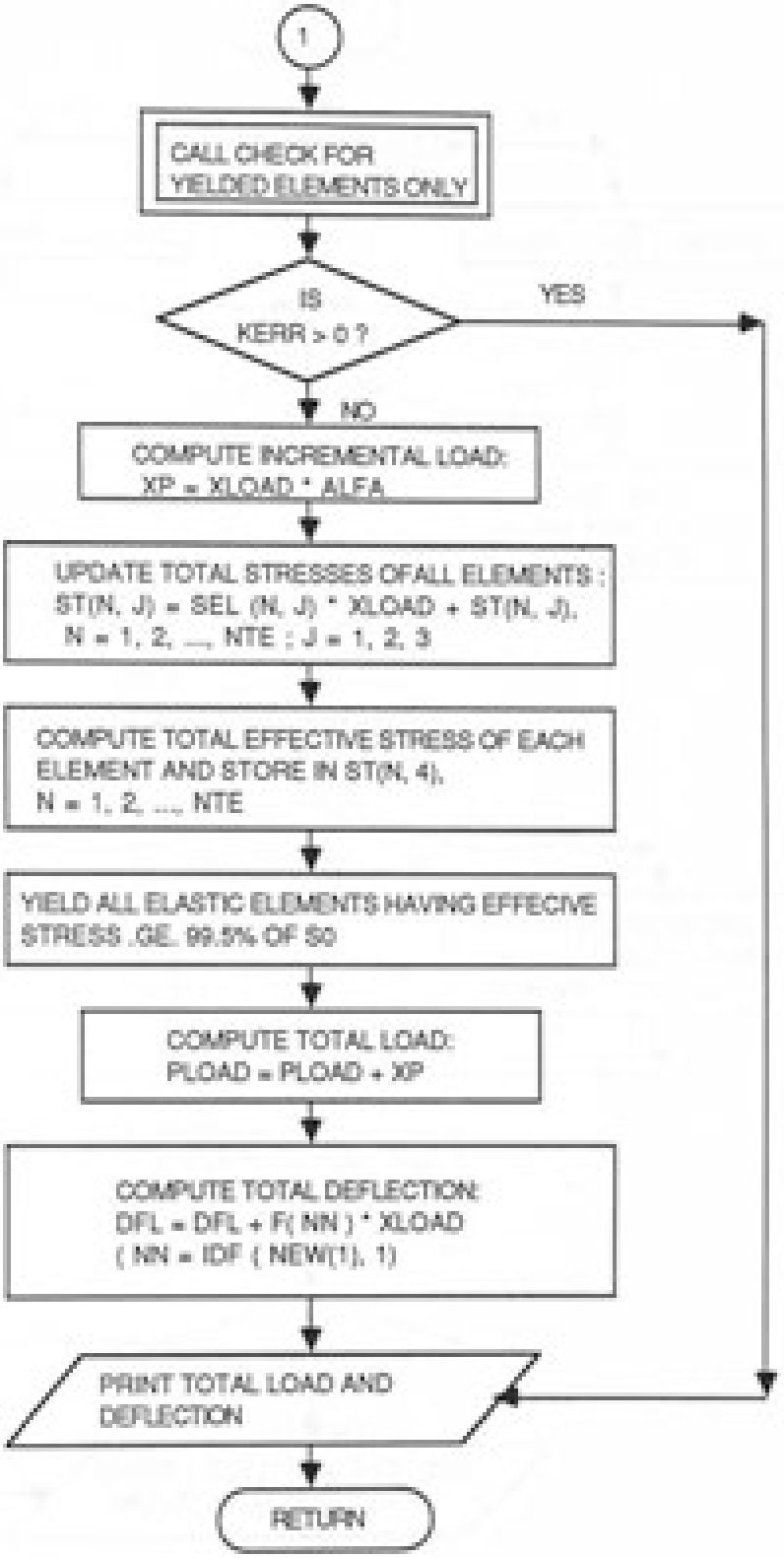

Fig.3.3(Cont'd) Flowchart of Subroutine PLASFL

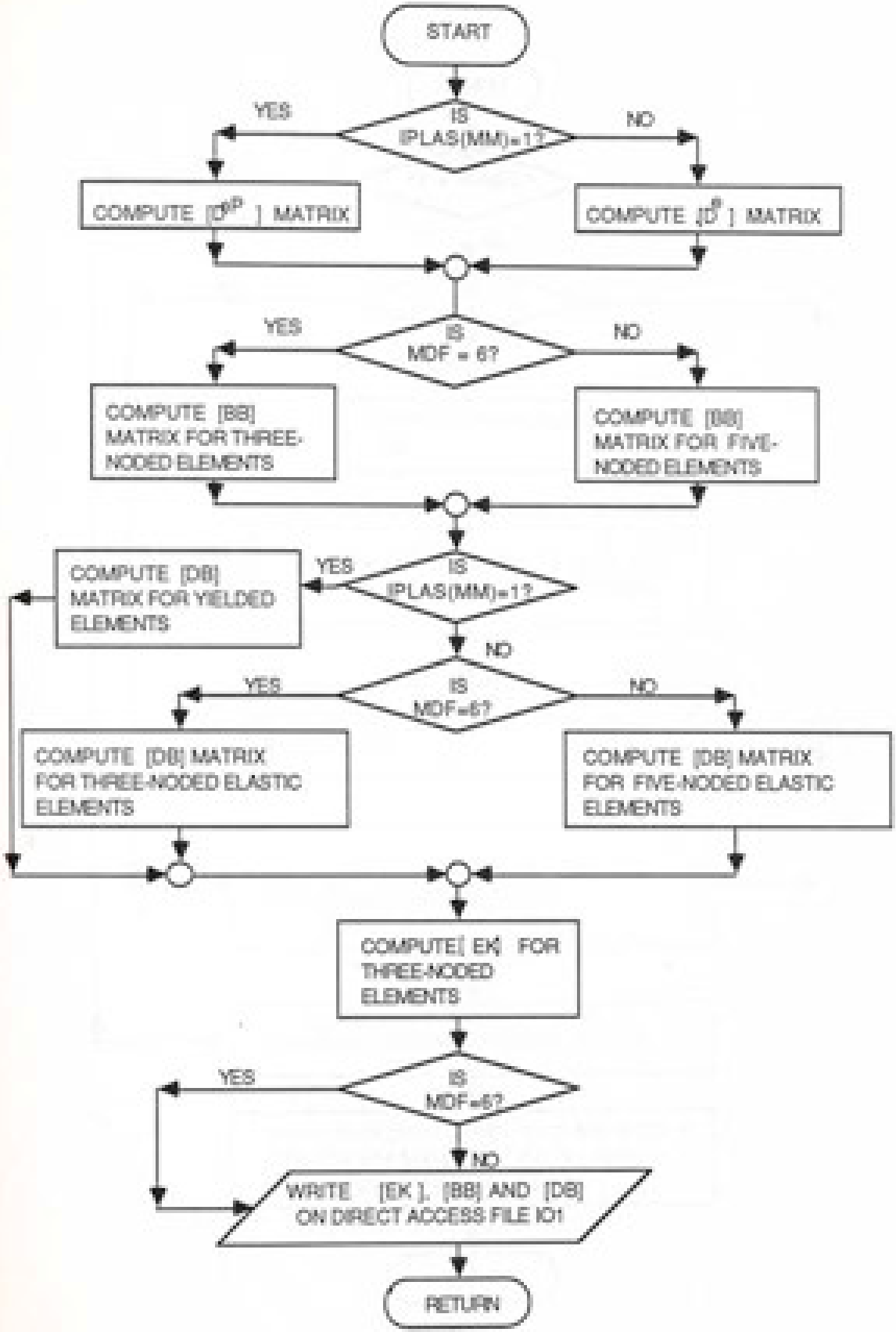

Fig. 3.4 Flowchart of Subroutine TRIAN3

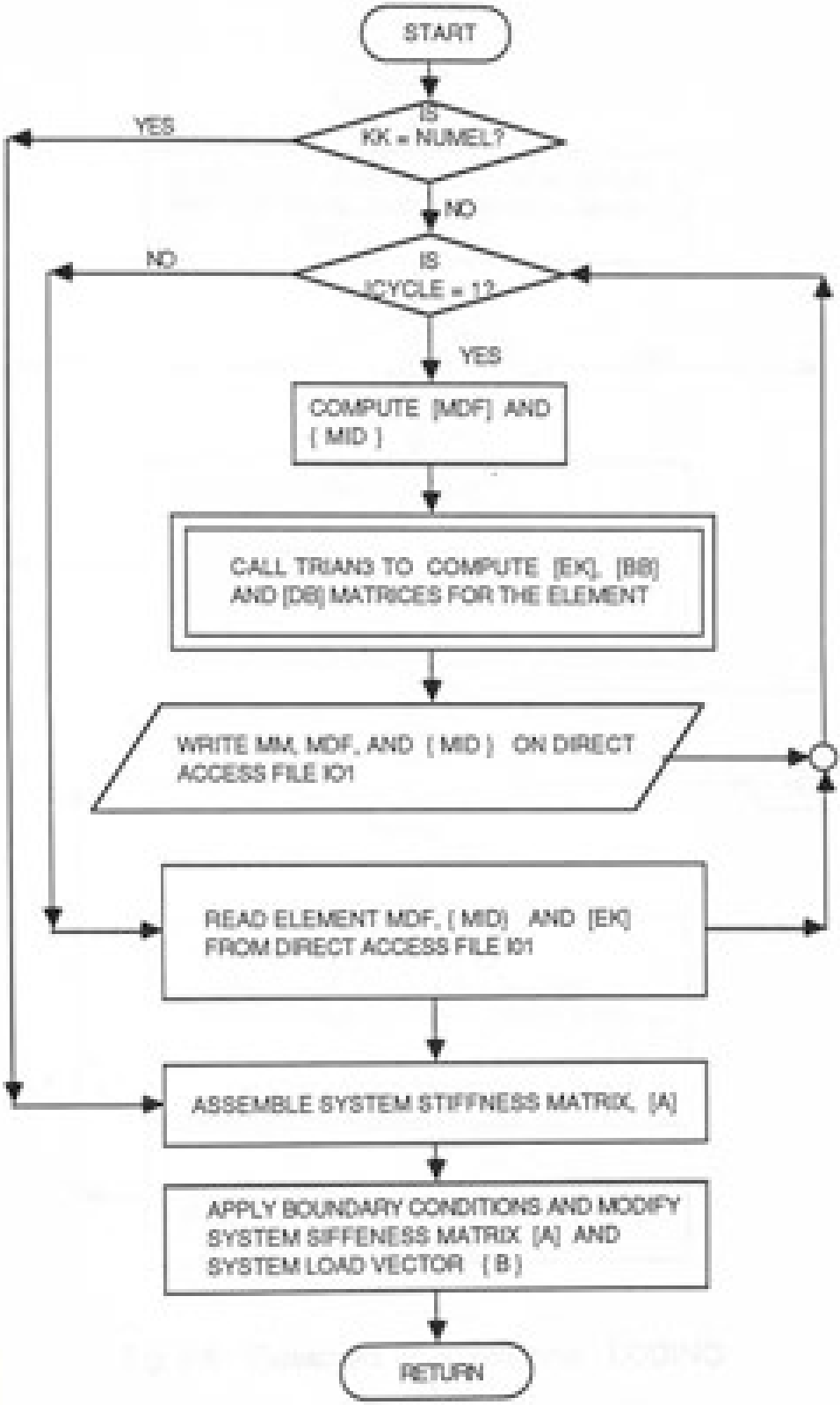

Fig. 3.5 Flowchart of Subroutine CYCLE1

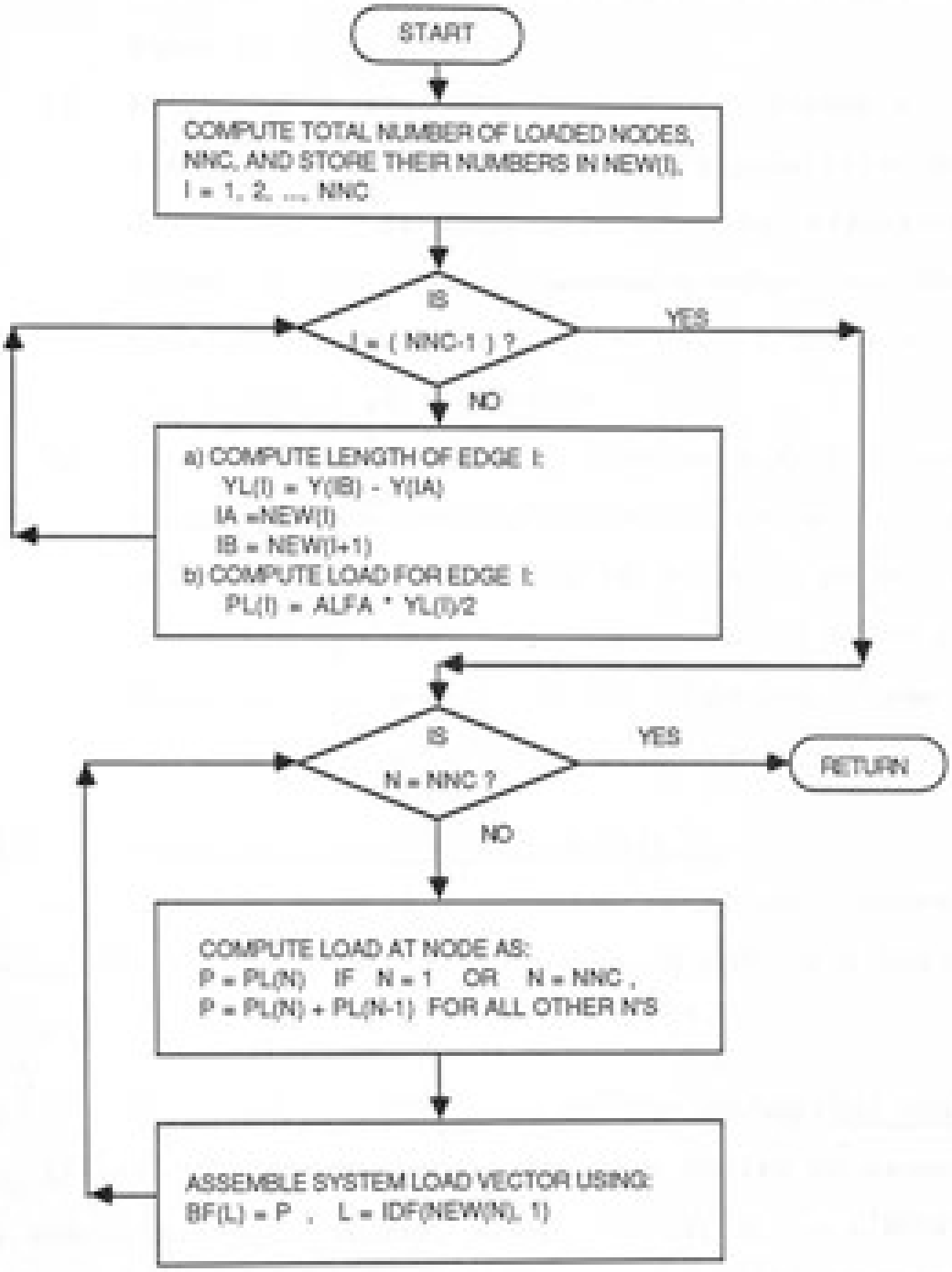

Fig. 3.6 Flowchart of Subroutine LODING

ment exceeds 86% (value arbitraily fixed) of the material fracture stress then IRANGE is set equal to 1.

(2) KPREV: This variable is used when IRANGE = 1. KPREV = 1 indicates that the analysis is to be discarded. This happens if the total effective stress of any element becomes greater than the material fracture stress. KPREV = 0 means that the analysis is acceptable.

(3) LOOPF: This variable is used as a flag to indicate if the redistribution of the energy of the fractured element is in process, which is indicated by LOOPF = 1, otherwise LOOPF = 0. Thus, if the energy of the fractured element has been completely dissipated then LOOPF = 0.

3.4.2 Stage II: Bandwidth Optimization

This stage is the same as Stage II of the computer program PLAST (see Fig. 3.1), as described in Section 3.2.2.

3.4.3 Stage III: Application of the Incremental Load

In this stage Subroutine LODING is called to assemble the system load vector, BF(I), I = 1, 2, ..., NDOF. Until the fracture of any element occurs, the analysis procedure follows Steps (1) to (7) of Section 3.2.3.

When an element fractures, its energy has to be re-

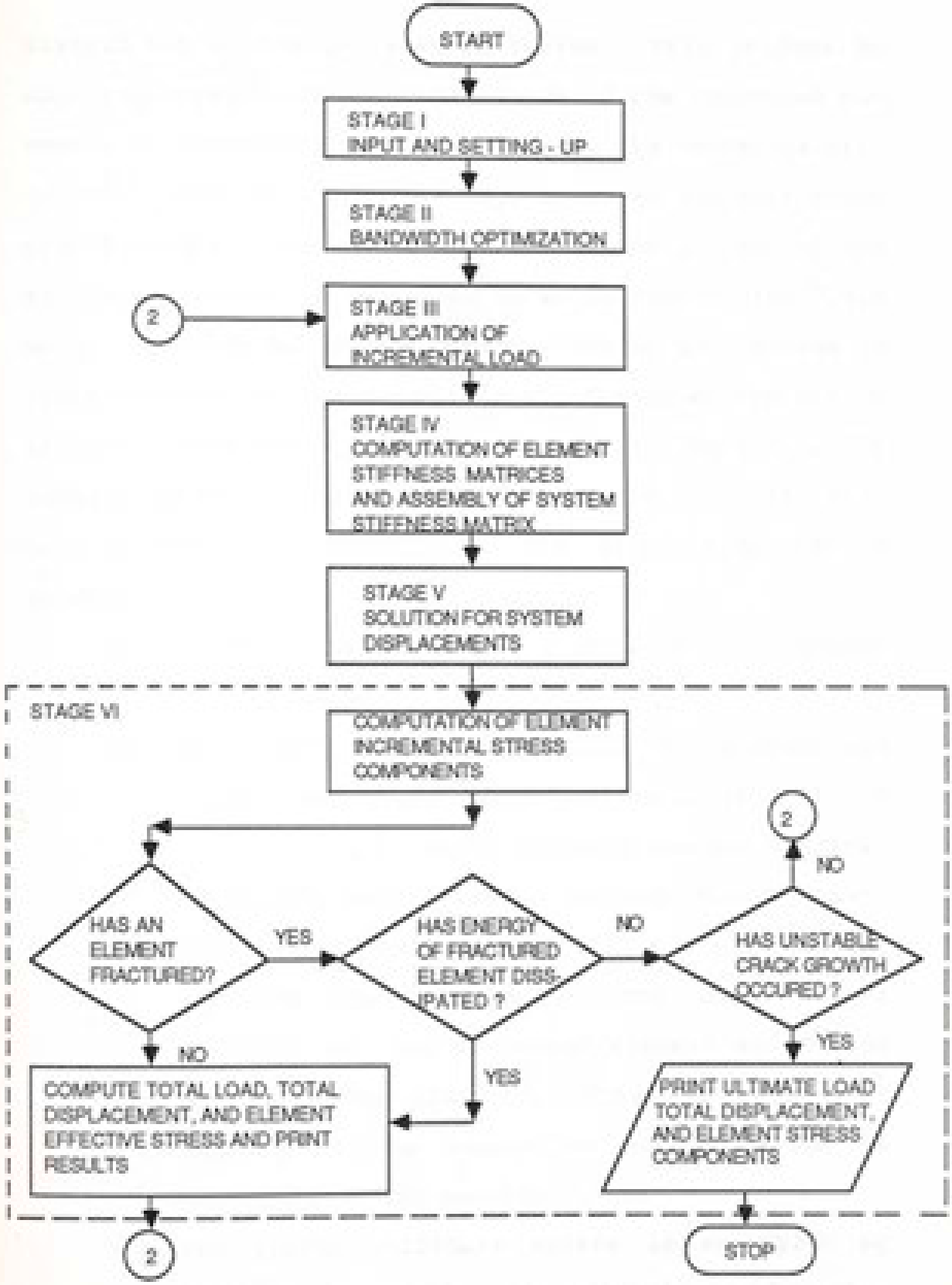

Fig. 3.7 Main Stages Of the Computer Program CRACK

distributed to the unfractured system. This is done by applying negative of the nodal loads of the fractured element, in increments, until either all the energy is distributed into the unfractured system or an unstable crack growth occurs. The computation of the nodal loads of the fractured element is explained later in Sub-section 3.4.6 under the title Subroutine NODFOR. During the process of redistribution of the energy of the fractured element no external loads are applied to the system. The flag LOOPF remains equal to 1 until the energy of the fractured element is completely dissipated. The procedure adopted is as follows:

(1) LOOPF is set equal to 1 in subroutine NODFOR when an element fractures.

(2) The system degrees-of-freedom of the fractured element are found using the vector IFDOF(I), I = 1, 2, ..., 6, which contains the six degrees-of-freedom pertaining to the fractured element.

(3) The system load vector, {BF}, is assembled by applying the negative of the nodal forces computed for the fractured element and stored as the vector {PAPPLY}. This vector is formulated in the subroutine NODFOR, which is described in Sub-section 3.4.6.

(4) The system stiffness matrix is assembled by calling either subroutine CYCLE1 or subroutine

CYCLE depending on the size of the system stiffness matrix, which is assembled with the fractured element removed.

(5) Steps (1) to (4) are repeated until all the energy of the fractured element is redistributed into the unfractured system and then LOOPF is again set equal to zero in subroutine NODFOR.

3.4.4 Stage IV: Computation of the Element Stiffness Matrices and Assembly of the System Stiffness Matrix

This stage performs the same functions as described in the Section 3.2.4. The main changes are summarized as follows:

(1) Since an incremental approach is used to march along the uniaxial stress-strain curve of the material till fracture occurs, there is a likelihood that at a certain incremental load step an element's effective stress may become greater than the material fracture stress. The results of this analysis have to be discarded and this analysis has to be repeated with a smaller value of the assumed incremental load. The check for this situation is made in every load cycle after the flag IRANGE (described in Section 3.4.1) becomes equal to 1.

(2) In every load cycle after IRANGE = 1 all the

element records formed in subroutine TRIAN3 are copied on a scratch file named IO3.

(3) If the effective stress of any element is not greater than the material fracture stress then the records of such elements are copied on the file IO1 (described in Sub-section 3.2.4), and the analysis is continued for the next load increment. But, if the effective stress of any element becomes greater than the material fracture stress then the results (and also the element records in IO3) are discarded. The load increment, ALFA, is reduced to half of the current value and the analysis is repeated using the previous element stiffness matrices records in file IO1. This process is continued till the effective stress of the most stressed yielded element is within 0.995 * SIGMAF $\leq$ SIGMAF $\leq$ 1.005 * SIGMAF, where SIGMAF is the material fracture stress. This algorithm is implemented in the subroutine PLASFL (described in Sub-section 3.4.6).

(4) If an element fractures, its stiffness matrix should not be assembled into the system stiffness matrix. This is accomplished by making use of a vector IFRACT(I), I = 1, 2, ..., NFRACT, where NFRACT is total number of frac-

tured elements and contains the element numbers of the fractured elements. This vector is formed in the subroutine PLASFL (described in Sub-section 3.4.6).

3.4.5 Stage V: Solution for System Displacements

This stage is the same as Stage V of the computer program PLAST, which was described in Sub-section 3.2.5.

3.4.6. Stage VI: Computation of Element Stress Components, Check for Element Fracture, Redistribution of Energy of Fractured Element, and Computation of Total Load

Subroutine PLASFL is called by the main program to compute the element stress components, to check for fracture of an element, to redistribute the energy of the fractured element, and to compute the total load. This subroutine calls subroutines STRES, FRCTUR, NODFOR and UPDAT. Specifically, the subroutine PLASFL performs the following functions:

Subroutine PLASFL:

(1) It reads the element degree-of-freedom numbers from the direct access file IO1 and using these the element nodal displacement vector, EF(I), I = 1, 2, ..., MDF, is extracted out from the system displacement vector, {B}.

(2) It then calls subroutine STRES to compute the element incremental strain components vector,

{STRANE}, and the element stress components vector, {SIGMA}, using the following equations, respectively,

$$\{STRANE\} = [BB]\{EF\} \tag{3.17}$$

$$\{SIGMA\} = [DB]\{EF\} \tag{3.18}$$

where [BB] is the element strain-displacement transformation matrix and [DB] is the element stress-displacement transformation matrix. These have been read from the direct access file IO1 in Step (1).

(3) The incremental stresses are computed and stored in an array SEL(I,J), I = 1, 2, ..., NUMEL and J = 1, 2, 3, 4. In this array the element incremental stress components, $\Delta\sigma_x$, $\Delta\sigma_y$ and $\Delta\tau_{xy}$, for the element I are stored in its first three columns, respectively, whereas, in the fourth column the incremental stress, $\Delta\bar{\sigma}''$, of the element is stored, which is computed using Eq. (2.109) of Chapter IV.

(4) (a) For the first load cycle the factor, YLOAD, is computed using the following expression:

$$YLOAD = \frac{SO}{SEL(N,4)} \tag{3.19}$$

where SO is the material yield stress and N is the element number.

(b) Steps (1) to (4) are repeated for all the elements and the minimum value of YLOAD for the finite element mesh is computed and stored as XLOAD. The element number having this value of the load is also stored as NYEL. So XLOAD is the incremental load which causes the element number NYEL to yield in the first cycle.

(c) All the element stresses are scaled by multiplying the element stress components computed in Step (3) by XLOAD. The element stress components are stored in an array ST(N,I), N = 1, 2, ..., NUMEL and I = 1, 2, 3, 4. The configuration of this array is the same as the array {SEL} defined earlier. Thus, matrix [ST] contains the total (cumulative) stress components for all the elements and also their effective stress in the last column.

(d) Now, the most stressed element (number = NYEL) is made to yield by making its effective stress, ST(NYEL, 4), equal to the material yield stress, SO, and its number is stored in an array NPL(J), J =

1, 2, ..., NYE, where NYE is total number of yielded elements. So the vector (NPL) contains the element numbers of the yielded elements.

(e) The incremental load which causes the most stressed element of the previous step to yield is now computed. As the load applied for the first load cycle is unity, so XLOAD is the incremental load, XP, i.e.,

$$XP = XLOAD \tag{3.20}$$

(f) The total load, PLOAD, is computed at the end of the current load cycle from

$$PLOAD = PLOAD + XP \tag{3.21}$$

where PLOAD is set equal to zero at the start of the program.

(g) The value of the total load, PLOAD, is printed and the program execution returns back to the main program.

(5) For later load cycles Steps (1) to (3) are repeated for all the elements. If LOOPF = 1 then the execution of the computer program goes to Step (8), otherwise, it goes to the next step.

(6) For all the elastic elements the value of RMIN is computed (given as r in Eq. (2.115) of Chapter II).

(7) The minimum of all the RMIN values is found and stored as XLOAD. The element number of the element having this value is stored as NYEL, which is the element number of the most stressed elastic element.

(8) Steps (1) to (7) are repeated for all the elements. Then the incremental load for this load cycle is computed from

$$XP = XLOAD * ALFA \tag{3.22}$$

if LOOPF = 1. Then subroutine NODFOR is called and the execution of the computer program returns to the main program, otherwise, it goes to the next step.

(9) If IRANGE = 1 the computer program execution goes to the next step, otherwise, it goes to Step (15).

(10) The total stress components for each element are computed and stored in a scratch array, [STF], which is obtained from

$$STF(N,J) = SEL(N,J) + ST(N,J) \tag{3.23}$$

where N is the element number and J = 1, 2, 3.

(11) The total effective stress of each element is computed using the stress values in the array [STF] and Eq. (2.57) of Chapter II. The effective stress of each element is stored in the fourth column of the array [STF]. The row number in this array corresponds to the element number.

(12) The number of the element having the maximum value in the fourth column of the array [STF] is found and stored as NYEL, which is the most stressed element. Then the subroutine FRCTUR is called to perform the following checks:

(a) If STF(NMOST,4) is within ± 0.5% of the material fracture stress, SIGMAF, then the element number, NMOST, is considered as a fractured element and KERR is set equal to 1.

(b) If STF(NMOST, 4) > SIGMAF the results of this run have to be discarded and the analysis has to be repeated using the previous element stiffness matrices (stored in file IO1), and setting the value of the incremental load applied, ALPHA, to ALFA/2 and the flag KPREV = 1.

(c) If STF(NMOST, 4) < SIGMAF then the results of this run are acceptable and the flag

KPREV is set equal to zero.

(13) If Step (12a) is true, i.e., an element has fractured, then the program execution goes to Step (14). If Step (12b) is true then the computer program execution is returned to the main program. If Step (12c) is true then the computer program execution goes to Step (15).

(14) (a) The element number of the fractured element is stored in the array IFRACT(I), I = 1, 2, ..., NFRACT, where NFRACT is the total number of fractured elements.

(b) The degrees-of-freedom of the latest fractured element are stored in the array IFDOF(I), I = 1, 2, ..., 6.

(c) The nodal forces of the fractured element are computed by calling subroutine NODFOR, which is described later in this section.

(15) The element incremental stress components (stored in the first three columns of the matrix [SEL]) and the corresponding incremental effective stress (computed in Step (3) for this load cycle) for all the elements are multiplied by XLOAD. Then these are then added to the appropriate rows of the previously computed total stress matrix, [ST]. This step is done for all the elements except the fractured

elements.

(16) The most stressed elastic element and all the elastic elements having their total element effective stress greater than or equal to 0.995 * SO are made to yield together by setting their effective stress equal to the material yield stress, SO.

(17) If IRANGE is not equal to 1 then the execution of the program goes to Step (18), otherwise, the element having the maximum value of the total effective stress (computed in Step (16)) is located and the following are checked for it:

(a) If SIGEFF $\geq$ SIGMAF then a message to choose a lower load increment is printed and the program execution is terminated.

(b) If SIGEFF $\geq$ (86%) * SIGMAF then IRANGE is set equal to one and the computer program execution goes to Step (18).

(18) If LOOPF $\neq$1 then the computer program execution goes to the next step, otherwise, it returns to the main program.

(19) The total load is computed by updating PLOAD in Eq. (3.21) and the computer program execution returns to the main program.

Subroutine NODFOR:

The purpose of this subroutine is to accomplish the following: compute the nodal forces of the fractured element; apply the negative of these nodal forces to the unfractured system in increments until the full load levels are reached; and to check for unstable crack growth. Specifically, it performs the following steps:

(1) If LOOPF = 1 then the execution of the computer program goes to Step (8).

(2) The current total effective stress, ST(N,4), of all the yielded elements are stored in an array FY(N), N = 1, 2, ..., NYE, where NYE is the total number of yielded elements.

(3) The nodal forces of the fractured element, N, are computed using the following relationship:

$$FN(I) = THM * AREA * [BB(I,J) * STF(N,J)] \quad (3.24)$$

where I = 1, 2, ..., 6; J = 1, 2, 3; THM is the thickness; AREA is the area of the element; [BB] is the element strain-displacement transformation matrix (as given by Eq. (2.32) of Chapter II); and matrix [STF] contains the values of the total stress components of the element in its first three columns and the value of the total effective stress of the ele-

ment in its fourth column.

(4) The negative of the vector {PN} is saved as vector PNOD(I), I = 1, 2, ..., 6.

(5) The element in vector {PNOD} which has the largest magnitude is located and designated as PNMAX. Say it occurs in the Kth row of the vector {PNOD}.

(6) The vector {PNOD} is normalized such that its Kth row element is set equal to 1 and all the other row entries are divided by PNMAX.

(7) The incremental load, DELW, is computed from

$$DELW = ALPHA * PNMAX \tag{3.25}$$

Then LOOPF is set equal to one and the computer program execution goes to Step (15).

(8) The total stress components of all the unfractured elements are computed and stored in a scratch array, [STF], as follows:

$$STF(N,J) = SEL(N,J) + ST(N,J) \tag{3.26}$$

where N is the element number; J = 1, 2, 3; [SEL] is element incremental stress components array; and [ST] is the element total stress components array obtained from the previous load cycle.

(9) The total effective stress is computed for all

the elements using Eq. (2.57) of Chapter II and is stored in the respective row of the fourth column of the matrix [STF].

(10) The most stressed elastic element, N, is the one for which the effective stress value is largest. If the value of the effective stress of this element is greater than the material yield stress, SO, then the run is discarded, and a new analysis is initiated after setting the value of the incremental load applied, ALPHA, to ALPHA/2. Then execution of the computer program returns to the subroutine PLASFL.

(11) When the next load increment is applied it may happen that some of the yielded elements near the crack tip start getting unloaded rather than picking up the load. If an element unloads then its modulus of elasticity should be taken equal to the elastic modulus of elasticity of the material. Thus, the original elastic element stiffness matrix has to be used for such an element. The unloading elements are detected by comparing the new total effective stress of the yielded elements, computed at the end of the incremental load cycle, with its value at the end of the previous incre-

mental load cycle. If the former value is less than the latter value then that element is said to be an unloading element and the element number of these elements are stored in an array ISE(K), K = 1, 2, ..., NSE, where NSE is the total number of unloading yielded elements. If such an element occurs during an incremental load cycle then the analysis performed for this incremental load cycle is discarded. The new system stiffness matrix of the unfractured system is computed using the elastic stiffness matrix for the unloading element. The incremental nodal loads are again reapplied and the Steps (1) to (10) are repeated. Then it would be found that the unloading element will start picking up load and will move elasticity till it intersects the nonlinear portion of the uniaxial stress-strain curve of the material. (This is ascertained by comparing the value of the total effective stress of the element with the value in the corresponding row of the vector {FY}, which is formed in Step (2) of subroutine NODFOR.) Then the stiffness matrix of this element will be changed to be equal to the original elasto-plastic stiffness matrix, which it possessed just before unloading

occurred. There may be a situation in which, during an incremental load cycle, as an unloading element is made to become a loading element by using its elastic element stiffness matrix another element may start unloading. So the procedure has to be repeated in cycles ideally till all unfractured elements become loading elements. To keep computer costs down, in the computer program developed a limit on the number of such cycles is put as four. It is expected that by the end of this process of repeating the four re-adjustment cycles for an incremental load cycle there would be no unloading elements. If this does not occur then the remaining unloading elements are treated as loading elements with their element stiffness matrices equal to their respective elasto-plastic element stiffness matrices. Then some error would be carried over to the next load increment.

(12) The total stress components of all the unfractured elements are computed by adding the incremental stresses computed for this load cycle to the total stresses already computed at the beginning of this load cycle, i.e., by using the following relationship:

$$ST(N,J) = SEL(N,J) + ST(N,J) \qquad (3.27)$$

where N is the element number and J = 1, 2, 3. Next, the total effective stress for all the unfractured elements is computed and stored in the fourth column of the matrix [ST]. The element having the maximum value of the total effective stress is now located. This is the most stressed yielded element.

(13) If the total effective stress of the most stressed yielded element is greater than or equal to the material fracture stress then unstable crack growth is said to occur. Then KERR is set equal to one and the execution of the computer program is made to return to the subroutine PLASFL and finally terminated. Otherwise, the execution proceeds to the next step.

(14) Using the values of the total effective stress computed in Step (12), all the elastic elements having the total effective stress value, ST(N,4), within 0.995 SO $\leq$ ST(N,4) $\leq$ SO are made to yield together by setting their total effective stress value equal to the material yield stress, SO.

(15) The load achieved for the fractured element is

updated and stored as PNTEMP, which is computed from

$$PNTEMP = PNLOAD + DELW \tag{3.28}$$

where DELW is the incremental load applied given by Eq. (3.19).

(16) (a) If PNTEMP is within an allowance of ± 0.0005 * PNMAX then the energy of fracture element is said to have been distributed into the unfractured system. If this is true then LOOPF is set equal to zero and the computer program execution returns to the subroutine PLASFL.

(b) If PNTEMP is greater than or equal to 0.9 * PNMAX then the next incremental load to be applied is computed as follows: first DELW is computed using

$$DELW = PNMAX - PNLOAD \tag{3.29}$$

and then the fraction of incremental load applied, ALPHA, is computed using

$$ALPHA = DELW/PNMAX \tag{3.30}$$

(c) If the above two checks are not found to be true then PNTEMP is stored as PNLOAD. Thus, PNLOAD is the total load achieved

during the energy distribution.

(17) The incremental nodal forces of the fractured element are computed from

$$PAPPLY(I) = ALPHA * PNMAX * PNEL(I) \quad (3.31)$$

where I = 1, 2, ..., 6. Then the execution of the computer program returns to the subroutine PLASFL.

3.5 FLOWCHARTS OF MAIN PROGRAM AND SUBROUTINES FOR PROGRAM CRACK

This section presents the flowcharts of the main program and some of the important subroutines for computer program CRACK. The flowchart of the main program is shown in Fig. 3.8. The flowcharts of the subroutine PLASFL and NODFOR are shown in Figs. 3.9 and 3.10, respectively. These and the other subroutines have been described earlier in Section 3.4.

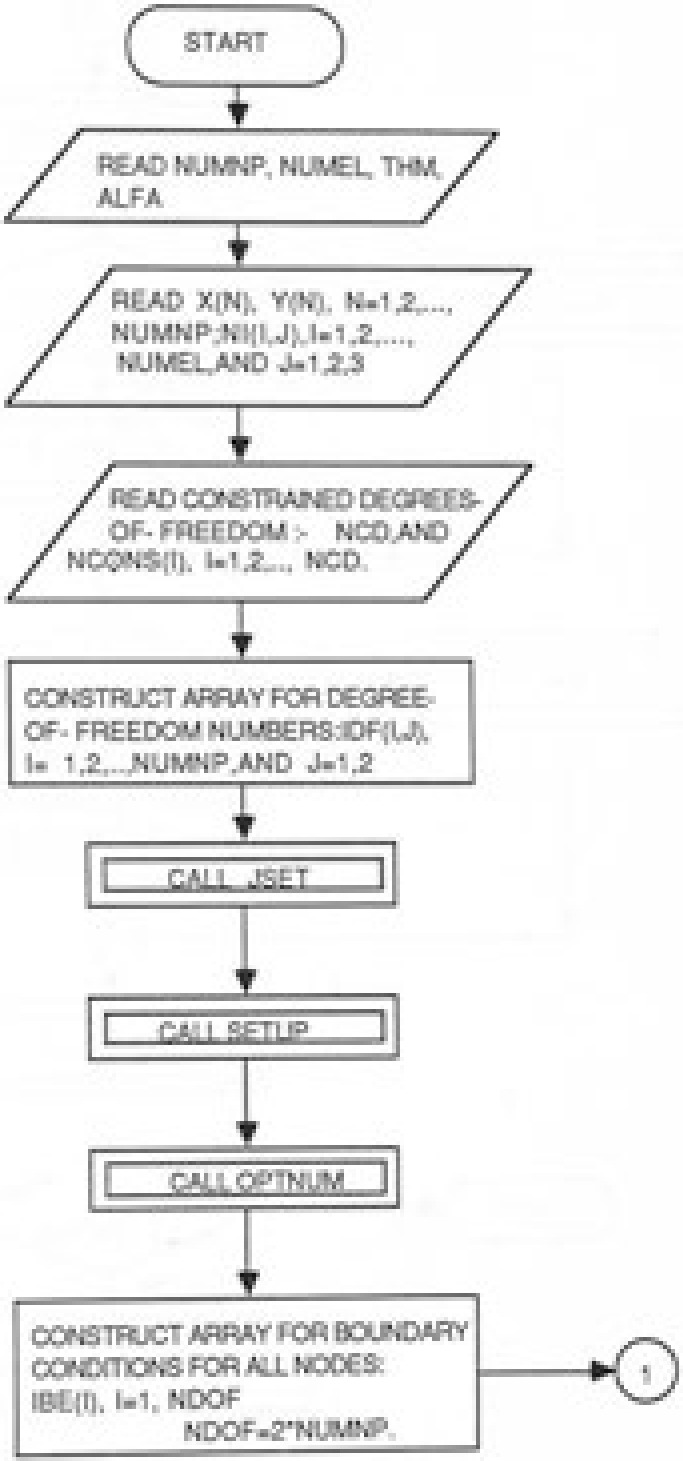

Fig. 3.8 Flowchart of the Main Program CRACK

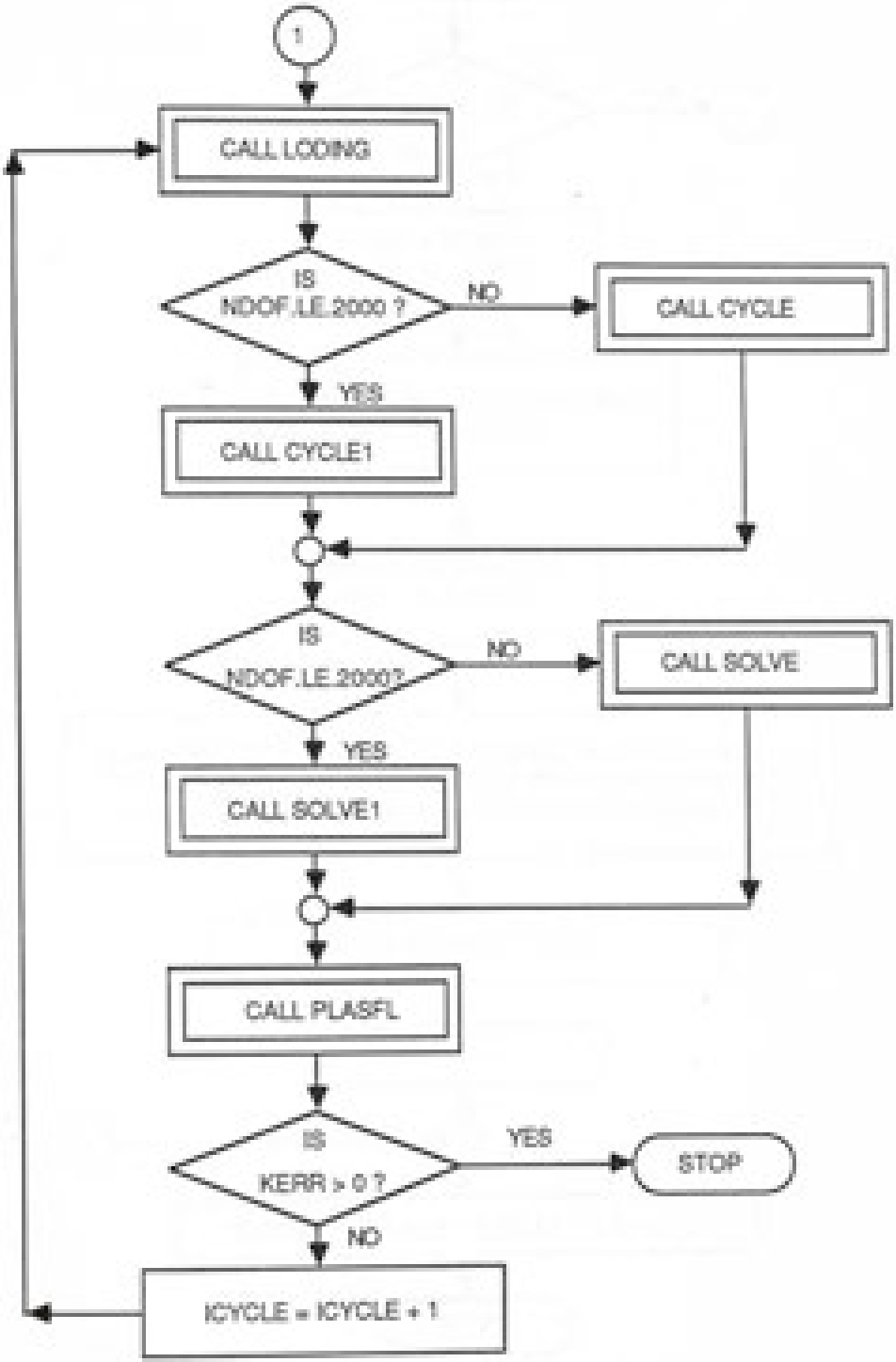

Fig. 3.8 (Cont'd) Flowchart of the Main Program CRACK

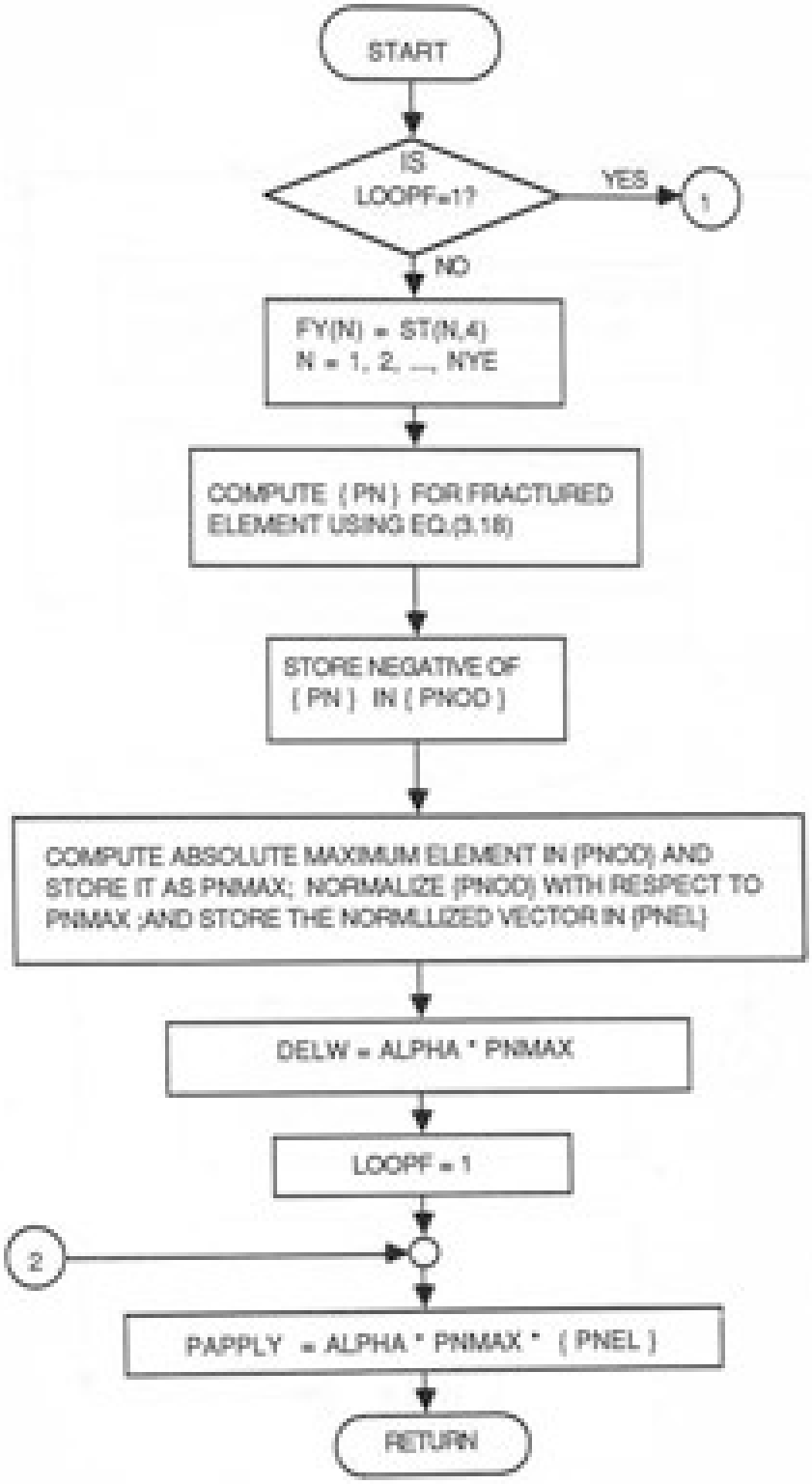

Fig. 3.9 Flowchart of Subroutine NODFOR

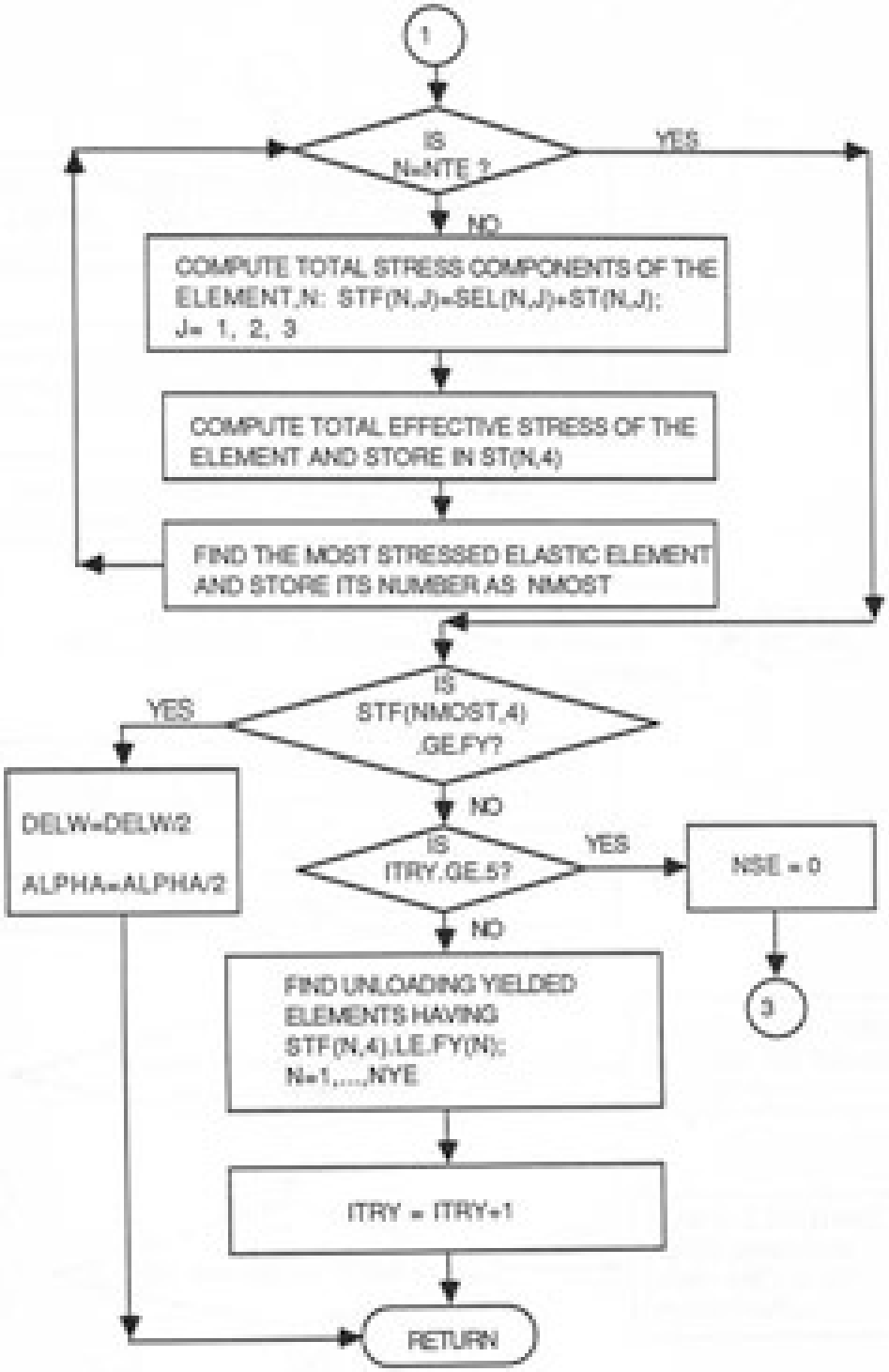

Fig. 3.9 (Cont'd) Flowchart of Subroutine NODFOR

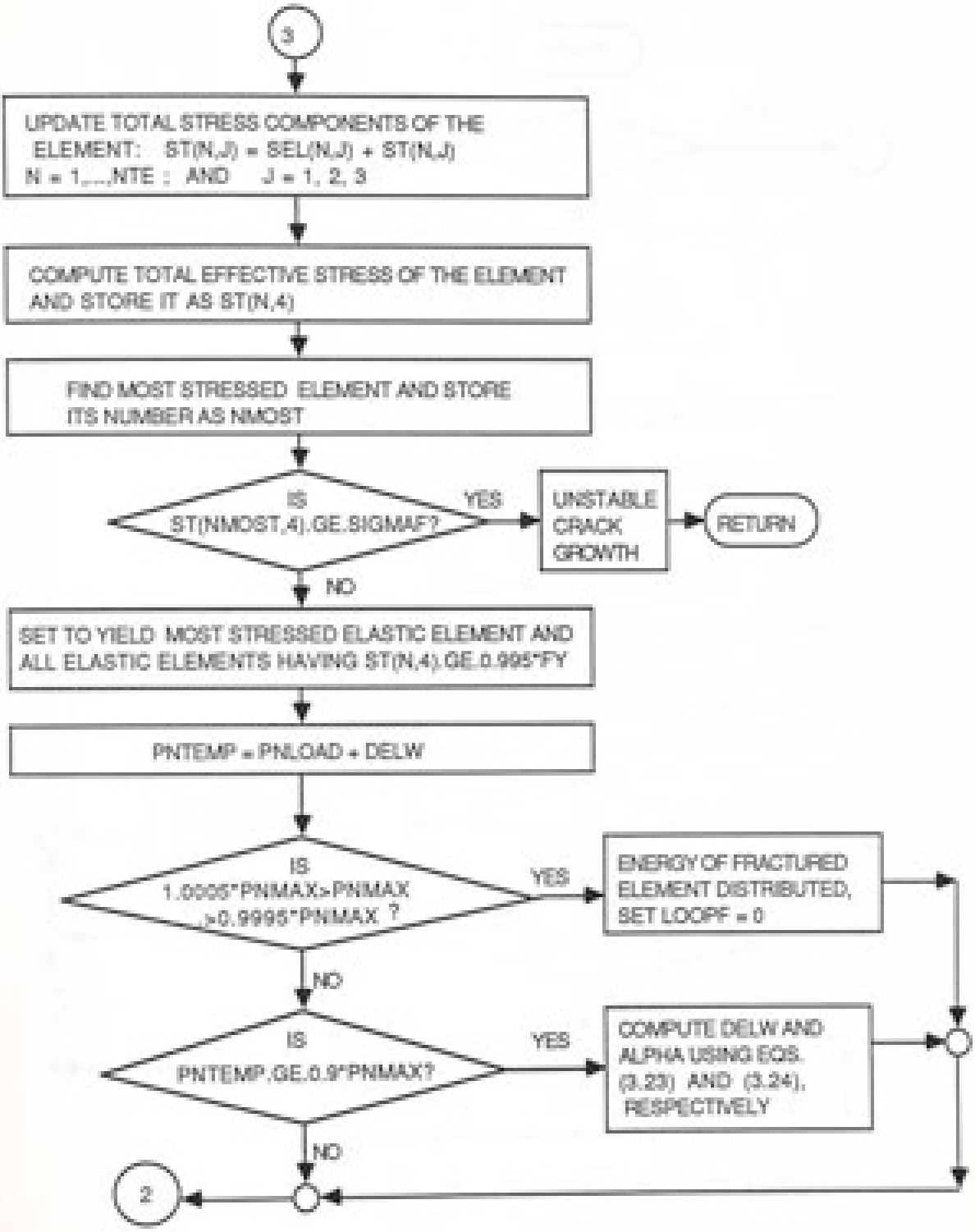

Fig. 3.9 (Cont'd) Flowchart of Subroutine NODFOR

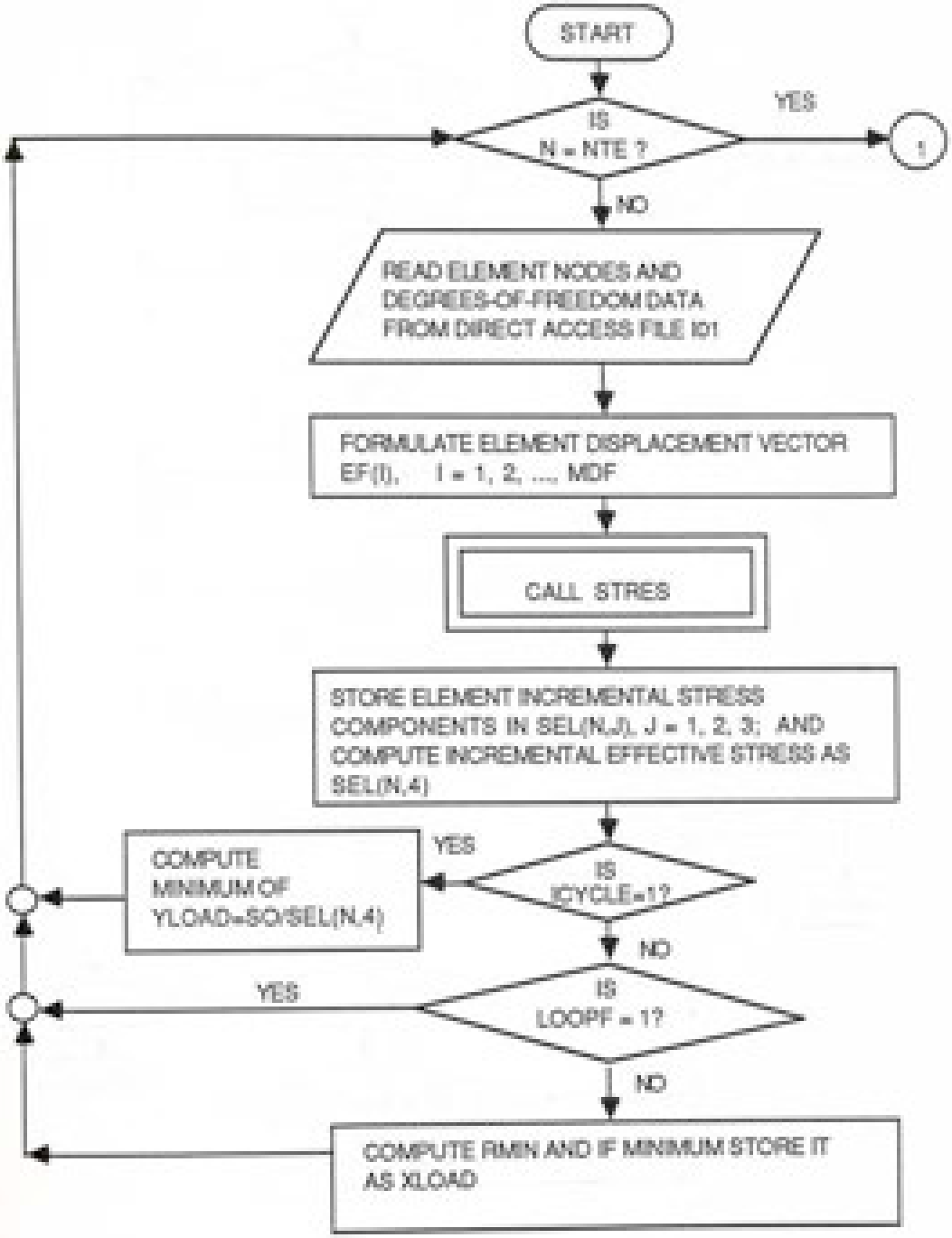

Fig. 3.10 Flowchart of Subroutine PLASFL

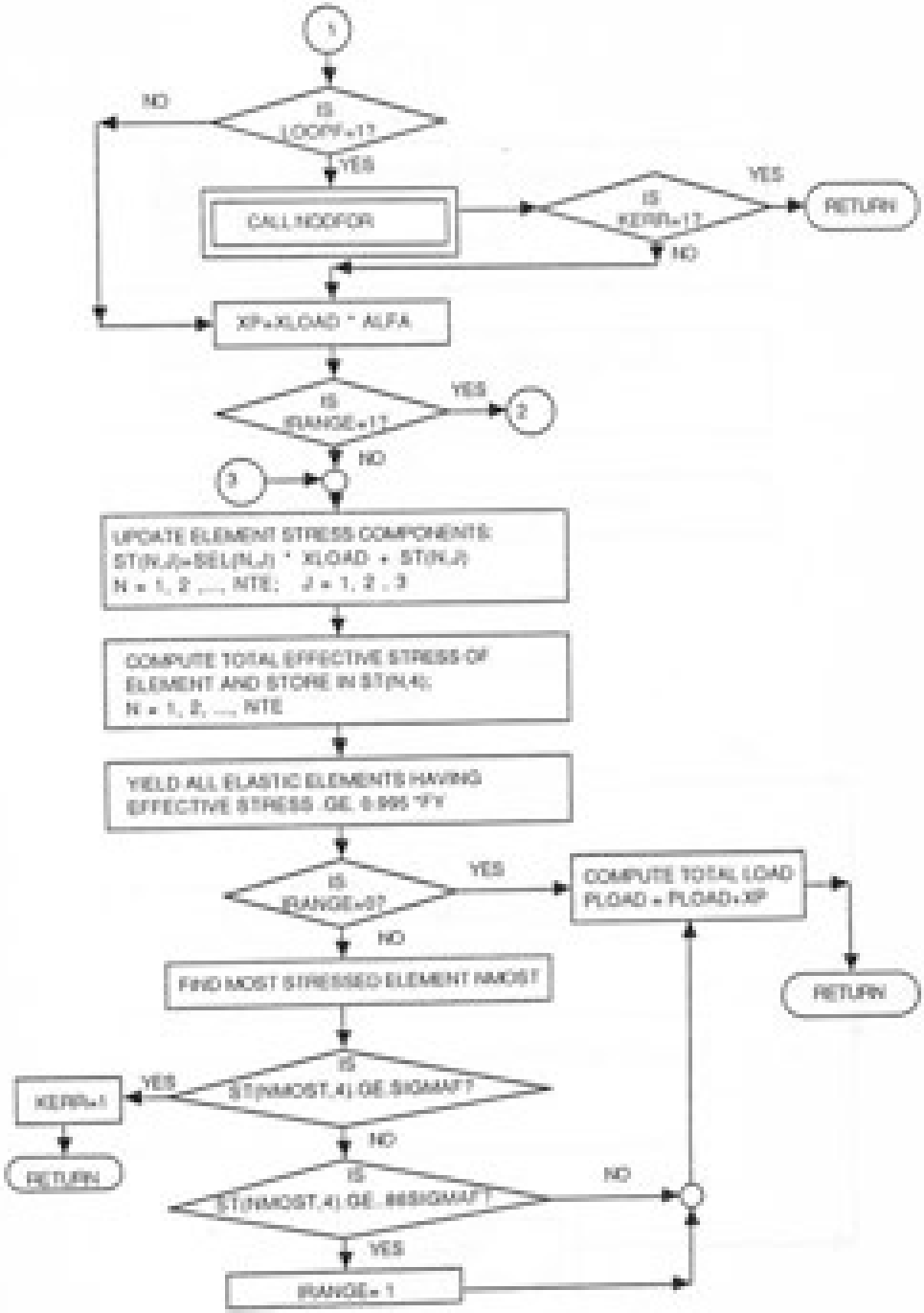

Fig. 3.10 (Cont'd) Flowchart of Subroutine PLASTL

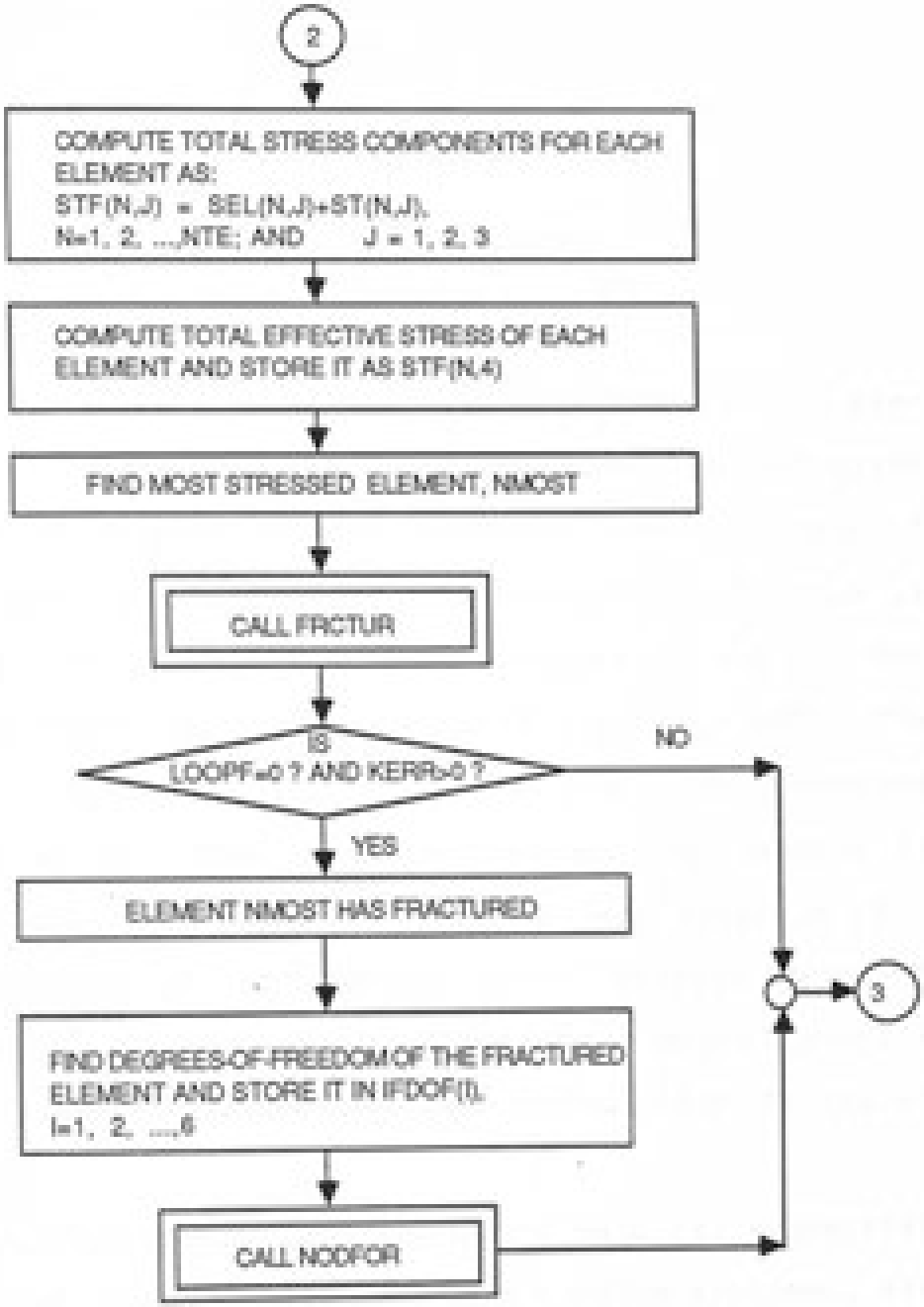

Fig. 3.10 (Cont'd) Flowchart of Subroutine PLASFL

CHAPTER IV

NUMERICAL VERIFICATIONS

4.1 INTRODUCTION

In this chapter, the mathematical formulations presented in Chapter II and the two computer programs described in Chapter III are verified with the help of two numerical examples. The first numerical example is concerned with the failure load analysis of a V-notched tension specimen using the computer program PLAST. The results of this example problem have been also presented by Yamada et al. [32]. The second numerical example is concerned with the ultimate fracture load analysis of a center pre-cracked rectangular panel tension specimen using the computer program CRACK. Experimental results for this example problem have been presented by Miller et al. [24].

In Section 4.2, the geometry and material properties of the first example, the V-notched tension specimen, are given. Details of the finite element modelling for this specimen are presented in Section 4.3. Finally, in Section 4.4, the numerical results obtained for this

problem using the computer program PLAST are presented and compared with results available in literature.

In Section 4.5, the geometry and material properties for the second numerical example, the center pre-cracked rectangular panel tension specimen, are given. Details of the finite element modelling for this specimen are presented in Section 4.6. Finally, in Section 4.7, the numerical results obtained for this problem using the computer program CRACK are presented and compared with results available in the literature.

4.2 GEOMETRY AND MATERIAL PROPERTIES FOR THE TEST V-NOTCHED TENSION SPECIMEN

The V-notched tension specimen, as presented by Yamada et al. [32], is chosen as the numerical example to verify the results predicted by the computer program PLAST developed in this study. The geometry of the specimen chosen is shown in Fig. 4.1. Due to its symmetry about both the x- and the y- axis, only a quarter panel needs to be analyzed. The boundary conditions thus imposed on this quarter panel are shown in Fig. 4.2. The load P in this figure represents the total load per half width of the actual specimen.

The material is considered to be elastic perfectly plastic with yield stress, F_y, equal to 30 Kg/mm^2. Poisson's ratio, ν, is taken equal to 0.3 and the Young's modulus of elasticity, E, is taken equal to 20,000

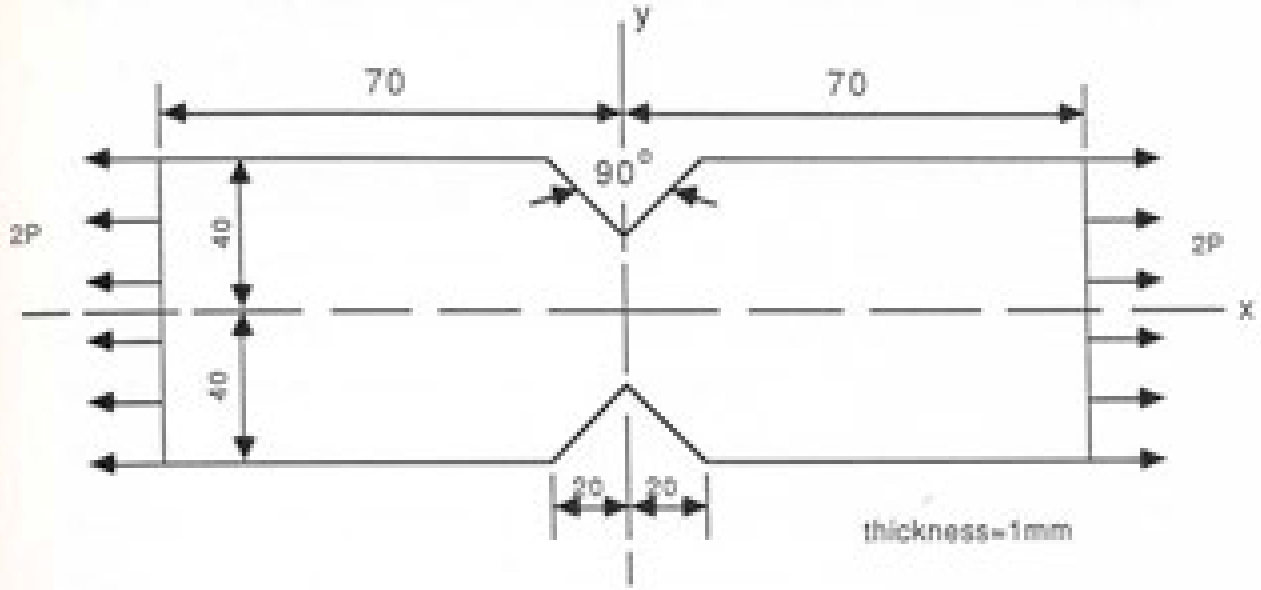

Fig. 4.1 Test V-notched Tension Specimen

(Note: All dimensions in mm)

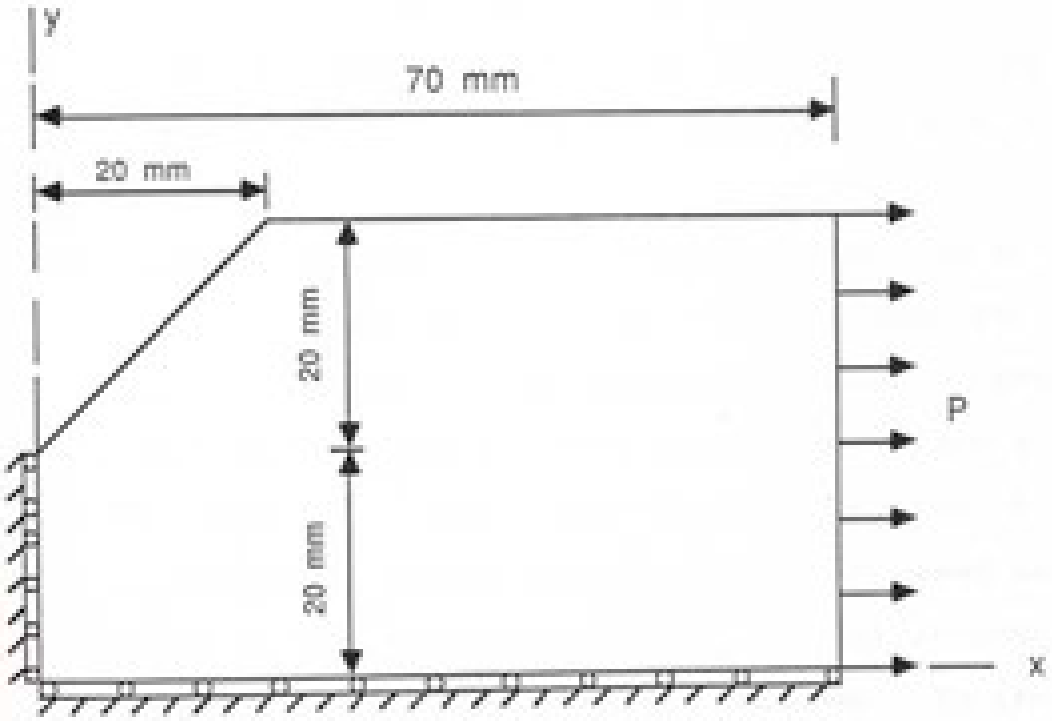

Fig. 4.2 Boundary Conditions for the Quarter Panel Considered for the Analysis of the Test V-notched Tension Specimen

Kg/mm^2. The material stress-strain curve used is shown in Fig. 4.3.

4.3 FINITE ELEMENT MODELING OF THE TEST V-NOTCHED TENSION SPECIMEN

The quarter panel, shown in Fig. 4.2, is modeled using constant stress-strain triangular shaped finite elements. Six meshes are considered. They will be referred to as mesh #1 through mesh #6 throughout this discussion. The geometric configuration of these meshes are shown in Fig. 4.4 and the salient features of these meshes are summarized in Table 4.1. In all the mesh patterns, smaller elements have been taken in the region expected to yield (i.e., the region near the V-notch).

As can be seen from Table 4.1, the following factors have been considered in choosing the various finite element meshes:

(1) Grading of mesh: To investigate the convergence of the results, for the same mesh pattern, the size of the smallest element in the mesh was decreased. Thus, in mesh #'s 1 and 4, in mesh #'s 2 and 5, and in mesh #'s 3 and 6, the minimum area of the element is decreased in each of the latter cases by about 44% in comparison to the respective former case. To investigate convergence of results, rather than refining mesh #'s 4 and 5 further, it was

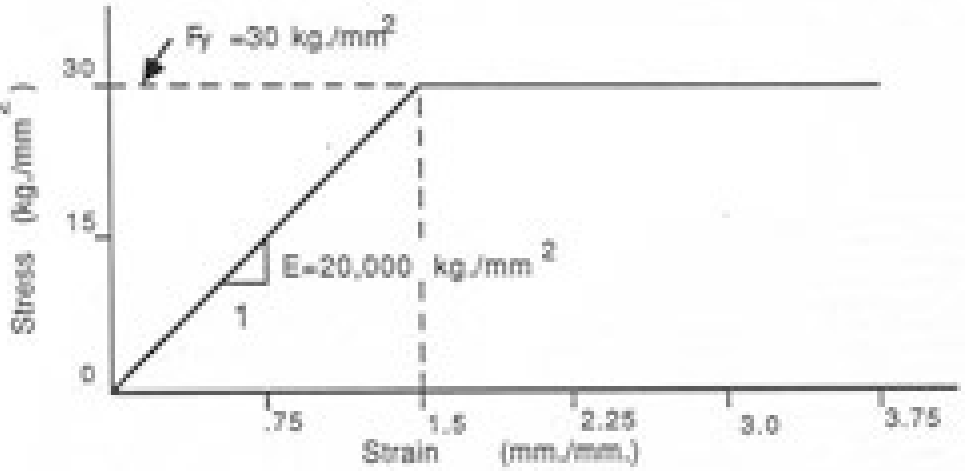

Fig. 4.3 Material Stress-Strain Curve for the Test V-Notched Tension Specimen

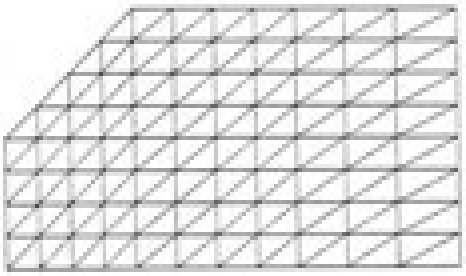

(a) Mesh #1

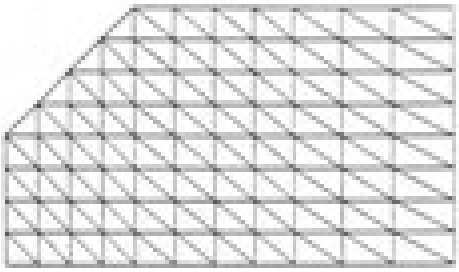

(b) Mesh #2

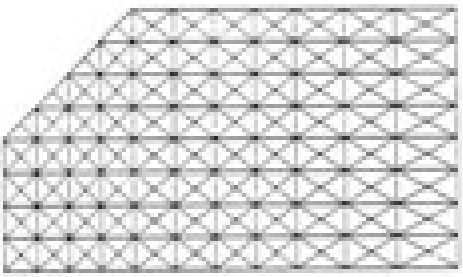

(c) Mesh #3

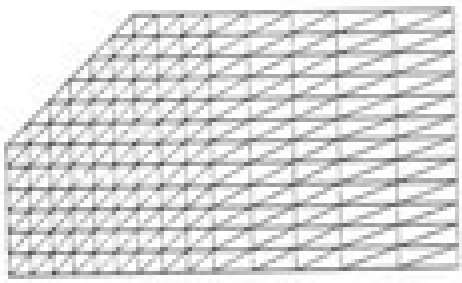

(d) Mesh #4

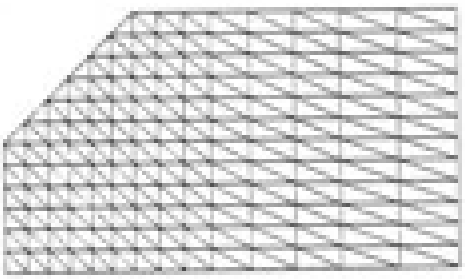

(e) Mesh #5

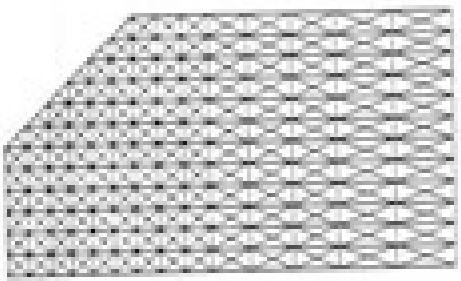

(f) Mesh #6

Fig. 4.4 Meshes Considered for Analysis of the Test V-notched Tension Specimen

Table 4.1 Mesh Grading and Element Orientation For the Test V-notched Tension Specimen

Mesh Designation	Mesh Pattern	Number of Nodes	Number of Elements	Minimum Area (mm^2)
#1		98	160	12.5
#2		98	160	12.5
#3		180	320	6.25
#4		174	320	5.54
#5		174	300	5.54
#6		327	600	2.76

decided to compare these results with those obtained by mesh #6, in which the minimum element area is 50% of the former meshes.

(2) Orientation of the elements: It should be noted that in mesh #'s 1 and 2 (and similarly in mesh #'s 4 and 5) the shape of the elements is a right angled isosceles triangle. But, the orientation of these triangles is different in the two meshes. These meshes are used to investigate the effect of the element orientation on the results predicted.

(3) Shape of the elements: In mesh #3, equilateral triangular elements are used in the expected yield zone, whereas, in mesh #'s 4 and 5, right angled isosceles triangular elements are used. In both these mesh patterns the number of elements are about the same. The minimum area of the element in mesh #3 is about 113% of that used in mesh #'s 4 and 5. These meshes are used to investigate the effect of the shape of the element on the results predicted.

4.4 NUMERICAL RESULTS OBTAINED FOR THE TEST V-NOTCHED TENSION SPECIMEN

The six meshes chosen for the test V-notched tension specimen (see Fig. 4.4) were analyzed using the computer program PLAST and the results for the following items are

presented:

(1) Load-displacement history,

(2) first yield load and failure load,

(3) yield patterns, and

(4) Central Processor Unit (CPU) computer time taken to perform each analysis.

The results obtained are compared with similar results reported by Yamada et al. [32], wherever possible. The results obtained are discussed in the light of the three factors used as a basis for selecting the six meshes, which have been discussed earlier in Section 4.3.

4.4.1 Prediction of Load-Displacement History

The values of the load level and the corresponding maximum displacement predicted by the computer program PLAST were plotted until failure occurred in the specimen. These plots of load versus displacement are referred to as the load-displacement history and give an idea about the ductility of the material.

To investigate the convergence trend of the results predicted, the load-displacement histories obtained for mesh #'s 1 and 4, mesh #'s 2 and 5, and mesh #'s 3 and 6, are plotted separately as Figs. 4.5(a), 4.5(b) and 4.5(c), respectively. Referring to Fig. 4.4, it should be noted that in each of these mesh groupings the mesh element pattern is the same except that one mesh is much

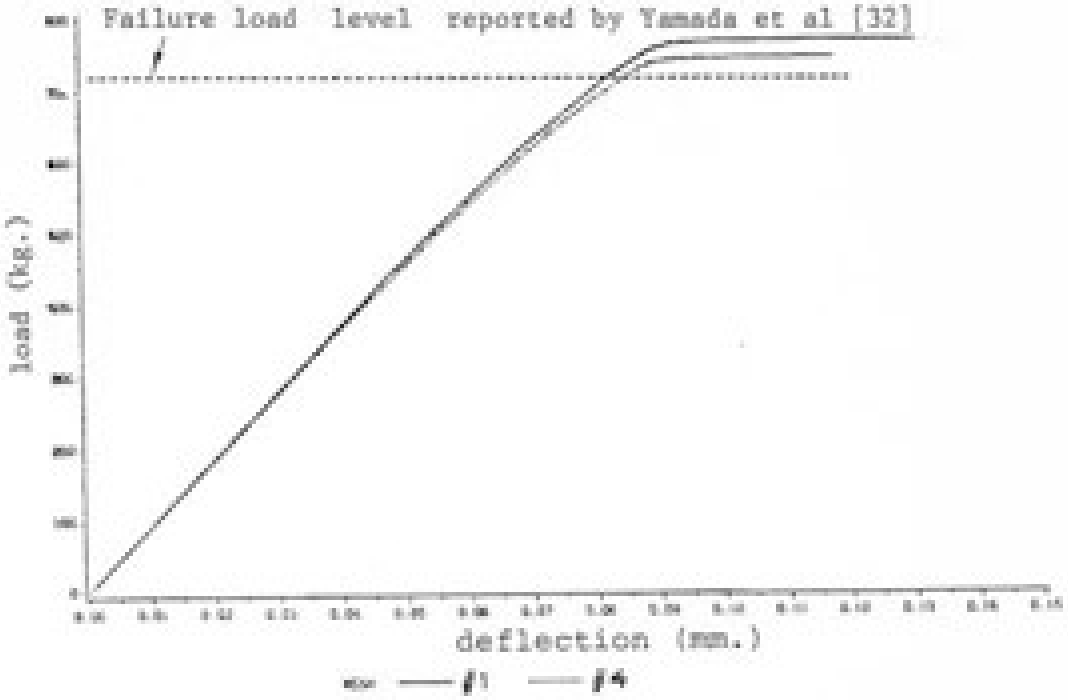

(a) Plot for mesh #s 1 and 4

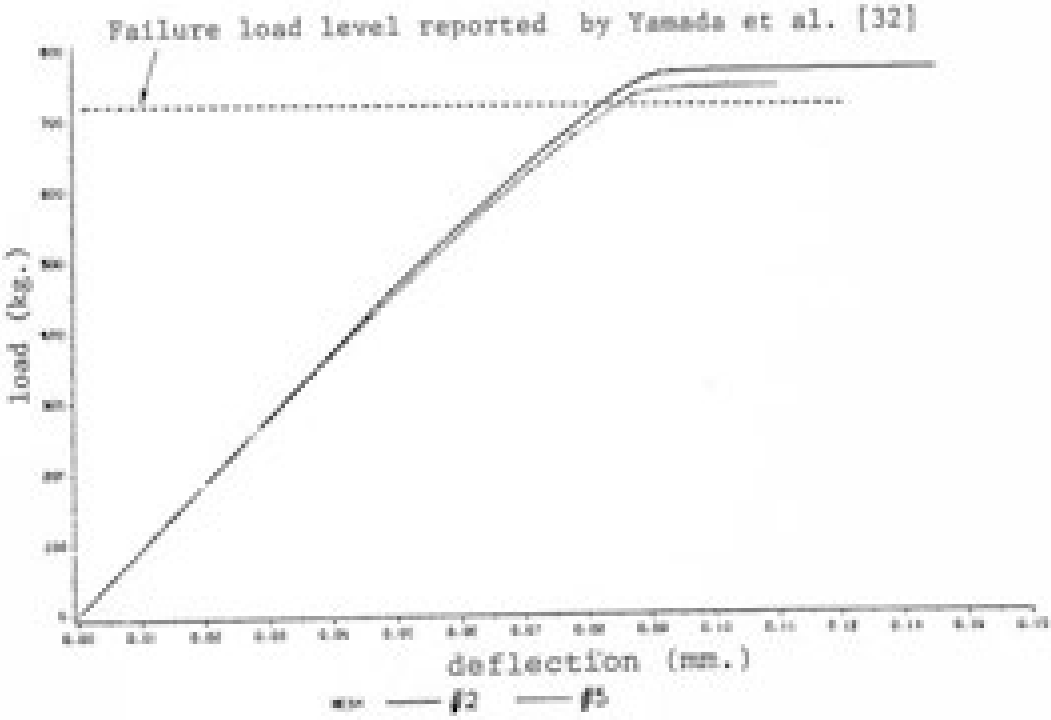

(b) Plot for mesh #s 2 and 5

Fig. 4.5 Load-Displacement History Comparision for the Test V-notched Tension Specimen

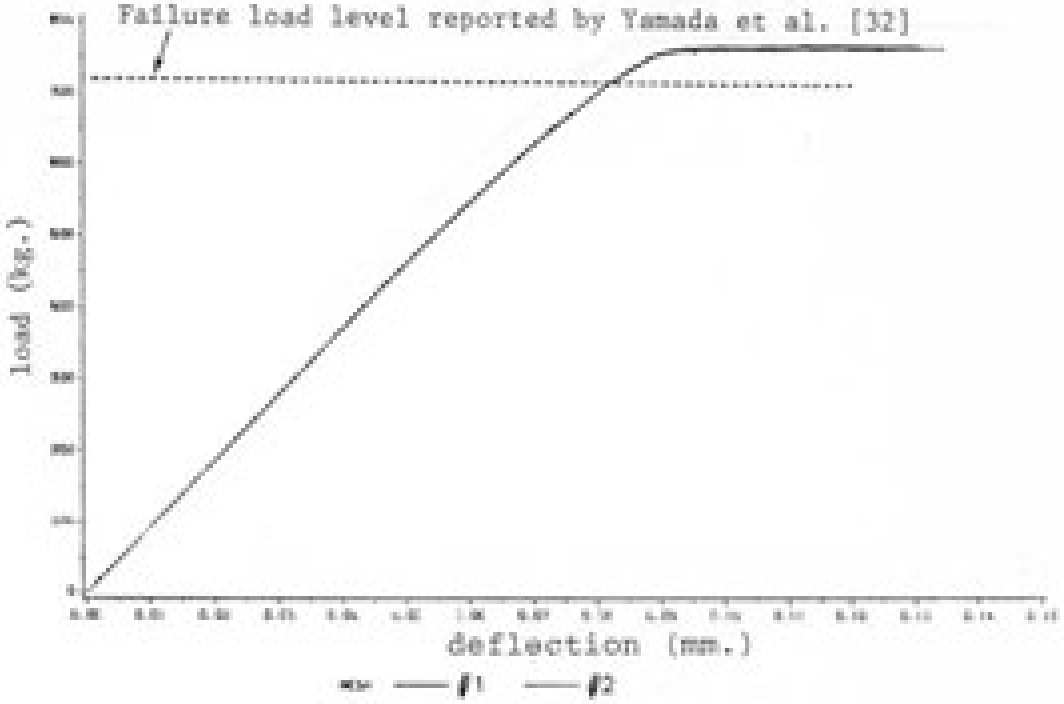

(c) Plot for mesh #s 1 and 2

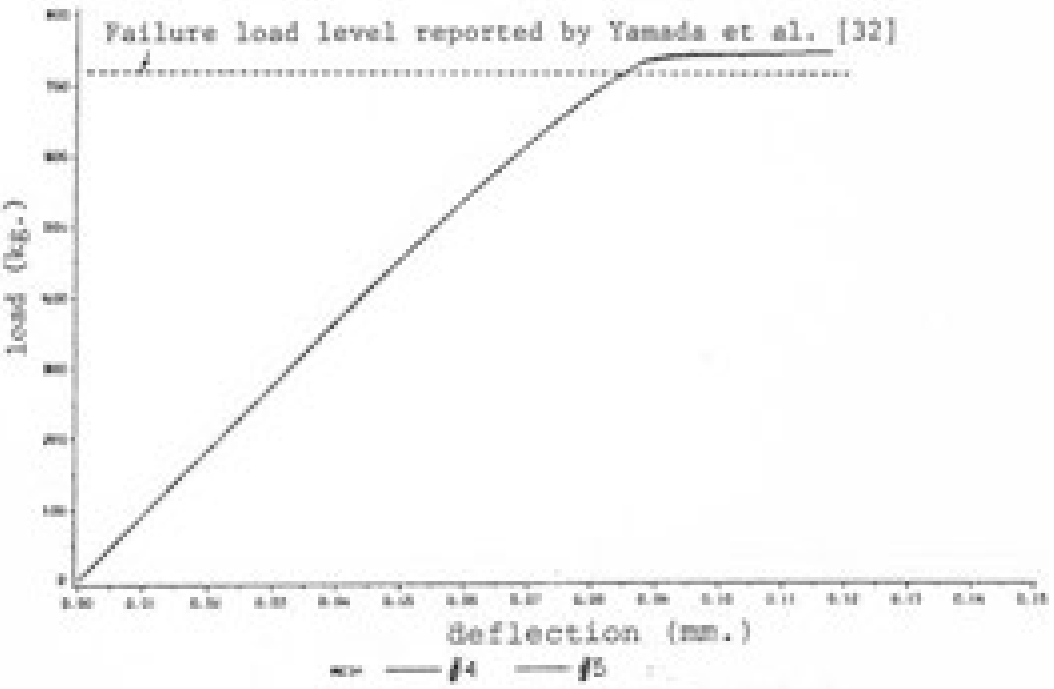

(d) Plot for mesh #s 4 and 5

Fig. 4.5 (Cont'd) Load-Displacement History Comparision for the Test V-notched Tension Specimen

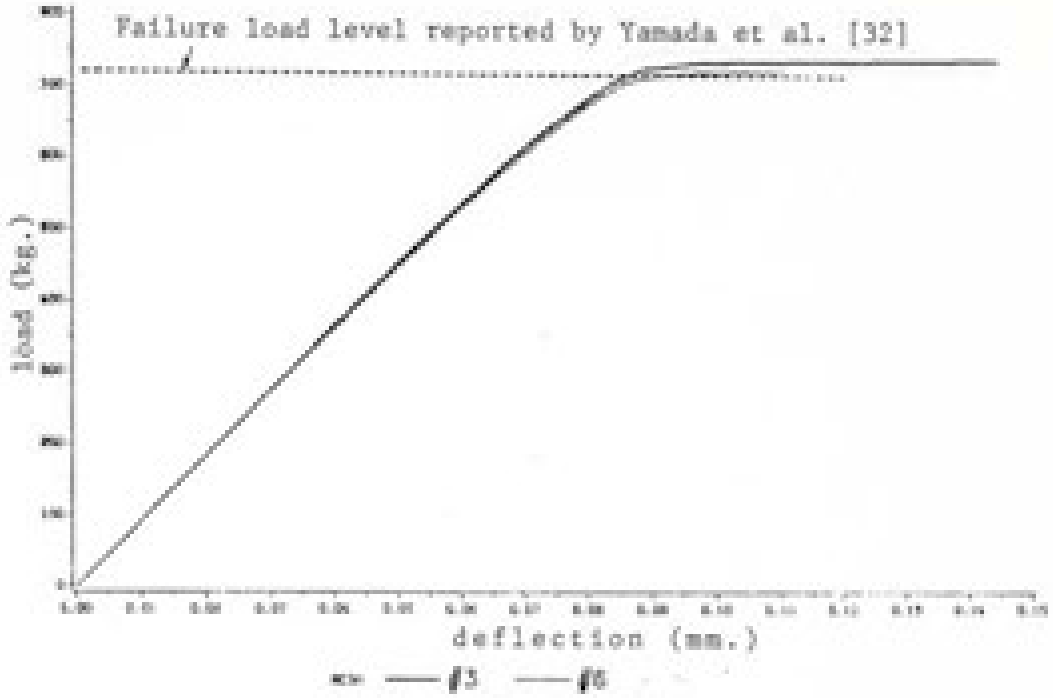

(e) Plot for mesh #s 3 and 6

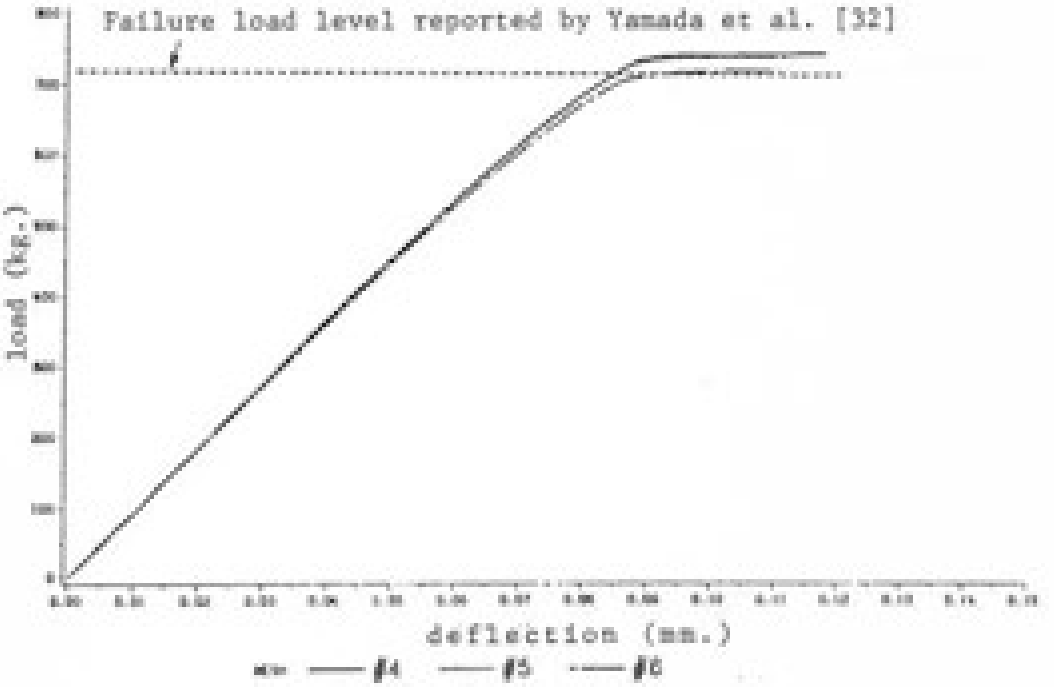

(f) Plot for mesh #s 4, 5 and 6

Fig. 4.5 (Cont'd) Load-Displacement History Comparision for the Test V-notched Tension Specimen

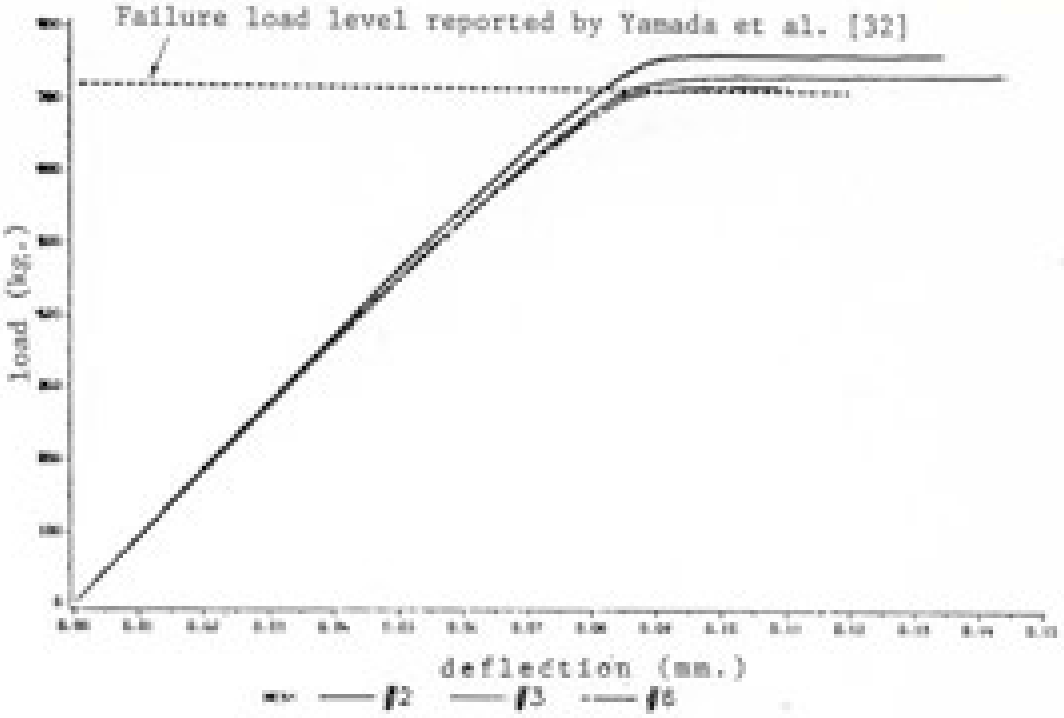

(g) Plot for mesh #s 2, 3 and 6

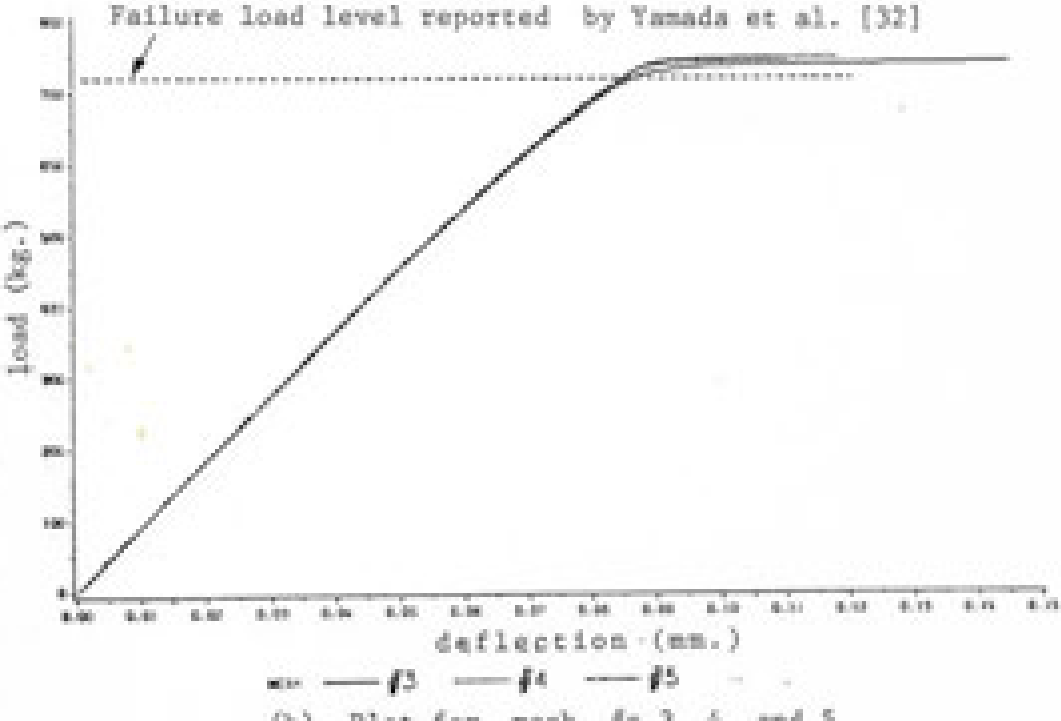

(h) Plot for mesh #s 3, 4 and 5

Fig. 4.5 (Cont'd) Load-Displacement History Comparision for the Test V-notched Tension Specimen

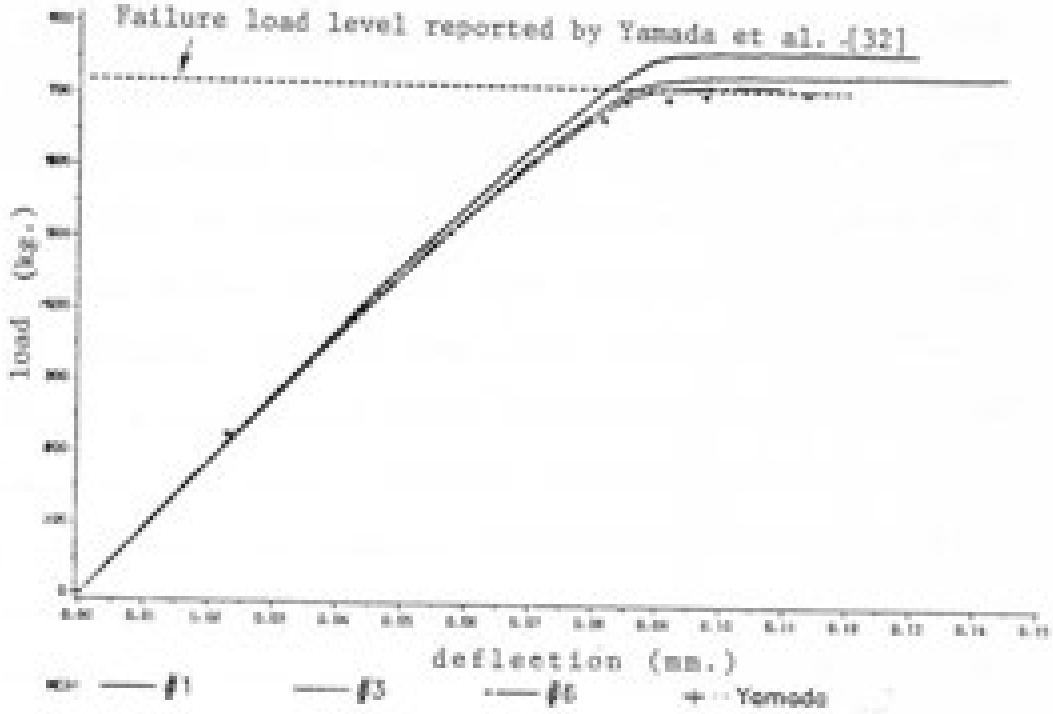

(i) Plot for mesh #s 1, 3 and 6

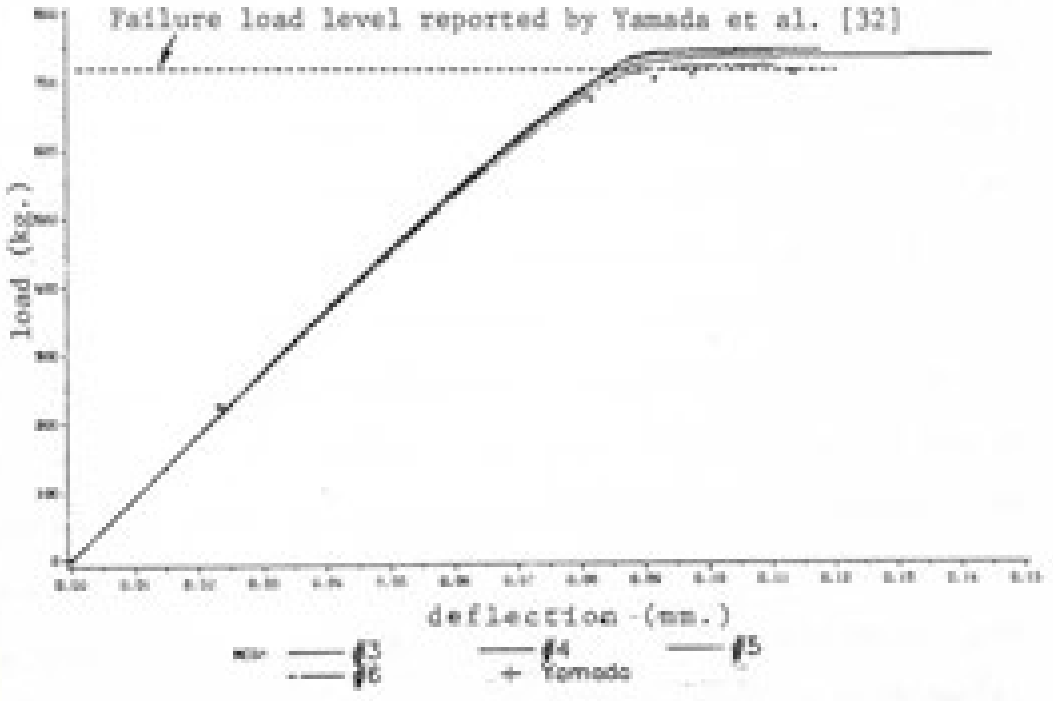

(j) Plot for mesh #s 3, 4, 5 and 6

Fig. 4.5 (Cont'd) Load-Displacement History Comparision for the Test V-Notched Tension Specimen

finer than the other. In Figs. 4.5(a) to 4.5(j) the horizontal dotted line represents the failure load level reported by Yamada et al. [32]. As expected, in each case, it can be seen that the cruder mesh predicted higher load values for the same displacement. As the mesh is refined, in each case, the failure load prediction shows a converging trend towards the value reported by Yamada et al. [32]. However, the cruder mesh predicts a much higher displacement (11.97% higher for mesh #1 over mesh #4, and 30.91% higher for mesh #3 over mesh #6) just before failure occurs. The value of the initial yield, the failure load and the corresponding failure deflection predicted by all the six meshes and those reported by Yamada et al. [32] are summarized in Table 4.2. The percentage difference between these results and those reported by Yamada et al. [32] are given in Table 4.3. Each of the meshes studied predicted a higher failure load level than that reported by Yamada et al. [32]. The load-levels predicted by mesh #1 are farthest away, whereas, those predicted by mesh #6 are closest to those reported by Yamada et al. [32]. The results obtained for mesh #3 are in-between the two curves. To relatively compare the three mesh patterns, in which mesh #1 is the crudest (minimum element area = 12.5 mm^2), and mesh #6 is the finest (minimum element area = 2.74 mm^2), their load-displacement histories are grouped together in

Fig. 4.5(i). In this figure the plus (+) sign represent the values picked up from the plots given by Yamada et al. [32]. From this figure it can be concluded that as the mesh is refined, particularly in the expected yield zone, the finite element results will converge. In the paper published by Yamada et al. [32] the mesh grading used for the quarter panel has not been reported. Because of computer costs involved no further refinement in mesh grading was tried, since the objective of this study was to simply verify the plasticity computer program (PLAST) before extending it to analyze fracture mechanics problems.

To investigate the effect of element orientation on the prediction of load-displacement history, results for mesh #'s 1 and 2 and for mesh #'s 4 and 5 are grouped together and are shown as Figs. 4.5(c) and 4.5(d), respectively. It should be noted from Fig. 4.4, that in each group of these meshes only the orientation of the elements changes - mesh grading is the same in both the cases grouped together. From Figs. 4.5(c) and 4.5(d) and Tables 4.2 and 4.3 it can be concluded that mesh #'s 2 and 5 (i.e., ⧹) predict better results than mesh #'s 1 and 4 (i.e., ⧸), respectively, for failure load when compared with the results reported by Yamada et al. [32]. But, when comparing the difference in the results obtained for mesh #'s 1 with 2 and mesh #'s 4 with 5 it

is observed that the results predicted by the two element orientations is not very significant for failure load. It is interesting to note that mesh #4 predicted a much higher (about 6.4% higher) failure deflection than that predicted by mesh #3. However, the reverse happens when comparing the failure deflection results predicted by mesh #'s 1 and 2. This shows that for the element orientation used in mesh #1 as the mesh is refined the numerical model obtained is more ductile than the one obtained by refining mesh #2. Thus, though the failure load predictions are about the same, the failure deflection predictions will vary with the change in element orientation. The results predicted by mesh #5, both for failure load and deflection, are closer to those reported by Yamada et al. [32].

To investigate the effect of the shape of the triangular elements chosen on the prediction of load-displacement history, results for mesh #'s 3, 4, 5 and 6 are grouped together in Fig. 4.5(j). The results reported by Yamada et al. [32] are also indicated in this figure with a plus (+) sign. In mesh #'s 3 and 6 equilateral triangular elements are used in the expected yield zone (see Fig. 4.4), whereas, in mesh #'s 4 and 5 right angled isosceles triangular elements are used (see Fig. 4.4). Also, referring to Table 4.1, it can be seen that the mesh grading level for mesh #'s 3, 4 and 5 is

about the same, with mesh #3 having a slightly larger (11% larger than mesh #'s 4 and 5) minimum element area. Keeping these facts in mind and comparing the results shown in Fig. 4.5 and Table 4.3, it is concluded that mesh #3 predicted better results for load levels than mesh #'s 4 and 5. But, mesh #3 predicted a much larger failure deflection than that predicted by mesh #'s 4 and 5. This may be due to the larger elemental area used in the expected yield zone and the element orientation pattern used for mesh #3. The results of mesh #6, which is composed of equilateral triangular elements in the yield zone is the closest to those reported by Yamada et al. [32]. For this mesh the difference in the result predicted by the computer program PLAST and that reported by Yamada et al. [32] for initial yield load is +0.5% and that for failure load is +1.4%.

In summary, the aforementioned discussion shows that if a crude finite element mesh composed of three-noded triangular elements is used, then the shape and orientation of the elements used to discretize the expected yield zone would effect more the failure deflection prediction than the failure load prediction. However, as the meshes are refined, within the limit, results would converge to about the same values.

4.4.2 Prediction of Initial Yield Load and Failure Load

The results for the initial yield load and the failure load for the six meshes predicted by the computer program PLAST and those reported by Yamada et al. [32] have been presented earlier in Tables 4.2 and 4.3. From these tables the following is concluded:

(1) As the mesh is refined the results predicted for both the initial yield and the failure loads show a convergence trend.

(2) A cruder mesh predicts a much higher initial yield load.

(3) The error in the initial yield load predicted by a crude mesh is much more than the error in the predicted failure load.

(4) Use of equilateral triangular shaped elements in the expected yield zone seems to predict better both the initial yield load and the failure load. As the mesh is refined faster convergence may be expected by the use of such elements in the mesh. Acute angled triangular shaped elements should be avoided.

4.4.3 Prediction of Yield Patterns

Considering the yield patterns presented in Figs. A.1 to A.6 of Appendix A, it can be observed that the location of the initial yield is independent of the mesh

Table 4.2 Summary of load and Deflection Results For test V-Notched Tension Specimen

Mesh Designation	Initial Yield Load (kg.)	Failure Load (kg.)	Deflection at failure (mm^2)
#1	416.8	774	0.131
#2	426.7	771	0.135
#3	336.6	741	0.144
#4	342.7	748	0.117
#5	351.7	745	0.110
#6	278.5	725	0.110
Yamada*	277.2	715.3	0.120

* From Reference [32]

Table 4.3 Summary of Percent Difference Of the Initial Yield Load, Failure Load , and Deflection Predicted at Failure by the Computer Program PLAST with the Results reported by Yamada et al. [32] for the Test V-notched tension Specimen

Mesh Designation	Initial Yield Load	Failure Load	Deflection at Failure
#1	50.4	8.2	9.2
#2	53.9	7.8	12.5
#3	21.4	3.7	20.0
#4	23.6	4.6	-2.5*
#5	26.9	4.1	-8.3*
#6	0.5	1.4	-8.3*

* Negative sign denotes that the value predicted by the computer program PLAST is lower than that reported by Yamada et al. [32]

grading or the mesh orientation (see part (a) of each of the Figs. A.1 to A.6 of Appendix A). In all the six cases studied the first yield starts at the tip of the V-notch, which is obvious because the highest stresses are developed at this location due to the application of the load.

To study the rate of yielding plots for load versus area yielded are drawn, as shown in Figs. 4.6(a) to 4.6(g). These figures are drawn using the results tabulated in Table C.1 of Appendix C. The interpretation of these figures is done such that a curve having more steps shows a more gradual (or better) trend in yielding as compared to a curve having big jumps and, therefore, a lesser number of steps.

From Figs. 4.6(a) to 4.6(g) it can be seen that the finer meshes show a better trend in yielding than the coarser meshes. This is due to the fact that in the method used yielding of an element is considered rather than yielding of a material point. In a coarser mesh, since larger size elements are used, a larger area yields at a particular load level. Considering the effect of mesh grading on the rate of yielding, the results for mesh #'s 1 and 4, mesh #'s 2 and 5, and mesh #'s 3 and 6 are compared (see Figs. 4.6(a), 4.6(b) and 4.6(e), respectively). In all three set of cases, the finer mesh shows a more gradual trend in yielding than the coarse

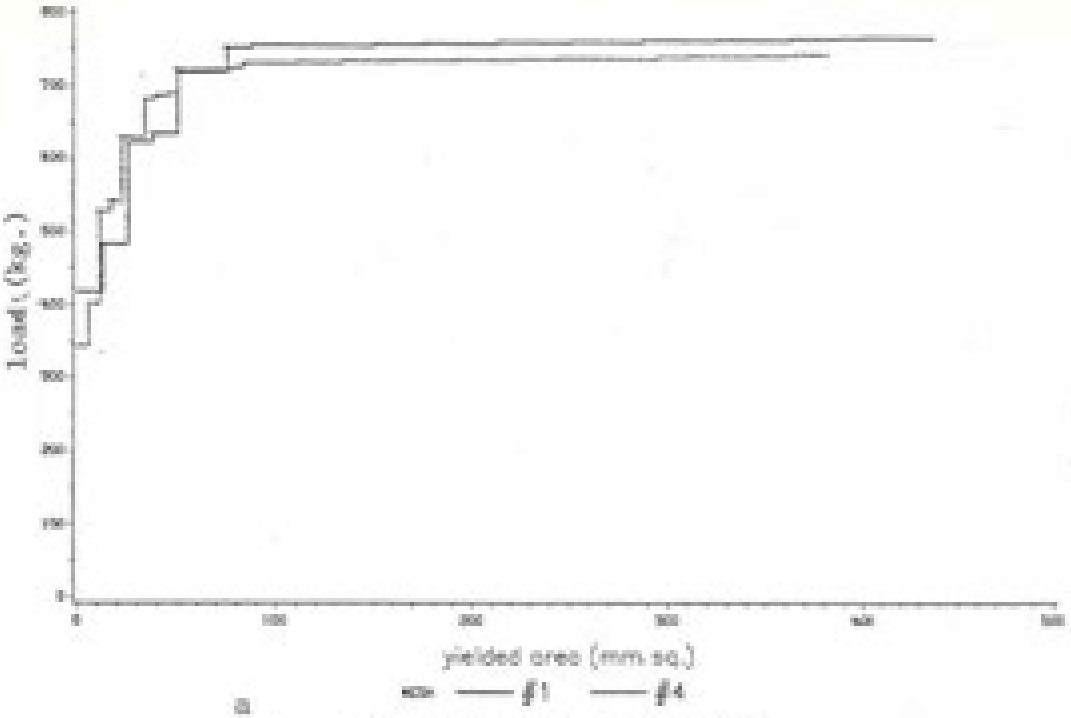

(a) Plot for mesh #s 1 and 4

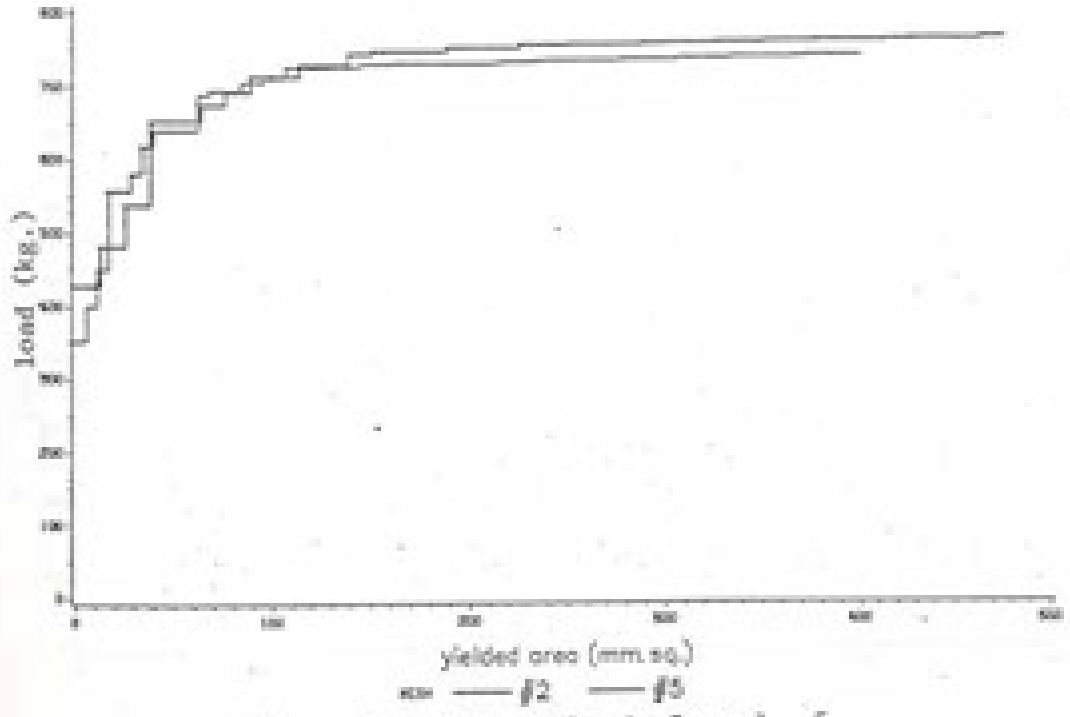

(b) Plot for mesh #s 2 and 5

Fig. 4.6 Load Versus Area Yielded Curves for the Test V-notched Tension Specimen

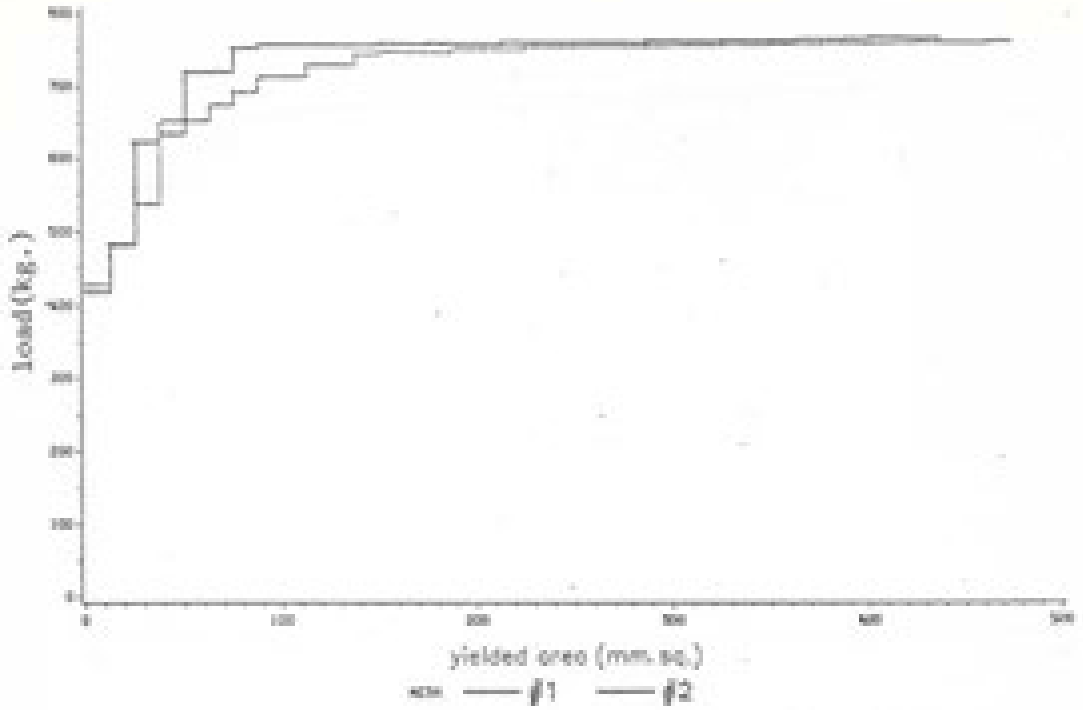

(c) Plot for mesh #s 1 and 2

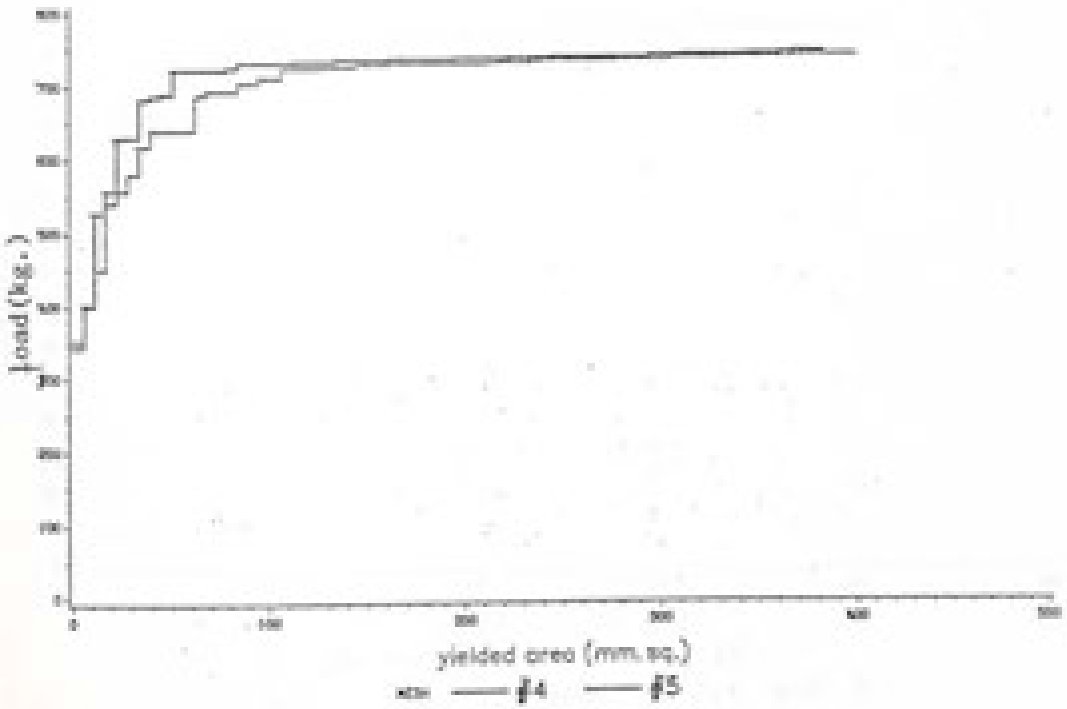

(d) Plot for mesh #s 4 and 5

Fig. 4.6 (Cont'd) Load Versus Area Yielded Curves for the Test V-notched Tension Specimen

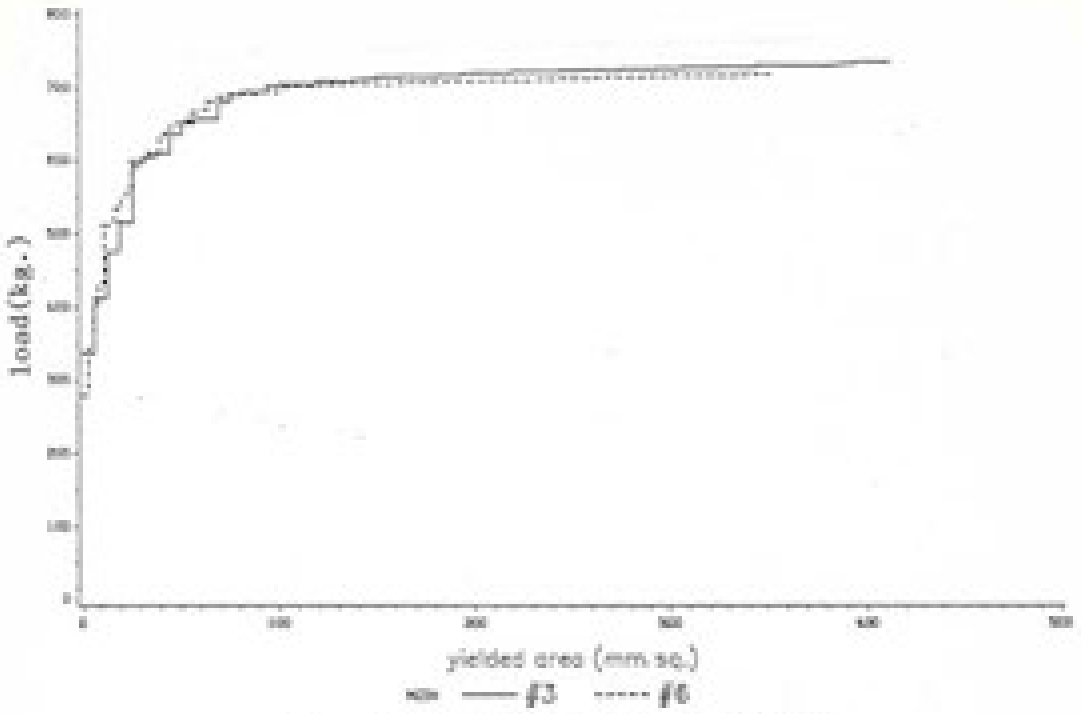

(e) Plot for mesh #s 3 and 6

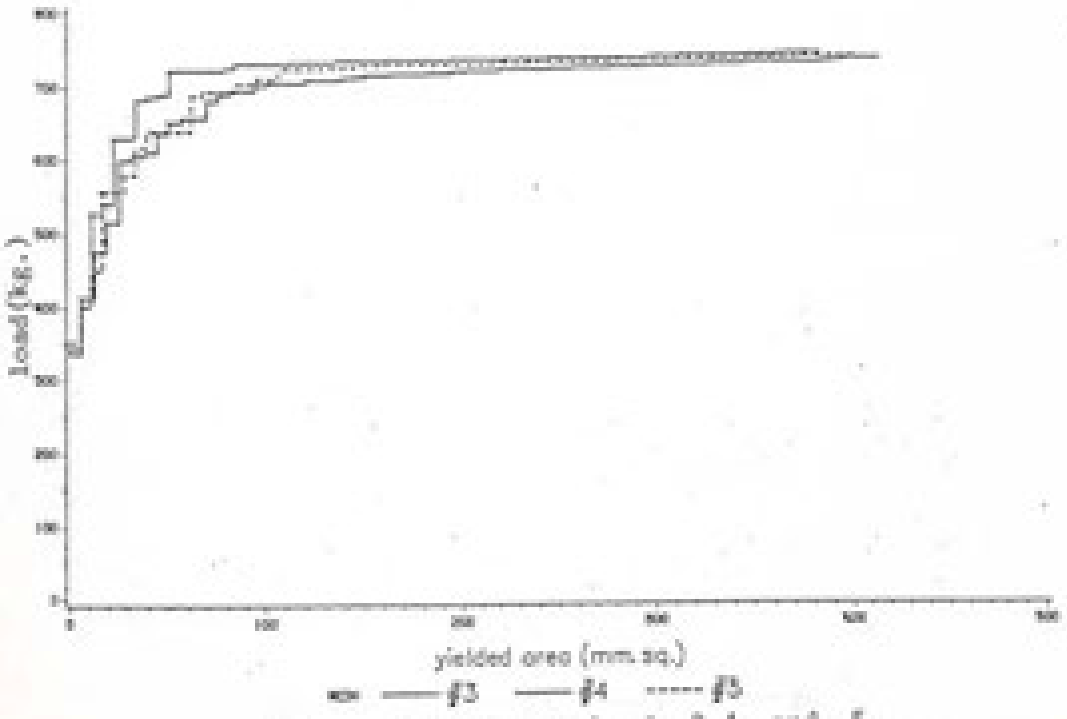

(f) Plot for mesh #s 3,4 and 5

Fig. 4.6 (Cont'd) Load Versus Area Yielded Curves for the Test V-notched Tension Specimen

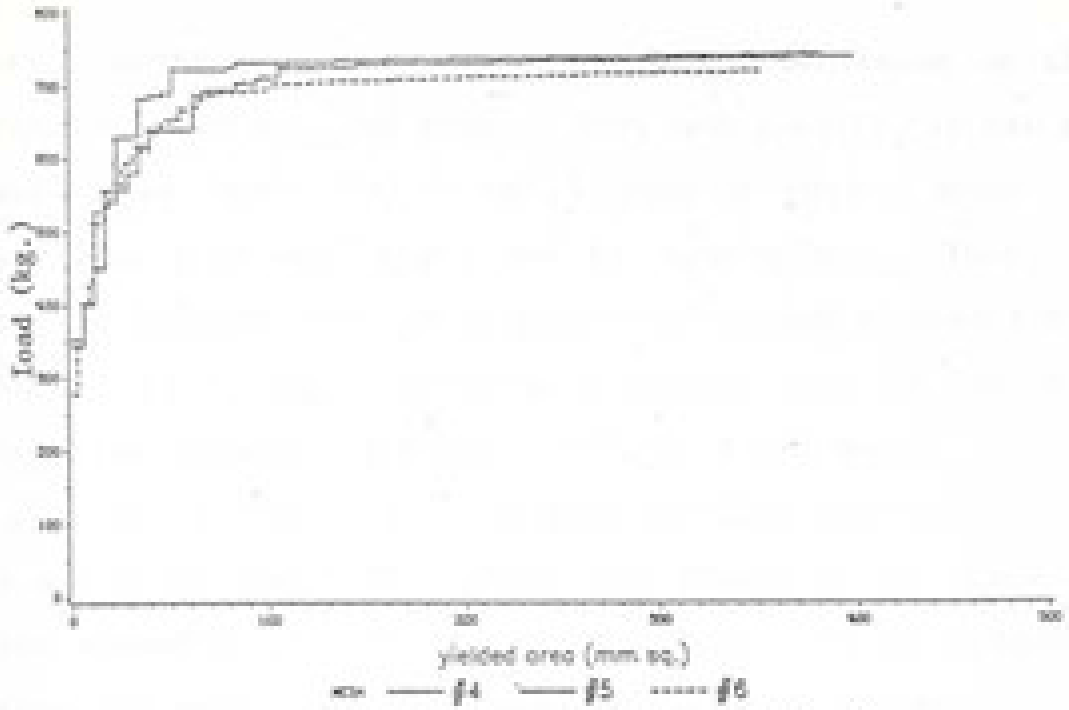

(g) Plot for mesh #s 4, 5 and 6

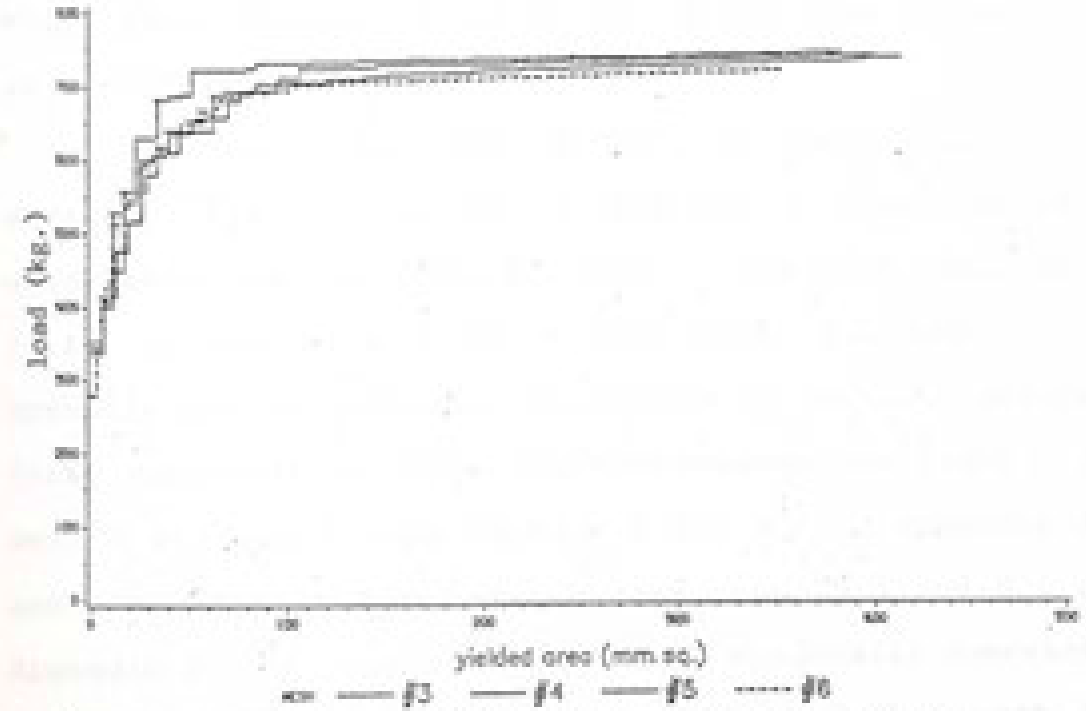

(h) Plot for mesh #s 3, 4, 5, and 6

Fig. 4.6 (Cont'd) Load versus Area Yielded curves for the test V-Notched Tension Specimen

one. Looking at the effect of mesh orientation on the rate of yielding (see Figs. 4.6(c) and 4.6(d)), it can be seen that mesh #'s 2 and 5 show a better trend in yielding than mesh #'s 1 and 4, respectively. Thus, it can be deduced that the element orientation of mesh #'s 2 and 5, (i.e. ◹) predicts a gradual rate of yielding than the element orientation of mesh #'s 1 and 4, (i.e., ◸). In Fig. 4.6(h) results obtained for mesh #'s 3, 4 and 5 are compared to study the effect of the shape of the elements on the rate of yielding. It is observed that the mesh with equilateral triangular elements shows a gradual trend for the rate of yielding than the mesh consisting of right angled triangular elements. In the same plot (Fig. 4.6(h)) curve for mesh #6 is also drawn, which gives the best trend as far as the rate of yielding is concerned.

Considering the yield patterns as the yielding progresses, Figs. A.1 to A.6 of Appendix A show that each orientation of the elements gives a distinct yield pattern. In mesh #'s 1 and 4 (see Figs. A.1 and A.4 of Appendix A) the yielding progresses in vertical strips, first downwards and then extends towards the right. In mesh #'s 2 and 5 (see Figs. A.2 and A.5 of Appendix A) and also in mesh #'s 3 and 6 (see Figs. A.3 and A.6 of Appendix A), the yielding progresses diagonally downwards starting from the V-notch. Yield patterns of mesh #6

(see Fig. A.6 of Appendix A) compare well with the yield patterns presented by Yamada et al. [32].

From Figs. A.1 to A.6 of Appendix A it can also be seen that the yield patterns obtained just before failure is somewhat similar in all the six meshes considered. Comparing the yielded area under the V-notch with the total area under the V-notch, the following is concluded: For the quarter panel considered, mesh #1 predicts the highest (18.3%) yielded area, whereas, mesh #6 predicts the lowest (13.6%) yielded area (see Table C.1 of Appendix C). Considering the total area yielded just before failure, the values in the last column of Table C.1 of Appendix C for each mesh are compared. Mesh #'s 1 and 4, mesh #'s 2 and 5, and mesh #'s 3 and 6 are compared to evaluate the effect of grading of the mesh on the total yielded area predicted just before failure. It can be seen that by decreasing the element area to about 50% the total yielded area just before failure decreases by 12%, 16% and 14%, respectively. Also comparing the values reported in Table C.1 of Appendix C for mesh #'s 3, 4 and 5 which have about the same mesh grading, it is observed that the total area yielded just before failure for these meshes is 17.2%, 15.9% and 16.6%, respectively, of the quarter specimen area. This shows that by the effect of element orientation (i.e., comparing ◪ to ◹) and the effect of element shape (i.e., isosceles

right angled triangle to an equilateral triangle) is not significant on the prediction of the total yielded area provided the mesh grading is kept the same in all the comparisons made. For the same mesh pattern a cruder mesh would predict a higher total yielded area.

Considering the effect of mesh orientation on the total yielded area predicted just before failure it can be seen by referring to Table C.1 of Appendix C that mesh #2 predicts a 8% higher value than mesh #1 and mesh #5 predicts a 4% higher value than mesh #1.

Finally, it can be concluded that a finer mesh predicts better yield patterns than a cruder mesh. Furthermore, a mesh composed of equilateral triangular elements in the expected yield zone predicts better results than the mesh composed of isosceles right angled triangular elements.

4.4.4 CPU Time

As mentioned in Chapter III, the computer program PLAST developed in this study is executed on the University of Oklahoma's IBM 3081 computer. The computer program developed by Yamada et al. [32] was run on an IBM 7090 computer. So a relative comparison of the CPU time for the execution of the two computer programs is not very appropriate. But a comparison of the CPU times taken to analyze the six meshes used in this study is

made in this sub-section. The CPU time taken to analyze these meshes by the computer program PLAST are tabulated in Table 4.4 and are categorized as follows:

(1) CPU time for initial data preparation: This includes the CPU time taken in reading of the input mesh information, setting-up of certain arrays needed to control the program execution and in the optimization of the nodal numbering scheme so as to yield a minimum half bandwidth for an input mesh.

(2) Average CPU time per load cycle: This includes the CPU time taken to compute the element stiffness matrices, assemble the system stiffness matrix, solve the resulting system stiffness equilibrium equations for nodal displacements, computation of the element incremental stresses and updating of the element total stresses in each incremental load cycle.

(3) Total CPU time for the program execution: This is the cumulative of the time taken to perform the analysis for all the load cycles till failure occurs.

From Table 4.4 it can be observed that the CPU time taken to conduct a complete failure analysis depends largely on the total number of elements used in the finite element mesh. For a finer mesh more computer time

is needed to read the input data and in setting-up of the arrays which control the program execution (for e.g., nodal degree-of-freedom numbers). In addition, at this stage the CPU time taken will also be a function of the node numbering scheme adopted for the input mesh. The computer program PLAST uses a bandwidth optimization subroutine. For an input mesh which is constructed using a grid pattern (for e.g., mesh #'s 1, 2, 5 and 6) it is easy to visualize the node numbering scheme which would yield a minimum half bandwidth of the system stiffness matrix, but that may not be the situation for other mesh patterns (for e.g., mesh #'s 3 and 6). For the six meshes studied Table 4.5 summarizes the maximum node difference, IDIFF, before (i.e., of input mesh) and after the bandwidth optimization. It can be seen that for mesh #'s 3 and 6 additional CPU time is used to renumber the input mesh nodes in order to yield a minimum half bandwidth. This is an important step to be done since the CPU time taken to solve the system equilibrium equation at each load increment will be greater if the half bandwidth is greater.

From Table 4.4 it can also be concluded that as the mesh is refined the number of load cycles needed to conduct the failure analysis increases. In the plasticity logic used to develop the computer program PLAST in each load cycle the load increment is computed so as to yield

Table 4.4 CPU Time Taken for the Execution of the Computer Program PLAST

Mesh Designation	Number of Nodes	Number of Elements	CPU Time for Input and Setting--up (sec.)	Average CPU Time Per Load Cycle (sec.)	Total Cycles Till Failure	Total CPU Time for Program Execution (sec.)
#1	98	160	3.3	2.2	23	52
#2	98	160	3.0	2.5	18	62
#3	180	320	9.5	7.2	36	287
#4	174	300	7.6	5.5	28	162
#5	174	300	7.2	5.0	25	168
#6	327	600	24.4	19.0	47	955

Table 4.5 CPU Time Taken for Input and Setting-up by Computer Program PLAST

Mesh Designation $\mathcal{N}$	Number of Nodes	Number of Elements	IDIFF Before Optimization	IDIFF After Optimization	CPU Time for Input and Setting--Up (sec.)
#1	98	160	9	9	3.3
#2	98	160	10	10	3.0
#3	180	320	98	18	9.5
#4	174	300	13	13	7.6
#5	174	300	14	14	7.2
#6	327	600	174	23	24.4

the remaining elastic elements in which the effective stress, σ_{eff}, falls within the range $0.995\ F_y \leq \sigma_{eff} \leq F_y$, where F_y is the yield stress of the material. For each of these elements, and for each of the previously yielded elements, the element stiffness matrix has to be updated to compute the incremental strains and stresses produced due to this incremental load. Thus, in this manner the yielding of the elements progresses. For a finer mesh since smaller size elements will yield in each successive load cycle so more load cycles will be needed to reach the yield pattern at failure. This was the reason that the CPU time for mesh #'s 1 and 2 is about the same (2.2 to 2.5 sec.). Similarly, the CPU time in mesh #'s 3, 4, and 5 is about the same (5.0 to 7.25 sec.). The CPU time for mesh #6 is the highest (19.0 sec.) because it has the least element area and the maximum number of elements. From Table 4.4 it can also be observed that the mesh pattern used for mesh #'s 1 and 4 (i.e., ◪) takes lesser total CPU time than the mesh patterns used for mesh #'s 2 and 5 (i.e., ◹). Looking at the effect of the shape of element it can be concluded that the use of equilateral triangular elements in the yield zone in mesh #3 increased the total CPU time to about 74% as compared to the isosceles right angled triangular elements used in mesh #'s 4 and 5, although the total number of elements and the minimum area for the three

meshes is about the same.

Finally, relating the discussion in this sub-section to that of Sub-section 4.4.1, it can be concluded that the use of a finer finite element mesh, especially with equilateral triangular elements cost more CPU time than a mesh with isosceles right angled triangular elements, but, the results converge towards the exact solution faster as the mesh is refined. So there is a trade-off between the computer cost and the degree of accuracy required.

4.5 GEOMETRY AND MATERIAL PROPERTIES FOR TEST CENTER PRE-CRACKED RECTANGULAR PANEL TENSION SPECIMEN

The center pre-cracked rectangular panel tension specimen, as presented by Miller et al. [24], and later also analyzed by Belie [3], Kumar [20] and Shammaa [31], is chosen as the numerical example to verify the computer program CRACK developed in this study. The geometry of the specimen chosen is shown in Fig. 4.7. Due to its symmetry about both the x- and the y-axis, only a quarter panel needs to be analyzed. The quarter panel and the boundary conditions thus imposed are shown in Fig. 4.8. The pre-cracked rectangular panel considered is subjected to a tensile load uniformly distributed on the edge areas. It should be noted that the nodal loads applied are parallel to the y-axis. To incorporate this type of loading necessary changes had been made in the Subroutine

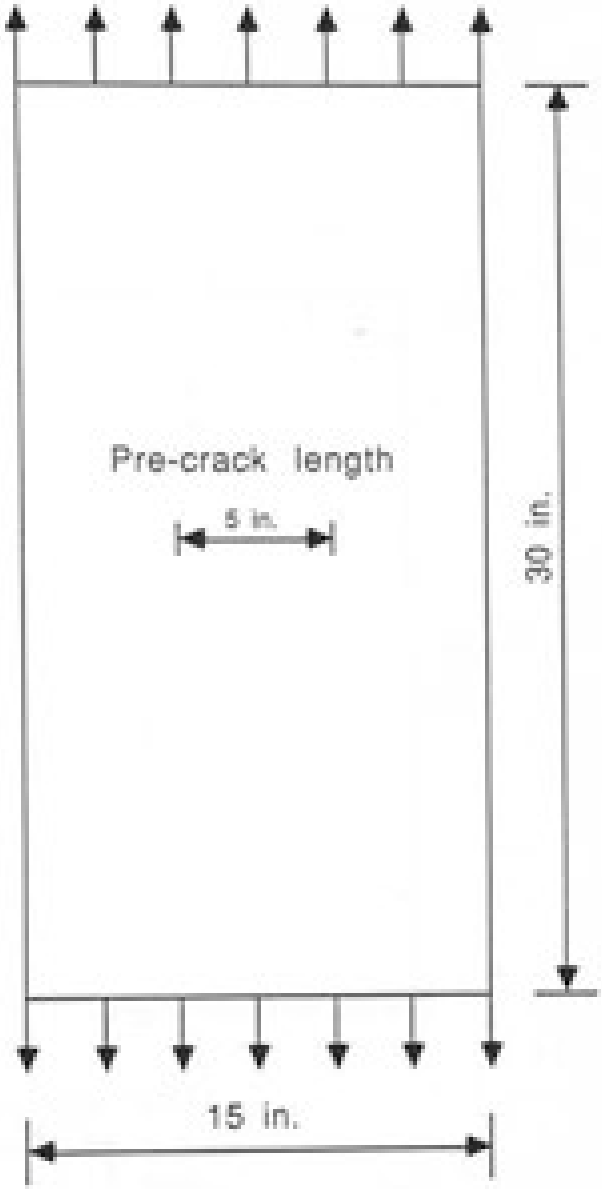

Fig. 4.7 Center Pre-Cracked Rectangular Panel Tension Specimen

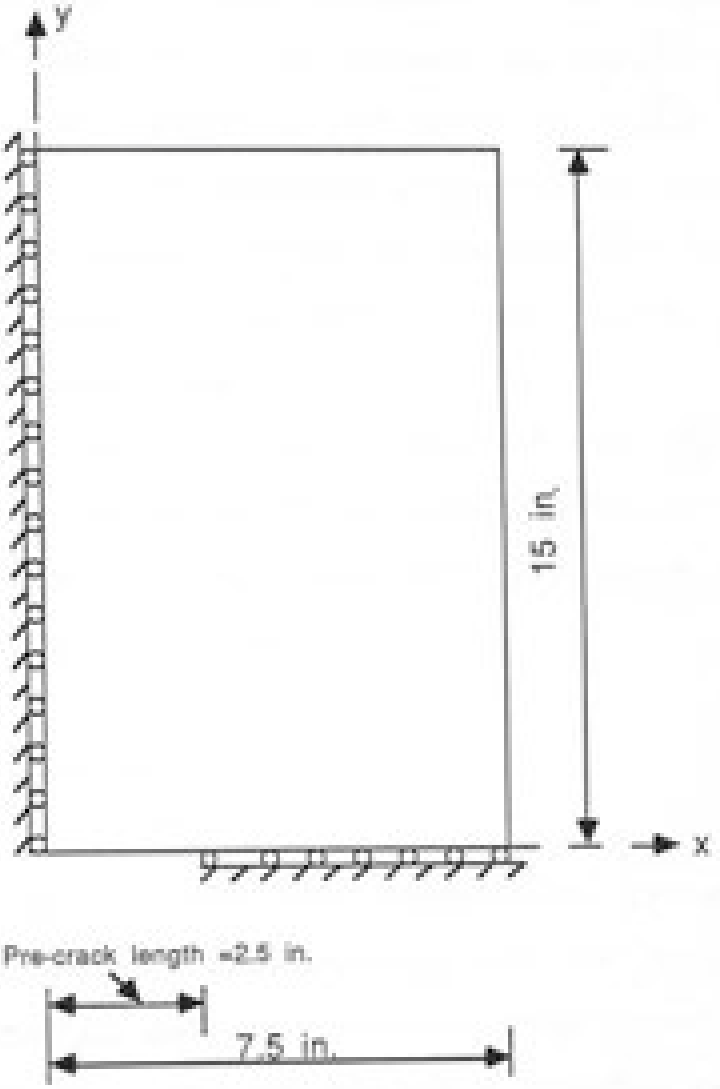

Fig. 4.8 Quarter Panel Considered For The Analysis of Center Pre-Cracked Rectangular Panel Tension Specimen

LODING, as described in Section 3.2.2 of Chapter III.

The test specimen is made of 2024-T3 aluminum. The uniaxial stress-strain curve for this material is given in Fig. 4.9. The nonlinear portion of the curve is divided into five linear segments. The values for the modulii of elasticity, the stress and strain of the end points of these segments are given in Table 4.6. The linearization of the material stress-strain curve is only needed in the present study to compute the value of the Neil's function, H' (as given by Eq. (2.72) of Chapter II), for yielded elements .

The different points selected on the material stress-strain curve are called yield points. The modulus of elasticity, E_i, for the ith linearized segment is obtained from [3, 15, 20, 31]

$$E_i = \frac{\sigma_i - \sigma_{i-1}}{\epsilon_i - \epsilon_{i-1}} \tag{4.1}$$

where σ_i and ϵ_i are the engineering stress and the engineering strain, respectively, for the ith yield point on the material uniaxial stress-strain curve. In order to compute the value of H' for a yielded element, Eq. (2.72) of Chapter II is used. In this equation the value of E is taken as E_i (as given in Table 4.6) and the value of E_t is taken as equal to E_i (as given in Table 4.6 for i = 2, 3, 4), where i denotes the segment number in which

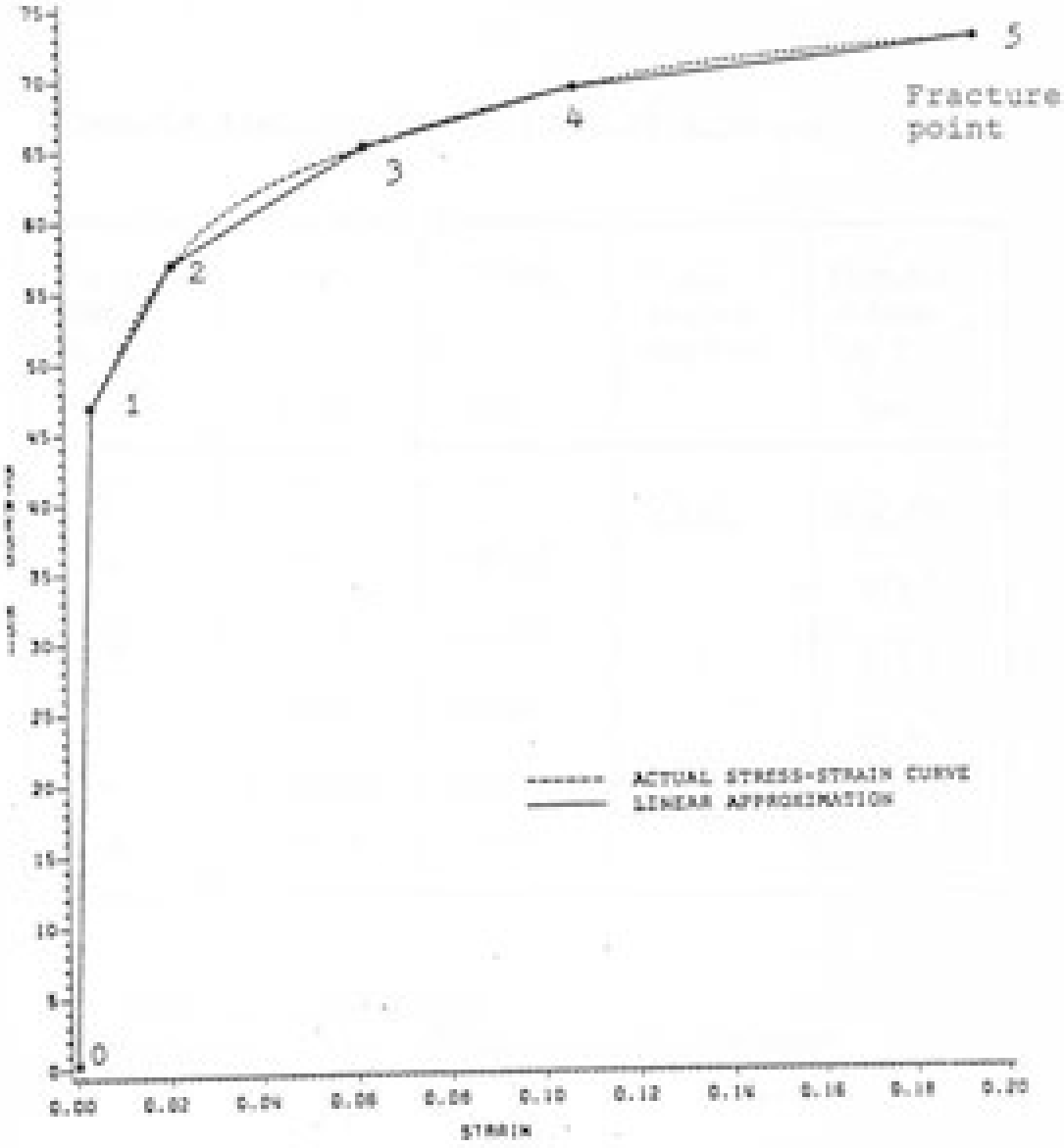

Fig. 4.9 Material Stress-Strain Curve for 2024-T3 Aluminum*

*Taken from reference [31]

Table 4.6 Material Properties of 2024-T3 Aluminum*

Yield Point Number	Strain (in./in.)	Stress (ksi)	Yield Region Number	Modulus of Elasticity, E_i** (ksi)
0	0.0	0.0	Elastic	10427.0
1	0.0045	46.923	1	579.7
2	0.02175	56.923	2	201.5
3	0.06375	65.394	3	43.5
4	0.10650	69.615	4	0.0
5	0.19500	73.462		

* Taken from reference [31]
** Subscript 'i' Denotes linearized segment number

the total effective stress ($\bar{\sigma}$) of the element falls within (i.e., $\sigma_{i-1} \leq \bar{\sigma} \leq \sigma_i$).

4.6 FINITE ELEMENT MODELING OF THE CENTER PRE-CRACKED RECTANGULAR PANEL TENSION SPECIMEN

The quarter panel shown in Fig. 4.8 is modeled using constant stress-strain triangular elements. As stated earlier, a very fine mesh is needed near the crack-tip where the yielding is expected to occur. In order to obtain a mesh configuration which has finer elements where required, the computer program developed by Shammaa [31] is used. This computer program has a moving mesh refinement capability. In this program the crude input mesh is gradually refined according to the values of the total effective stress of the yielded element. Three different finite element meshes were selected from Reference [31] to execute the computer program, CRACK, developed in this study. The minimum element areas taken for the different 'yield points' selected on the uniaxial stress-strain curve (see Fig. 4.9) for these three meshes considered are given in Table 4.7. In this table a value of minimum area equal to 999.0 indicates the fracture point on the uniaxial stress-strain curve of the material. A crude finite element mesh shown in Fig. 4.10 and the minimum areas specified in Table 4.7 were input in the computer program developed by Shammaa [31] for the ultimate fracture failure analysis. The geometric data of these

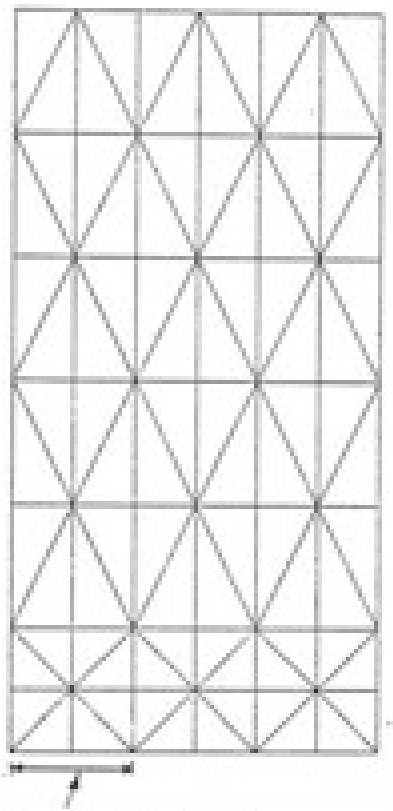

Fig. 4.10 Crude Finite Element Mesh Used to Prepare the Input Mesh Configurations for the Center Pre-Cracked Rectangular Panel Tension Specimen

Table 4.7 Minumum Element Area Required at the Yield Points Selected On the Stress-Strain Curve

Yield Point Number	Input Minimum Areas ($in.^2$)		
	For Mesh #1 **	For Mesh #1 ***	For Mesh #1 ****
0	0.781	0.781	0.781
1	0.700	0.700	0.700
2	0.700	0.100	0.100
3	0.700	0.100	0.030
4	0.700	0.100	0.010
5	0.700	0.100	0.003
6	999.0	999.0	999.0

* Taken from Reference [31]
** Shammaa's Run #2
*** Shammaa's Run #3
**** Shammaa's Run #6

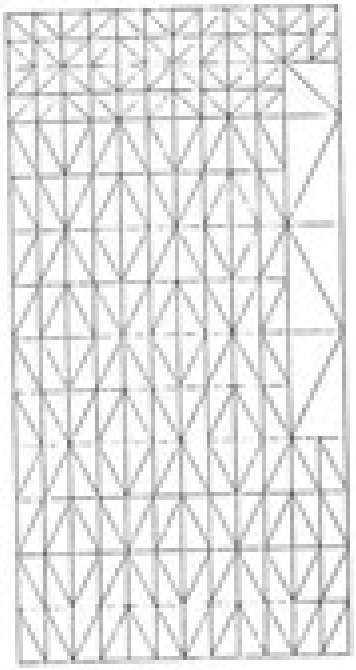

(a) Mesh #1

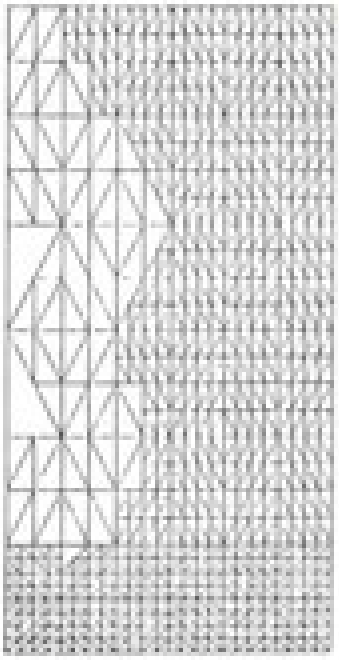

(b) Mesh #2

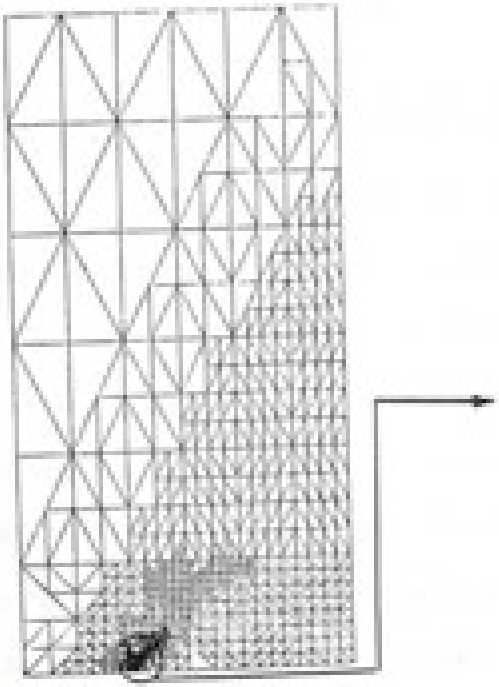

(c) Mesh #3

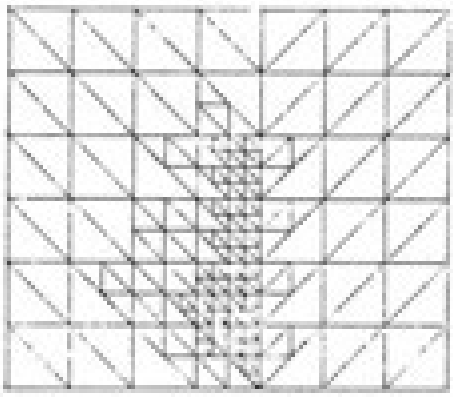

Enlarged View of the
Circled Portion

Fig. 4.11 Finite Element Meshes Considered for the Analysis of the Centre Pre-Cracked Rectangular Panel Tension Specimen

finite element meshes obtained from this computer program for each data set of Table 4.7 were saved. The three finite element meshes so obtained are taken as input meshes for the computer program CRACK developed in the present study. The details of these three meshes, called mesh #1, mesh #2 and mesh #3, are summarized in Table 4.8, and the mesh configurations are shown in Fig. 4.11.

4.7 NUMERICAL RESULTS OBTAINED FOR THE CENTER PRE-CRACKED RECTANGULAR PANEL TENSION SPECIMEN

The three input meshes, as described in Section 4.6, were analyzed using the computer program CRACK. Results for the various parameters considered are summarized in the subsequent paragraphs in this section.

4.7.1 First Yield Load and Ultimate Fracture Failure Load

The values for the first yield load and the ultimate fracture failure load, predicted by the computer program CRACK are summarized in Table 4.9 for the three meshes. In this table the results predicted by analyzing these meshes by the computer program developed by Shammaa [31] and those reported by Miller et al. [24] are also reported. Comparing the ultimate fracture failure load obtained in the present study to the experimental value reported by Miller et al. it was observed that the computer program predicted 45%, 39% and 29% higher values for

Table 4.8 Input Meshes Used In The Analysis of the Center Pre-Cracked Rectangular Panel Tension Specimen

Mesh Designation	Number of Nodes	Number of Elements	Minimum Area at the Crack Tip ($in.^2$)
#1	189	312	0.1953
#2	608	1077	0.0488
#3	977	1548	0.00005

mesh #'s 1, 2 and 3, respectively. The ultimate fracture failure load predicted by the computer program CRACK for mesh #'s 1, 2 and 3 is 31%, 23% and 11%, respectively, higher than the analytical value reported by Miller et al. Comparing the ultimate fracture failure load predicted by the present study for mesh #'s 1, 2 and 3 with mesh #'s 2, 3 and 6 of Shammaa (as referenced by Shammaa [31]), respectively, the percentage difference is +76%, +65% and +51%, respectively. Comparing the ultimate fracture failure load predicted by the computer program CRACK for mesh #3 to the ultimate fracture failure load predicted by the Shammaa's program using mesh #3 as the input mesh it is seen that the former predicts a 54% higher value than the later one.

Comparing relatively the results reported for mesh #'s 1, 2 and 3 in Table 4.9 it can be observed that mesh #1 (which has a 75% higher minimum element area than that for mesh #2) predicts a 38% higher value for the first yield load than mesh #2. And, mesh #3 (which has a minimum element area that is 976 times lower than mesh #2) predicts about a 5 times lower value for the first yield load than mesh #2. For the ultimate fracture failure load mesh #2 predicted a 12% lower and 14% higher value than mesh #'s 1 and 3, respectively.

Table 4.9 Summary of the First Yield Load And Ultimate Fracture Failure Load Predicted for the Center Pre-Cracked Rectangular PanelTension Specimen

Mesh Designation	Results Predicted by the Computer Program CRACK			Results Predicted by Shammaa's Computer Program [31]			Ultimate Fracture Failure Load Reported by Miller et al. [24]	
	First Yield Load (ksi)	Ultimate Fracture Failure Load (ksi)	Displacement at Ultimate Fracture Failure (in.)	First Yield Load (ksi)	Ultimate Fracture Failure Load (ksi)	Displacement at Ultimate Fracture Failure (in.)	Experimental (ksi)	Analytical (ksi)
#1	19.601	43.716	0.326	10.1	24.8	0.28		
#2	14.161	39.197	0.254	10.1	23.8	0.22	24.0	30.0
#3	2.877	33.839	0.089	10.1 * / 1.48 **	22.4 * / 21.9 **	0.21 * / 0.1 **		

* Using crude mesh as input mesh and gradually refining as per values indicated in the third column of Table 4.7

** Using Mesh #3 as the input mesh

4.7.2 Load-Displacement History

The load-displacement histories obtained for the finite element meshes considered are given in Figs. 4.12 and 4.13. In Figs. 4.12(a) to 4.12(c) the load-displacement histories for mesh #'s 1, 2 and 3, respectively, obtained from the computer program CRACK are compared to those obtained by the computer program developed by Shammaa [31]. It can be observed from Figs. 4.12(a) to 4.12(c) that the computer program developed by Shammaa [31] predicts lower values of loads when compared with similar results predicted by the computer program CRACK, whereas, the values obtained for displacements at the ultimate failure are about the same by the two computer programs. The main reason for this difference seems to be due to the differences in the analysis procedures adopted in the two studies. For the non-linear region of the material uniaxial stress-strain curve Shammaa performs an elastic analysis by simply changing the values of the modulus of elasticity, E, and the Poisson's ratio, ν, of the yielded elements depending on which linear segment their effective stress lies within. On the other hand, in the present study an incremental plasticity approach is used to model the behavior of the yielded elements in the nonlinear region of the material uniaxial stress-strain curve. Thus, in the present study the material behavior in the nonlinear range

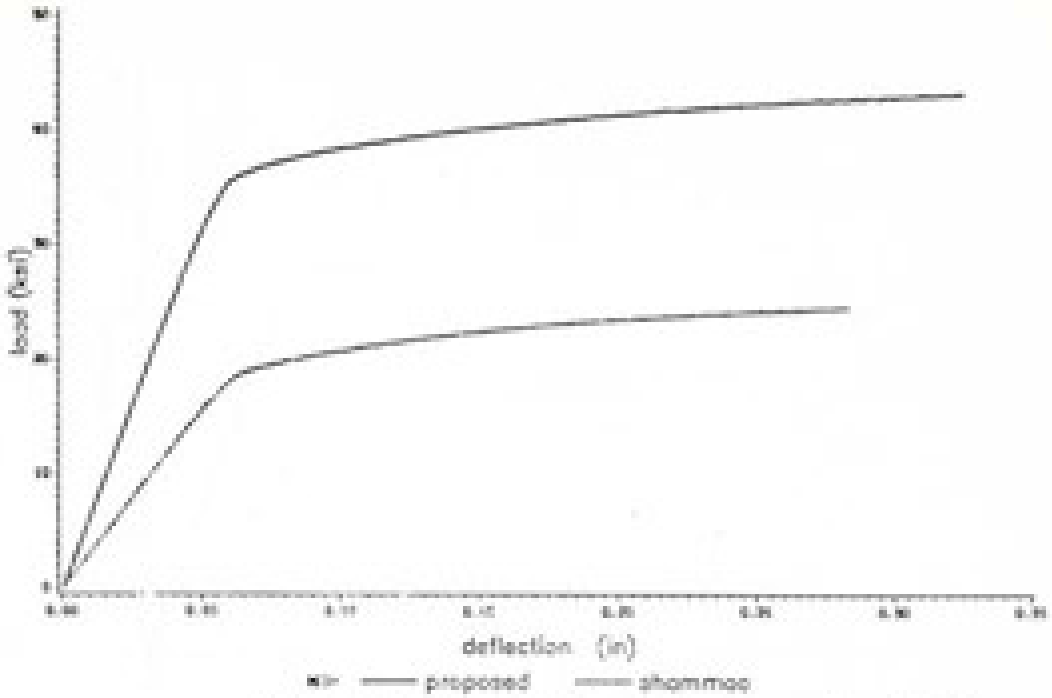

(a) Plot for mesh #1 and Shammaa's Run#2

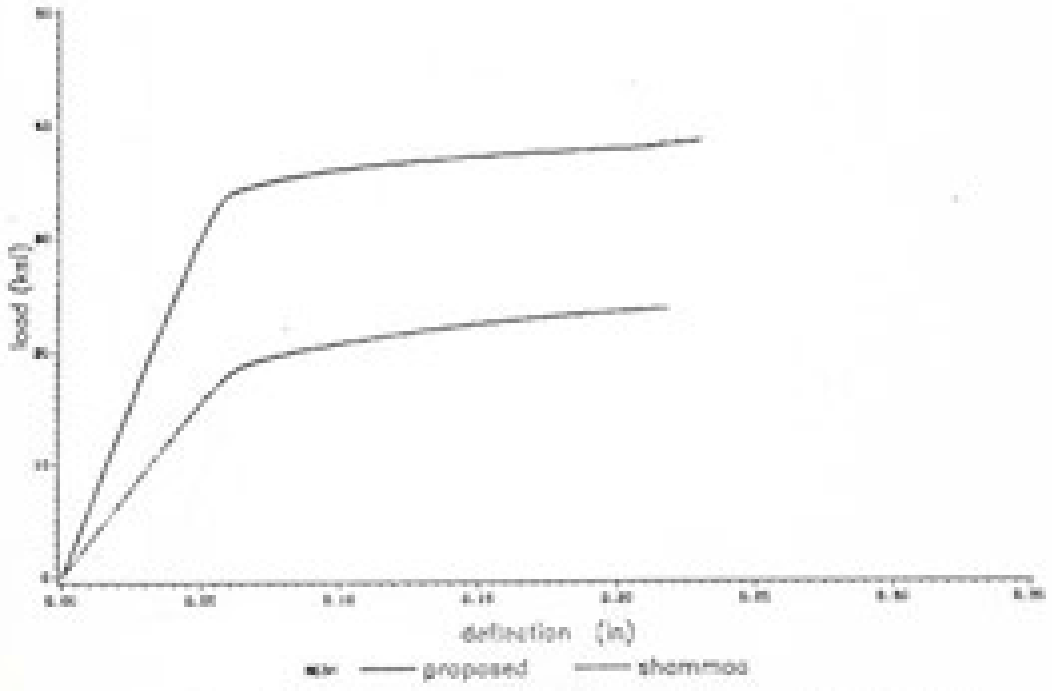

(b) Plot for mesh #2 and Shammaa's Run#3

Fig. 4.12 Load-Displacement History Comparision for the Three Meshes Analyzed my Program CRACK and by Shammaa's Program for the Center Pre-Cracked Rectangular Panel Tension Specimen

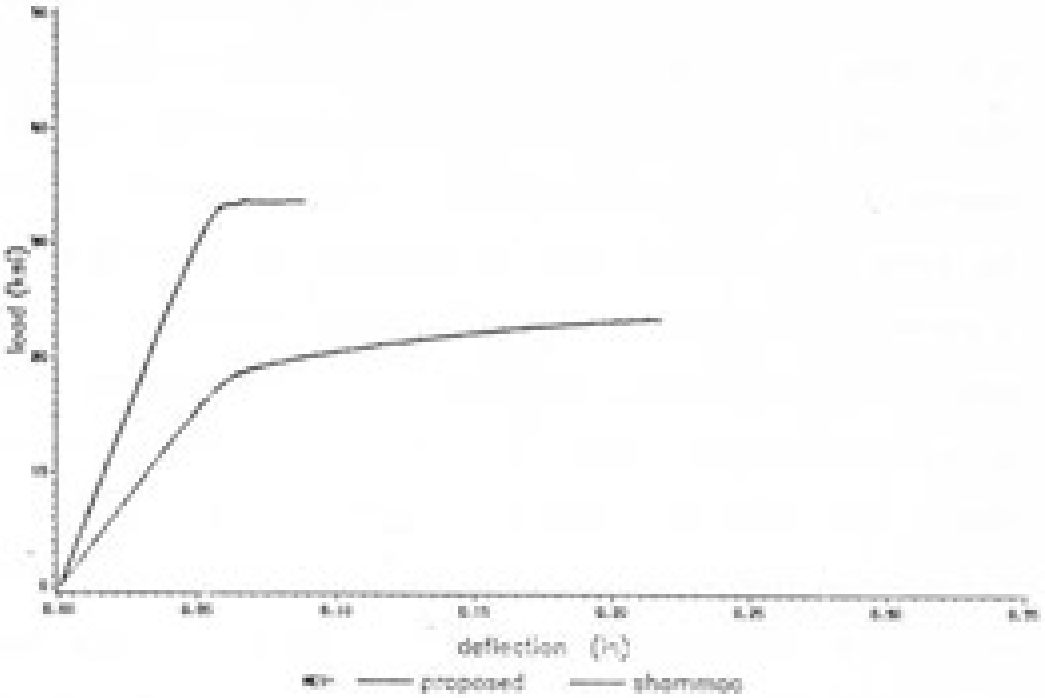

(c) Plot for mesh#3 and Shammaa's Run#6

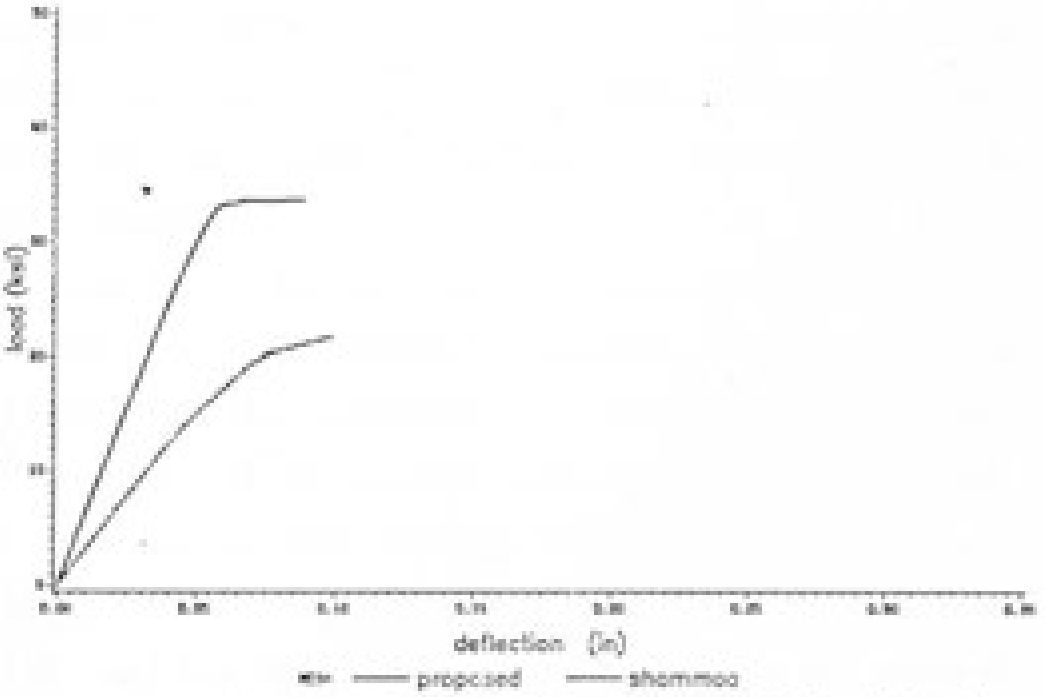

(d) Plot for mesh#3 by program CRACK and by Shammaa

Fig. 4.12 (Cont'd) Load-Displacement History Comparision for the three Meshes Analyzed By Program CRACK and by Shamma's Program for the Center Pre-Cracked Rectangular Panel Tension Specimen

is modeled more differently.

It can be observed from Fig. 4.12(c) that there is a significant difference in the failure displacement predicted by the two curves. The reason for the difference can be explained by looking at the values tabulated in Table 4.7, in which mesh #3 is obtained from Shammaa's computer program [31] by gradually refining the yielded element area from 0.7 sq. in. at first (initial) yield to 0.003 sq. in. at fracture. In Fig. 4.12(c) the load-displacement curve by Shammaa is for this gradually refined mesh, whereas, the load-displacement curve reported by the present study is the case when the final refined mesh is analyzed by the computer program CRACK. This comparison shows that the load-displacement results predicted are greatly dependent on the element area used not only for the fractured elements but also for the yielded elements. To confirm this it was decided to re-run mesh #3 (used for computer program CRACK) as the input mesh for the Shammaa's computer program and not requesting for any refinement. The load-displacement curve for this run is plotted with the load-displacement curve obtained by the present study in Fig. 4.12(d). From this figure it can be seen that using the refined mesh (as used for the present study) the computer program developed by Shammaa and that developed in this study predict similar displacement values at the ultimate

fracture failure.

In Fig. 4.13 the load-displacement histories obtained by the computer program CRACK for the three meshes analyzed are plotted and compared with the experimental result obtained by Miller et al. [24], which is shown by the horizontal line in this figure. Miller et al. have not reported any displacement results. It can be observed from this figure that all the curves have about the same slope in the linear portion. Also, it can be inferred from this figure that as the mesh is refined the failure load decreases and approaches towards the experimental value reported by Miller et al. [24].

4.7.3 Yield Patterns

The yield patterns for the meshes considered to analyze the pre-cracked rectangular panel tension specimen are given in Figs. B.1 to B.3 of Appendix B. The yielded elements are represented by the shaded area in these figures. Considering the location of the first yield it can be observed from part (a) of Figs. B.1 to B.3 of Appendix B that all the three meshes predicted the initial yield to occur in an element at the crack tip.

From Figs. B.1 to B.3 of Appendix B, it can also be observed that the yielding progresses towards the portion of the specimen above the uncracked length. The shape of the yielded zone predicted for mesh #'s 1 and 2 (see

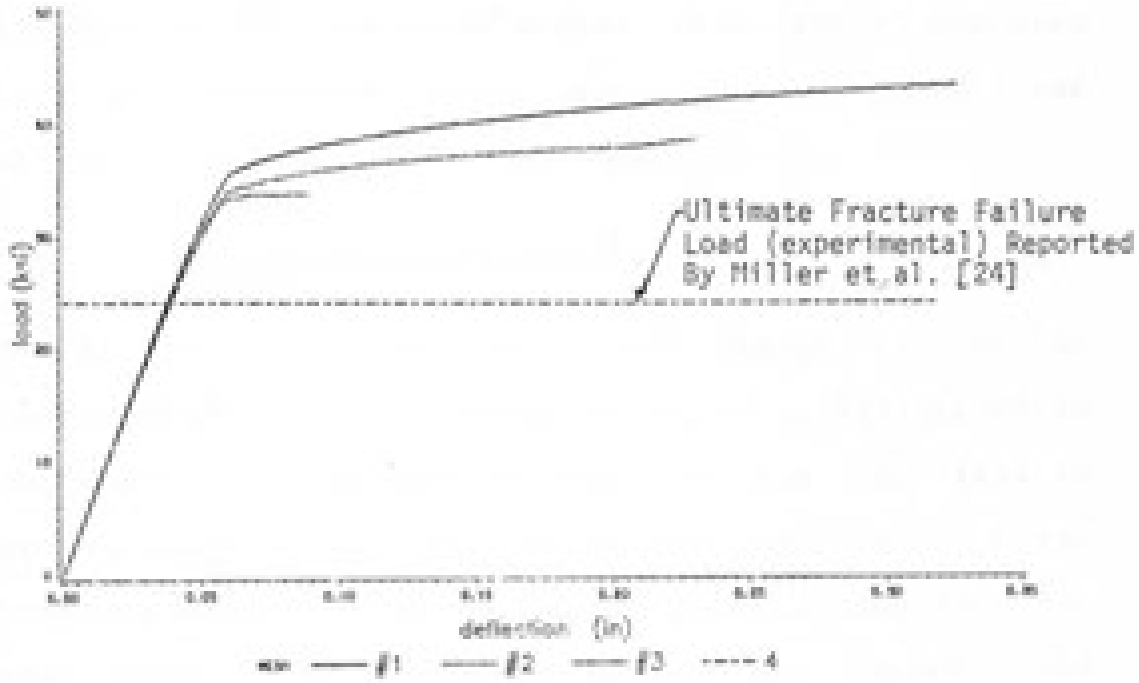

Fig. 4.13 Load-Displacement History Comparision for the Meshes Considered for the Center Pre-Cracked Rectangular Panel Tension Specimen

Figs. B.1 and B.2 of Appendix B) look somewhat similar: triangular region above uncracked length (along x-axis) yields. But the shape of the yield zone predicted for mesh #3 is different: yielding progresses diagonally upwards from the crack tip. At the ultimate fracture fracture, in all the three meshes, about 30% of the area above the uncracked length (along x-axis) yields (see part (f) of Figs. B.1 to B.3 of Appendix B).

4.7.4 Redistribution of the Energy of the Fractured Element

As discussed in Section 2.4 of Chapter II, when an element fractures it's energy has to be redistributed to the remaining unfractured system. In this study this is done by applying the negative of the nodal loads of the fractured element to the system in small increments. The nodal loads of a fractured element are computed and stored in a vector called {PNOD} in the computer program CRACK. The largest element in this vector is found and called PNMAX. The elements of the vector {PNOD} are normalized by dividing each value in this vector by PNMAX. The normalized load vector is then applied in increments to the system such that an increment of PNMAX is applied at each load redistribution step till the full load {PNMAX} is applied to the system. In the present study mesh #1 did not give any stable crack growth (i.e., before the complete nodal load level, PNMAX of the

first fractured element could be achieved another element fractured), mesh #2 and mesh #3 gave two and three stable crack growths, respectively. Figs. 4.14 and 4.15 show the load level achieved at the end of each load redistribution step for each stable crack growth for mesh #'s 2 and 3, respectively. The horizontal line in these figures shows the maximum value of the load to be achieved (PNMAX) for each fractured element. It can be observed from these figures that the desired full load level is achieved within the specified tolerance limits thus indicating that the dissipation of the energy of the fractured element into the unfractured system has been completed for each stable crack growth. It should be noted that all the meshes when analyzed by the computer program developed by Shammaa [31] predicted unstable crack growth.

4.7.5 Crack Propagation and Boundary Conditions for Each Stable Crack Growth

As mentioned in the previous sub-section, out of the three meshes considered for the analysis of the center pre-cracked rectangular panel tension specimen, mesh #1 did not give any stable crack growth, whereas, mesh #'s 2 and 3 gave two and three stable crack growths, respectively. As mentioned in Subsection 3.4.6 of Chapter III, if the fractured element is at the crack tip it's node at the crack tip (if the element node is on x-axis) is

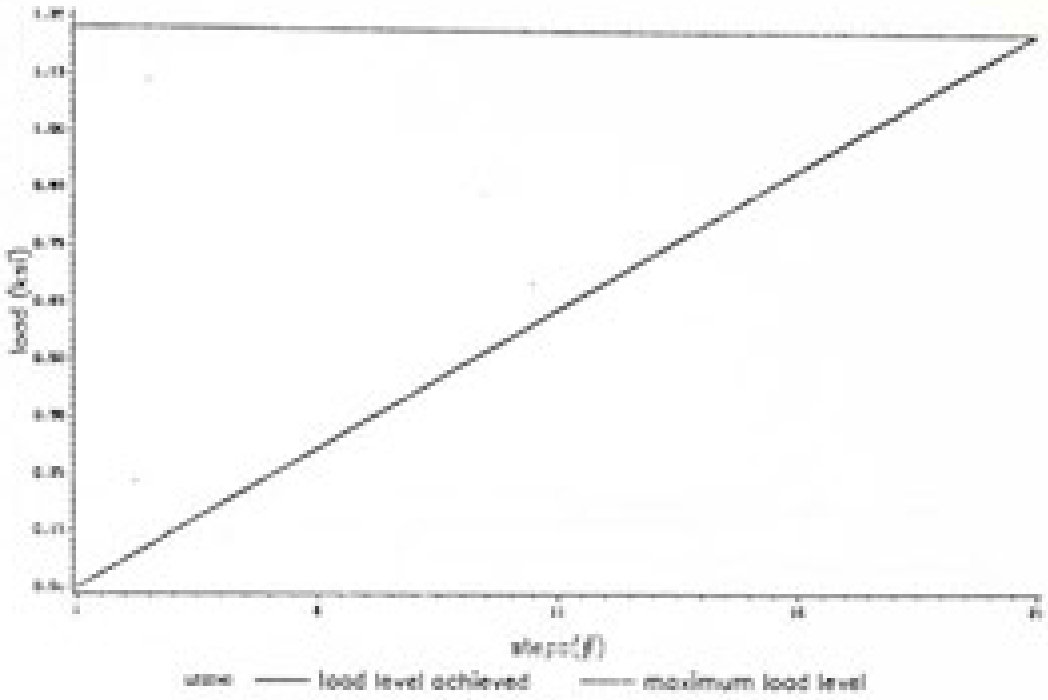

(a) For first fractured element

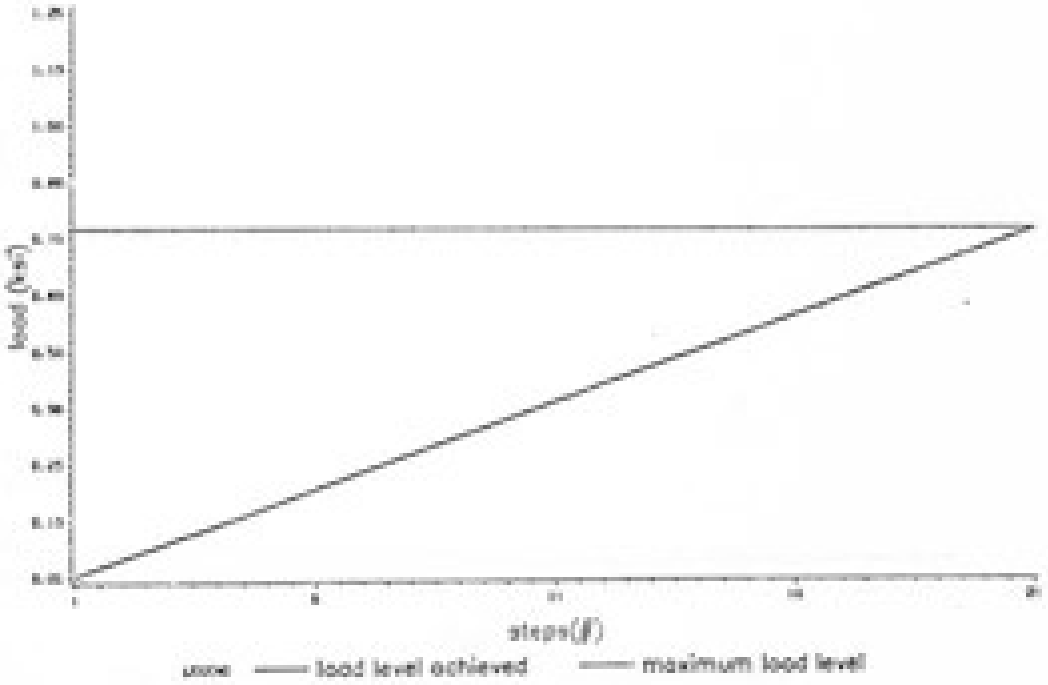

(b) For second fractured element

Fig. 4.14 Number of Load Steps Required to Redistribute the Energy of Fractured Elements For Mesh#2 Considered for the Center Pre-Cracked Rectangular Panel Tension Specimen

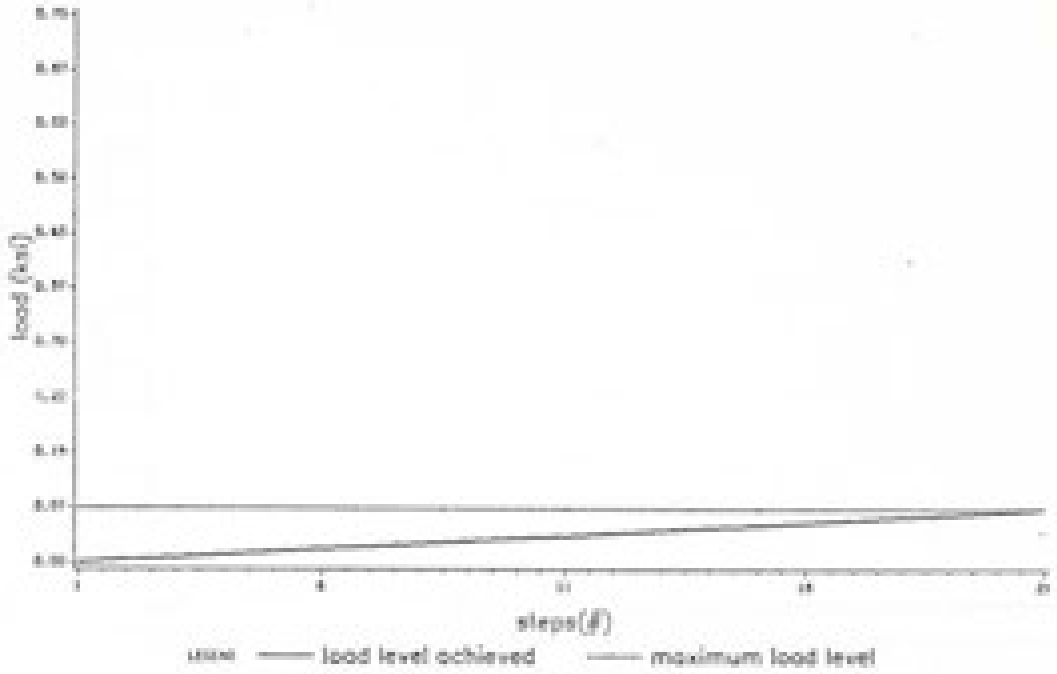

(a) For first fractured element

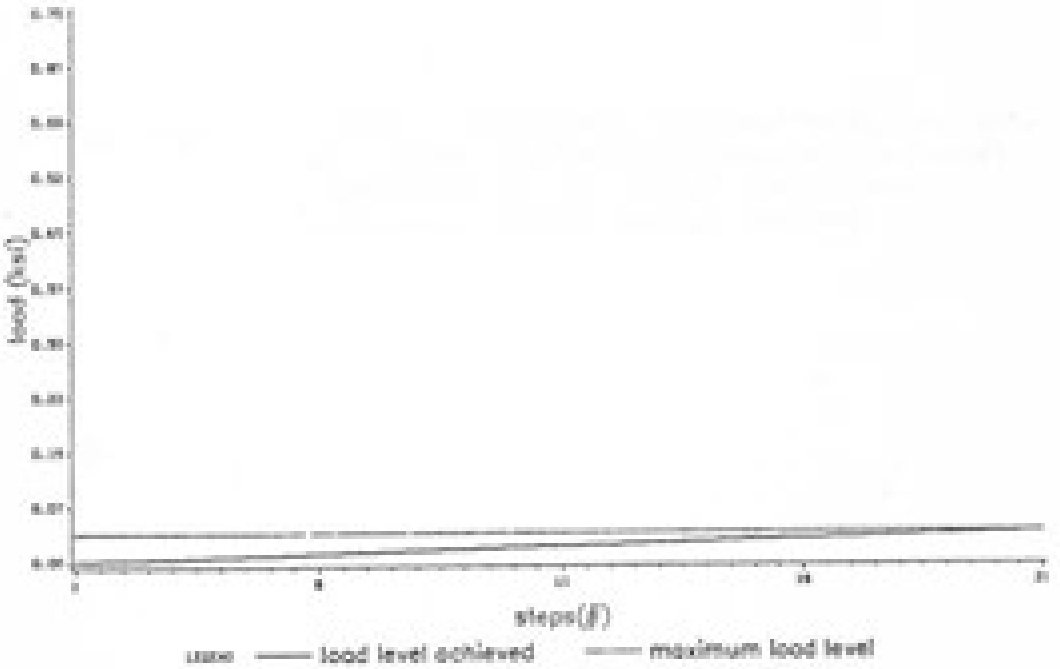

(b) For second fractured element

Fig. 4.15 Number of Load Steps Required to Redistribute the Energy of Fractured Element for Mesh #3 Considered for the Center Pre-Cracked Rectangular Panel Tension Specimen

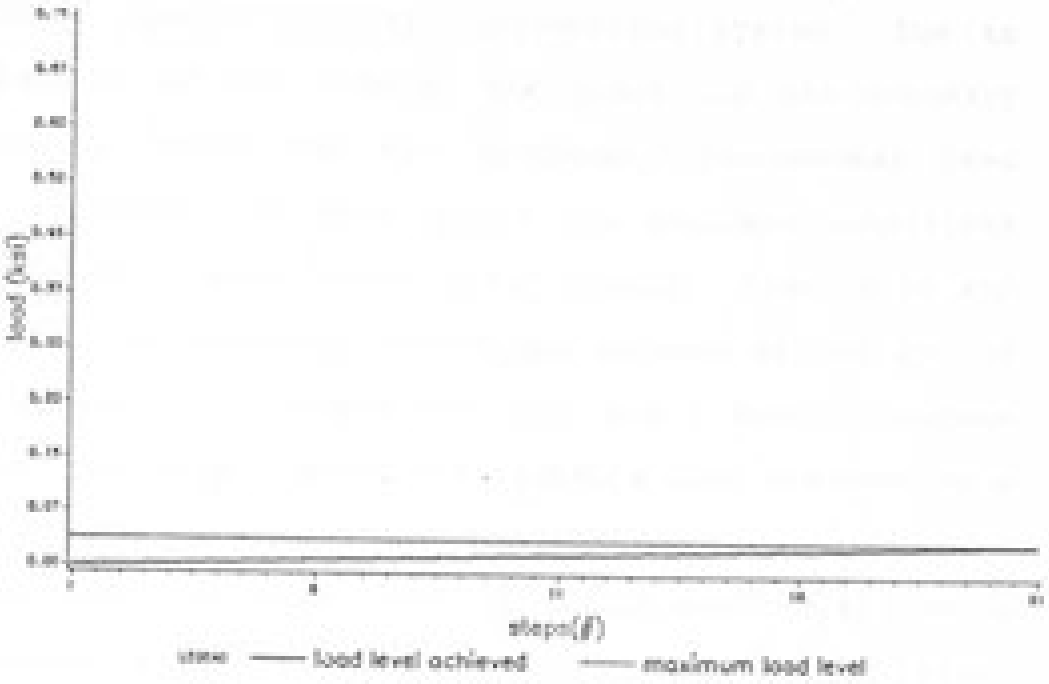

(c) For third fractured element

Fig. 4.15 (Cont'd) Number of Load Steps Required to Redistribute the Energy of Fractured Elements for Mesh#3 Considered for the Center Pre-Cracked Rectangular Panel Tension Specimen

released after the redistribution of the energy of the fractured element into the unfractured system. Due to the release of the node at the crack tip the boundary conditions change for the subsequent incremental load cycle analysis. In this manner the boundary conditions are modeled at each stable crack growth. Figs. 4.16 and 4.17 show the boundary conditions imposed at the end of each stable crack growth for mesh #'s 2 and 3, respectively. In these figures the elements that fracture have been shaded in black. It should be noted that these figures have not been drawn to scale and simply denote the results qualitatively. It can be observed from Figs. 4.16 and 4.17 that in both the meshes one node is released after the first stable crack growth and after that no other node is released until the ultimate fracture failure occurs. This is because in both the cases after the first element fractures the subsequent elements that fracture do not have a new node (i.e., a node which was not previously released) on the x-axis, which is one of the axis of symmetry. In the studies reported by Miller et al. [24] and Belie [3] for this problem, the crack length at any load level is measured up to the first roller support along the x-axis (see Figs. 4.16 and 4.17). In this study since fracturing of an element is considered rather than fracturing of a node, as done by Miller et al., it would be appro-

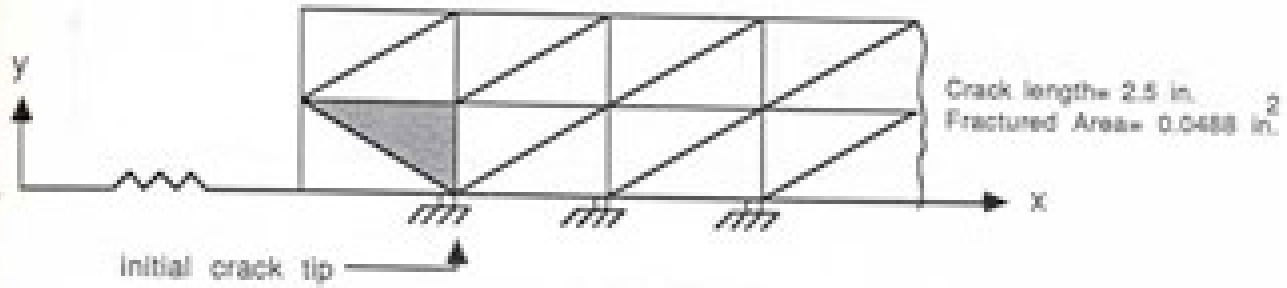

(a) Boundary Conditions at first fracture

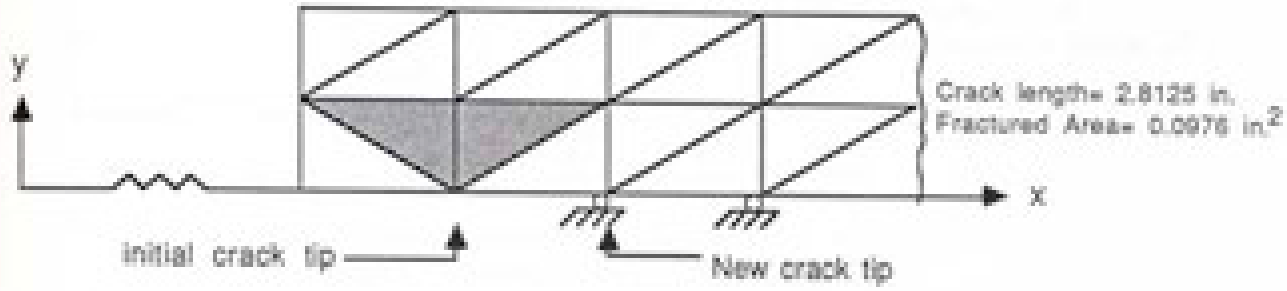

(b) Boundary Conditions after first element fractured
and before second element fractured

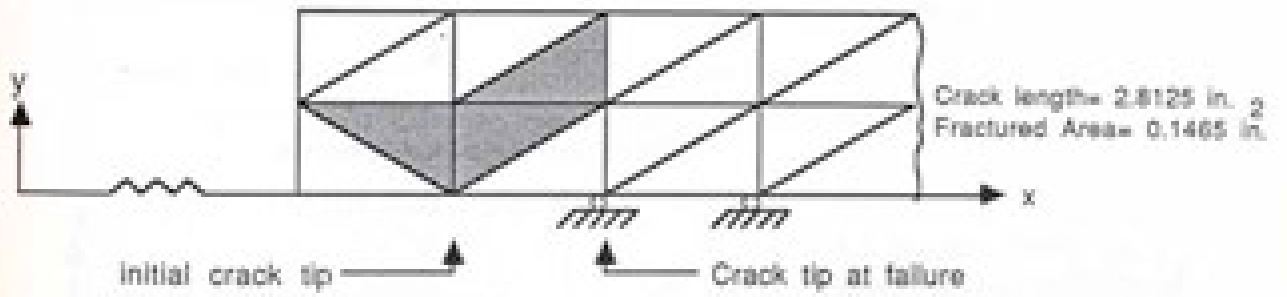

(c) Boundary Conditions at ultimate fracture failure

Fig. 4.16 Boundary Conditions For Mesh#2 for the Center Pre-Cracked Rectangular Panel Tension Specimen (Note: These Figures Are Not Drawn to the Exact Scale)

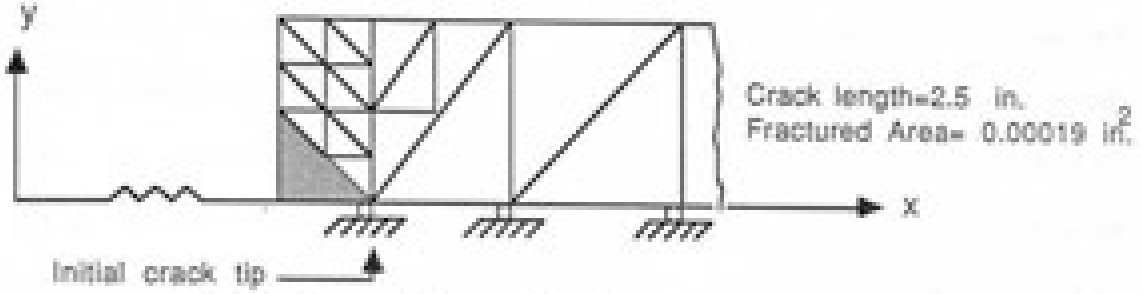

(a) Boundary condition at first fracture

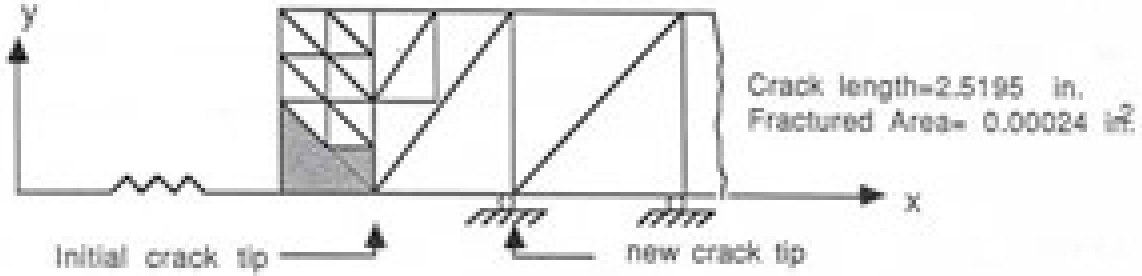

(b) Boundary condition after first element fractured and before second element fractured

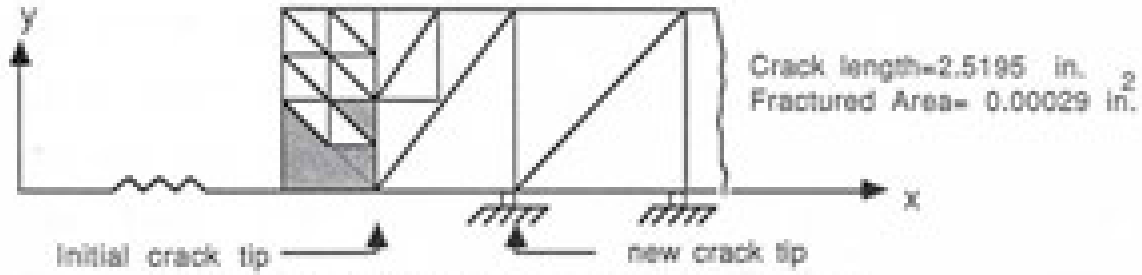

(c) Boundary condition after second element fractured and before third element fractured

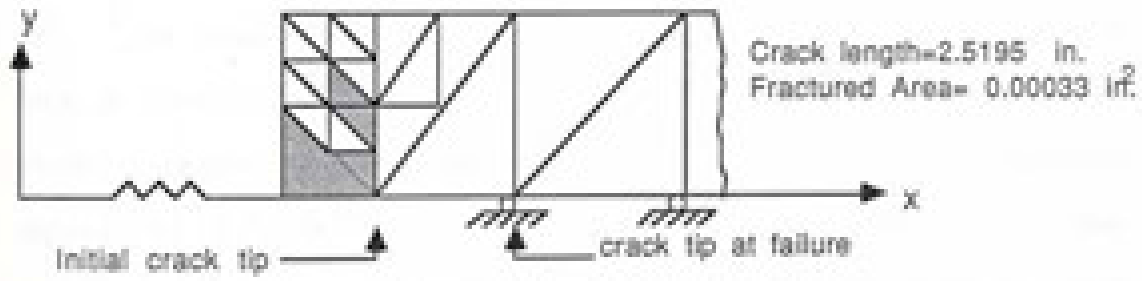

(c) Boundary condition at ultimate fracture failure

Fig. 4.17 Boundary Conditions for Mesh#3 for the Center Pre-Cracked Rectangular Tension Specimen (Note: these figures are about 1000 times bigger as compared to Fig.4.16)

priate to not only look at the propagation of the aforementioned crack length but to also consider the area of the elements that fracture. The more refined the mesh is, it should be then expected that the crack propagation path would be modeled more accurately. The results obtained for crack length and the area fractured for the three meshes analyzed in this study are shown in Figs. 4.16 and 4.17 and are also summarized in Table 4.10. These results are further explained and compared to results reported in the literature in the subsequent paragraphs of this sub-section.

As mesh #1 did not give any stable crack growth thus, there is no propagation in the crack length. For mesh #2, which gave two stable crack growths, the node at the crack tip is released after the first stable fracture, which equals to a crack propagation of about 0.3125 in. and the new crack length becomes equal to 2.8125 in. And, since after that no further node is released (see fracture path for mesh #2 in Fig. 4.17) the crack length just before ultimate fracture failure remains at 2.8125 in. The same is true for mesh #3, (see Fig. 4.17) which has a crack propagation of 0.0195 in. after the first stable crack growth and so the new crack length becomes equal to 2.5195 in., which remains the same until the ultimate fracture failure of the structure occurs (see Fig. 4.18). Belie [3] obtained a crack length of 2.766

Table 4.10 Summary of Total Load, Total Area Fractured and Crack Length At Each Successive Fracture For The Center Pre-Cracked Ractangular Panel Tension Specimen

Fracture Number	For Mesh #1			For Mesh #2			For Mesh #3		
	Total Load (ksi)	Total Area Fractured ($in.^2$)	Crack Length (in.)	Total Load (ksi)	Total Area Fractured ($in.^2$)	Crack Length (in.)	Total Load (ksi)	Total Area Fractured ($in.^2$)	Crack Length (in.)
1	43.716*	0.1953	2.5000	38.006	0.0488	2.5000	32.927	0.00019	2.5000
2	–	–	–	38.198	0.0976	2.8125	33.473	0.00024	2.5195
3	–	–	–	39.197*	0.1465	2.8125	33.772	0.00029	2.5195
4	–	–	–	–	–	–	33.839*	0.00033	2.5195

* Load at ultimate Fracture Failure

in. at ultimate fracture failure by using three noded triangular finite elements to discretize the problem. Both Shammaa [31] and Kumar [20] did not obtain any crack propagation for this problem since in their analyses the specimen failed just after the first element fracture occurred. It should be noted that all the three latter studies used "zero modulus-unload-reload" method to distribute the energy of the fractured element into the nonfractured system.

As mentioned in Sub-section 1.3 of Chapter I in the method suggested by Miller et al. [24] fracturing of a node is considered and the method is applied to model the failure along the lines of symmetry. Thus, the analysis of the center pre-cracked rectangular panel tension specimen by the method suggested by Miller et al. pre-fixes the direction of the crack propagation. In the present study since the fracture of an element is considered so the fracture path (i.e., area) is not pre-fixed.

4.7.6 Fracture Path and Load at Each Fracture

The fracture path for mesh #'s 2 and 3, drawn to scale, is shown in Figs. 4.18 and 4.19, respectively. In these figures the fractured elements are shaded in black. It can be observed from these figures that the fracture starts at the crack tip and proceeds diagonally upwards over the uncracked length. A similar fracture pattern

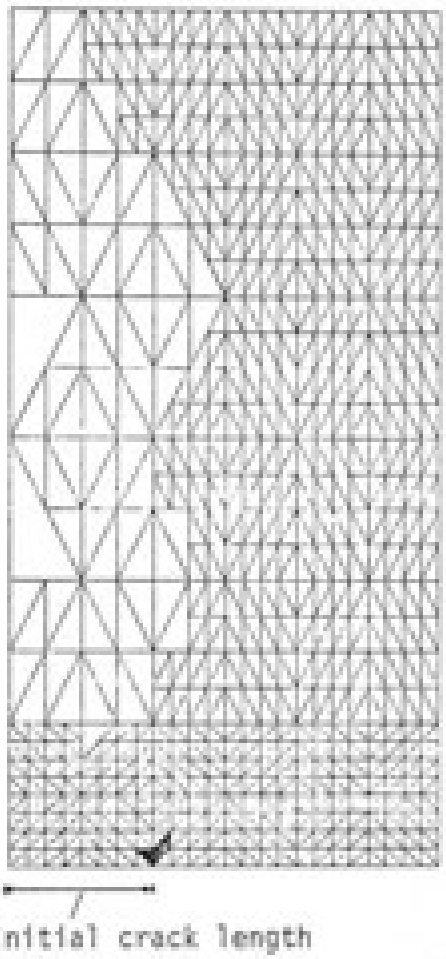

Fig. 4.B Fracture Path Predicted For Mesh#2 for the Center Pre-Cracked Rectangular Panel Tension Specimen

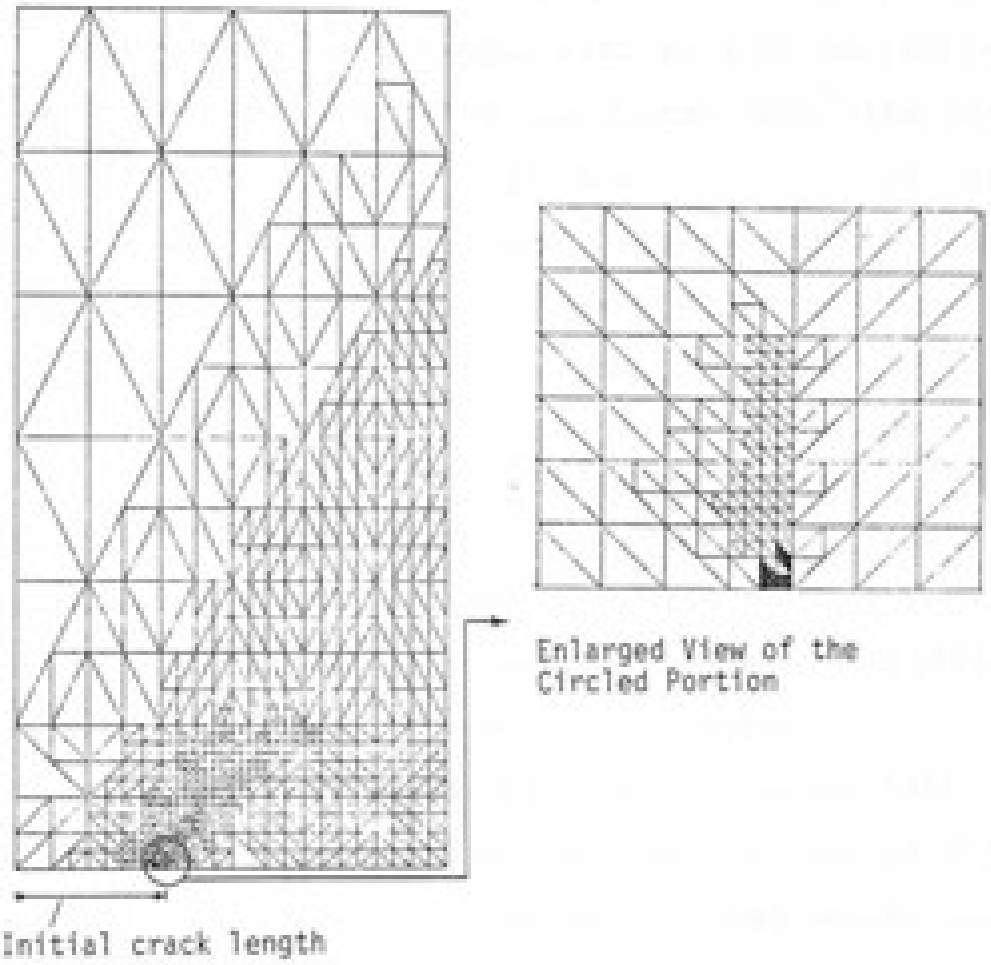

Fig. 4.19 Fracture Path Predicted For Mesh#3 for the Center Pre-Cracked Rectangular Panel Tension Specimen

has been reported by Belie [3].

The total loads as each successive element fracture occurs for mesh #'s 2 and 3 are tabulated in Table 4.10. In mesh #2 the total load increases by 0.5% and 2.5%, respectively, beyond the initial fracture load during the two successive fracture growth cycles, whereas, in mesh #3 (which is much finer that the former mesh) the total load increases by 1.63%, 0.9% and 0.2%, respectively, beyond the initial fracture load during the three successive stable fracture growth cycles.

4.7.7 Computer CPU Time

The computer CPU time taken by the three meshes analyzed by the computer program CRACK developed in the present study are summarized in Table 4.11. In this table the computer CPU time taken by the computer program developed by Shammaa [31] are also indicated.

From Table 4.11 comparing the CPU times taken by mesh #'s 1 and 2 analyzed by the computer program CRACK to the CPU times taken by executing these meshes using the computer program developed by Shammaa, it can be observed that the computer program CRACK takes 7.14% less CPU time for mesh #1 and 48.5%, i.e. more CPU time for mesh #2. In Table 4.11 for mesh #3 two CPU times are reported for executing the computer program developed by Shammaa. The first CPU time (45.0 min.) is the time

Table 4.11 CPU Time Taken To Analyze The Center Pre-Cracked Rectangular Tension Specimen

Mesh Designation	CPU Time Taken By Program CRACK (min.)	CPU Time Taken By Program Developed By Shammaa [31] (min.)
#1	4.2	4.5
#2	53.7	27.7
#3	283.4	176.0 * / 250.5 **

* Using crude mesh as input mesh and gradually refining as per values indicated in the third column of Table 4.7

** Using Mesh #3 as the input mesh

taken to analyze the crude mesh (see Fig. 4.10 and Table 4.7) and the second CPU time (250.5 min.) is the CPU time taken when mesh #3 is taken as the input mesh. Comparing the CPU time taken for analyzing mesh #3 by the computer program CRACK to the CPU time taken for analysis the similar mesh by Shammaa's computer program it is found that the latter took 11.61% less CPU time. Since the computer time and costs for mesh #3 itself were quite significant no further cases of mesh refinement were executed using the computer program CRACK. From Fig. 4.13 it can be seen that as the finite element mesh is refined for the center pre-cracked rectangular tension specimen the results predicted do show a convergent trend toward the experimental ultimate fracture failure load reported by Miller et al. [24]. Hence, it is expected that a much finer mesh than mesh #3 in the expected yield zone would predict the failure load closer to the experimental value.

CHAPTER V

SUMMARY, CONCLUSIONS AND RECOMMENDATIONS

5.1 SUMMARY

In the present study two computer programs are developed to analyze nonlinear elasto-plastic problems using the finite element method. The first computer program is called "PLAST". It's analytical formulation is developed based on the incremental plasticity theory and it has the following capabilities:

(i) Locates initiation of yielding and the initial yield load based on a selected yield criterion.

(ii) Predicts the yield patterns at different load levels of the structural system.

(iii) Predicts the failure load based on the failure criterion suggested by Yamada et al. [32], in which failure is said to occur when the incremental plastic strain becomes a negative number during any load increment.

(iv) Predicts the load-displacement history of the structure up to failure.

The second computer program developed is called

"CRACK". It is an extension of the computer program PLAST so as to possess the following additional capabilities:

(i) Locate the crack initiation and predict the path of crack propagation.

(ii) Predict stable and unstable crack growth.

(iii) Predict the load-displacement history of the structure up to collapse or ultimate fracture failure of the structure. It should be noted that the mode of failure here is defined differently than that defined by Yamada et al. [32].

(iv) Directly predict the ultimate fracture load and the corresponding deflection of the structure comprised of elasto-plastic materials.

The two computer programs are written in FORTRAN 77 for the IBM 3081 computer at the University of Oklahoma.

The first computer program PLAST uses an isotropic plasticity hardening model to march along the nonlinear portion of the material uniaxial stress-strain curve. Incremental plasticity theory and the von Mises yield criterion are used for the analytical formulation. Constant stress-strain triangular finite elements are used to discretize the structural system and small displacement theory is used to describe the strain-displacement relationships.

To start the analysis a unit load is applied to the system and the system nodal displacements are computed, which are used to compute the incremental strain and the incremental stress components for each element. The incremental effective stress for each element is then computed and the element having the maximum value of this effective stress is made to yield by setting it's effective stress equal to the material yield (initial yield) stress. The stresses of all the remaining elastic elements are scaled accordingly. Then a small assumed incremental load is applied and the analysis is carried out using the elasto-plastic material matrix, $[D^{eP}]$, for the yielded element. The system incremental nodal displacements are computed, which are used to compute the incremental strain and stress components for each element. The incremental effective stress of each element is then computed, which is used to find the most stressed elastic element, as done before. A load scaling factor is then computed such that if the assumed incremental load is multiplied by this scaling factor the most highly stressed elastic element will yield. All the incremental strain and stress components computed for the assumed incremental load are then multiplied by this scaling factor and the results are added to the strain and stress components computed at the end of the previous load cycle. This gives the total strain and stress components

for each element, which are used to compute the total effective stress of each element. Finally, the incremental plastic strain is computed for all the yielded elements as the final quantity for this load cycle. If this value is negative for any yielded element then failure due to excessive yielding is said to occur [32]. The total load at the end of this load cycle is reported as the failure load and the execution of the computer program is terminated. If the value of the incremental plastic strain is positive for all the yielded elements then the analysis proceeds with the application of the incremental load applied for the next load cycle. This process is continued till the failure of the structure occurs due to excessive yielding, as defined before in each load cycle an automated logic is encorporated in the computer program to locate the elastic elements which have a total effective stress, $\bar{\sigma}_{eff}$, less than or equal to 99.5% F_y and yield them all together by setting their total effective stress equal to the material yield stress, F_y. This is done simply to speed up the program execution.

In the computer program CRACK the failure criterion suggested by Yamada et al. [32] is removed and replaced by the criterion that if the effective stress of an element computed based on von Mises theory becomes equal to the fracture stress of the material then that element

will be considered to have fractured. Thus, the analysis is carried out on similar lines, as described for the computer program PLAST, until the total effective stress of an element becomes equal to the material fracture stress. Before application of any further load the strain energy of this element has to be redistributed into the remaining unfractured elements. This is done by using an "element nodal load release" method, in which the negative of the nodal loads of the fractured element are applied to the system in increments till the full load levels are achieved. This would prestress the remaining unfractured elements in the vicinity of the fractured element. This procedure is described in the subsequent paragraph.

In the "element nodal load release" method first the nodal loads of the fractured element are computed and an array containing the negative of these nodal loads is formed. This array is normalized with respect to the maximum value in the array, say PNMAX. The system load vector is assembled using this normalized array and considering that these loads are only acting at the nodal degrees-of-freedom of the fractured element. A small increment of PNMAX is applied to the system (without application of any external loads). The system stiffness matrix is assembled such that the fractured element is not considered in the assembly. The system stiffness

equilibrium equations, so obtained, are solved for the system nodal displacements, which are used to compute the incremental stress components for each element. These are added to the total stress components which were computed at the end of the previous load cycle (i.e., when fracture occurred) to give the total stress components for each element for the current load cycle. The total effective stress for each element is then computed. All the yielded elements having their total effective stress for the current load cycle less than their total effective stress at the end of the previous load cycle are called unloading yielded elements. If there is any such unloading yielded element present then that load redistribution cycle is discarded and the system stiffness matrix is reassembled using the elastic element stiffness matrix for such elements. The analysis is repeated using this new system stiffness matrix and the previous system load vector. To decrease computer costs this procedure of checking for unloading yielded elements is performed for a pre-fixed (say four) number of iteration cycles with the expectation that by the end of these iteration cycles the unloading yielded elements will start picking up the stress and become loading elements (which they should be). The total load achieved by the fractured element is then computed by adding the increments of PNMAX applied. The energy redistribution is said to be

completed when the total load achieved by the fractured element becomes equal to the PNMAX, within some allowable tolerance limit. Further external load increments are then applied until another element fractures. Again the strain energy of this element is redistributed into the remaining unfractured system. Unstable crack growth is said to occur if another element fractures before the strain energy of a fractured element has been completely redistributed into the unfractured system. The total load at this stage is reported as the ultimate fracture failure load of the system and the execution of the computed program is terminated.

The computer program PLAST is verified for the V-notched tension specimen presented by Yamada et al. [32]. The computer program CRACK is verified for the center pre-cracked rectangular panel tension specimen, presented by Miller et al. [24] and which has been also analyzed by Belie [3], Kumar [20] and Shammaa [31].

5.2 CONCLUSIONS

The following conclusions are drawn by using the computer program PLAST for the analysis of the V-notched tension specimen:

(1) The computer program predicted results for initial yielding, load-displacement history and failure load due to excessive yielding that

compared very well with the results reported by Yamada et al. [32].

(2) The computer program was also successfully verified to ascertain the effect of the use of the three-noded triangular finite elements, as far as mesh grading, orientation and shape of elements are concerned, on the prediction of the results. Three mesh patterns (orientation and shape of element are kept the same in a mesh pattern only mesh grading is changed) were adopted to analyze the test V-notched tension specimen. The following conclusions are drawn:

(a) In each case, as expected, a coarser mesh predicted a higher value of the failure load than a finer mesh. Keeping the mesh pattern the same as a mesh is refined the load-displacement history shows an upper bound convergence trend.

(b) For the same order of mesh grading it was found that a mesh containing equilateral triangular shaped elements in the expected yield zone predicted better results for failure load and yield patterns. However, the computational cost for such a mesh would generally be greater than the mesh obtained by joining the diagonals of a

grid. This is due to the fact that the half bandwidth of the system stiffness matrix for a mesh containing equilateral triangular shaped elements would usually be larger.

(c) The choice of the shape and the orientation of the triangular elements in the yield zone have a greater effect on the results predicted by a coarser mesh. This effect was observed to be more significant for the maximum displacement predicted just before failure rather than the load level predicted at failure. Thus, it is recommended that if a coarser mesh has to be used, based on limitations of computational costs, the use of equilateral triangular elements in the expected yield zone may be a better choice to obtain more accurate results.

(d) Due to mesh refinement, in the limit, the load-displacement history predicted by different mesh patterns would tend to converge towards the same answers.

The following conclusions are drawn by using the computer program CRACK for the analysis the center precracked rectangular panel tension specimen:

(1) The computer program PLAST when extended to perform fracture analysis gave satisfactory results for prediction of initial fracture, stable crack growth and load-displacement history up to ultimate fracture failure. To extend the program PLAST to predict crack initiation the yielding failure criterion suggested by Yamada et al. [32] was removed and replaced by the criterion that if the effective stress of an element, computed based on von Mises yield theory, becomes equal to the fracture stress then the element would be considered to have fractured. This failure criterion predicted results that compared with the analytical results reported by Miller el al. [24], Belie [3], Kumar [20] and Shammaa [31] for the same problem.

(2) As the mesh in the expected yield zone was refined the load-displacement history predicted showed an upper bound convergence trend. In this study the problem was analyzed for only three mesh gradings, due to high computer costs involved (the crudest mesh took about 4 minutes of computer CPU time and cost $56, whereas, the finer mesh took about 283 minutes of computer CPU time and cost $3,962). It is expected that

the results would have improved more (especially the prediction of the failure load level) if the area of the yielded elements in the mesh was decreased further. The finest finite element mesh analyzed by the computer program CRACK predicted 29% higher ultimate fracture failure load as compared to the experimental value reported by Miller et al. [24].

(3) The level of grading of the mesh in the expected yield zone significantly effects the value predicted for the maximum displacement at failure. Both the computer programs, i.e., the computer program CRACK developed in this study and the moving mesh refinement computer program developed by Shammaa [31], predicted a higher value for a cruder mesh relative to that predicted by a finer one. However, it was observed that if the gradual mesh refinement option is implemented using Shammaa's computer program then a much larger (for the mesh #3 in this study it was found to be twice as large) maximum failure displacement value is sometimes obtained, relative to the value predicted if the mesh was refined such that the area of each yielded element (i.e., at first yield) is equal to the desired fracture element area. Thus, it

may be desirable to refine the input coarser finite element mesh such that when any element yields for the first time then it is sub-divided (i.e., it is refined) such that the minimum sub-elemental areas inside this element become equal to the minimum element area for the fractured element. The smaller the area adopted, the more accurately the fracture path would be modelled.

(4) A significant difference is observed between the load-displacement histories predicted by the computer program CRACK and that predicted by executing the computer program developed by Shammaa [31] for the same mesh. The reasons for this difference can be attributed to the difference in the modeling of the material behavior in the nonlinear range of the uniaxial material stress-strain curve and the procedure adopted to redistribute the energy of the fractured element into the unfractured system. Shammaa approximated the material uniaxial stress-strain curve of linear segments with each segment material properties being unique, defined by its modulus of elasticity, E_i (= slope of the segment), and its Poisson's ratio, ν_i. Thus, during any incremental load cycle

Shammaa performs an elastic analysis by simply changing the values of the modulus of elasticity, E_i, and the Poisson's ratio, ν_i, of the yielded elements depending on which linear segment their effective stress lies within. On the other hand, in the present study an incremental plasticity approach and von Mises yield criterion are used to model the behavior of the yielded elements in the nonlinear region of the uniaxial material stress-strain curve. Thus, in the present study the material behavior in the nonlinear range is modeled differently.

(5) The fracture mechanics computer program developed in this study predicted stable crack growth for two of the meshes for which Shammaa's [31] method failed to do so. In the "element nodal load release" method presented the energy of the fractured element is gradually re-distributed into the unfractured system within the specified error limits.

(6) In the formulation presented by Miller et al. [24] fracture of a node is modeled such that the crack is propagated in a pre-fixed direction. On the other hand, in the present study since the fracturing of an element is con-

sidered, so the fracture path (i.e., area) is not pre-fixed.

5.3 RECOMMENDATIONS

The following recommendations are made for the extensions of the study presented in this thesis:

(1) In the incremental plasticity model implemented in this study the tangential stiffness at the beginning of the load increment is used to compute the element stiffness matrix of the yielded elements. This would produce some disbalance in the system equilibrium equations and this error would accumulate as the number of incremental load steps increases. In the problems analyzed, since the load increments were computed to be very small this error was not much. But this may not be the case for all problems. So, it may be appropriate to incorporate an iterative logic to update the element stiffness matrix of the yielded elements such that during each load analysis cycle the disbalance is within some specified tolerance. This, of course, would increase computer the costs in order to gain accuracy.

(2) A general kinematic hardening model should be incorporated, which accounts for both expansion

and translation of the yield surfaces. Also, apply these for different failure theories, for e.g., von Mises, St. Venant, Tresca, Mohr Coulomb, etc.

(3) Incorporate a library of two- and three-dimensional finite elements in the computer program, such as, four- and eight-noded two-dimensional quadrilateral isoparametric elements, three-dimensional eight-noded isoparametric brick elements, etc.

(4) Incorporate the effects of changes in thickness and temperature.

(5) Extend the analysis to model the behavior of structural systems which have more than one crack present. Modeling of opening and closing of such cracks, depending on the level, should be considered.

BIBLIOGRAPHY

[1] Armen, H. Jr., Isakson, G. and Pifko, "Discrete Element Methods for the Plastic Analysis of Structures Subjected to Cyclic Loading", International Journal for Numerical Methods in Engineering, Vol. 2, 1970, pp. 189-206.

[2] Barsoum, R.S., "A Convergent Method for Cyclic Plasticity Analysis With Application to Nuclear Components", International Journal for Numerical Methods in Engineering, Vol. 6, 1973, pp. 227-236.

[3] Belie, R.G., "Fracture Prediction in Plane Elasto-Plastic Problems by the Finite Element Method", a dissertation submitted to the University of Oklahoma, Norman, 1978, in partial fulfillment of the requirements for the degree of Doctor of Philosophy.

[4] Bert, C.W., Mills, E.J., and Hyler, W.S., "Effect of Variation in Poisson's Ratio on Plastic Tensile Instability", Journal of Basic Engineering, Trans. AMNE, Vol. 890, 1967, pp. 35-39.

[5] Carey, G.F., "A Mesh-Refinement Scheme for Finite Element Computations", Computer Methods in Applied Mechanics and Engineering, Vol. 7, Jan. 1976, pp. 93-105.

[6] Carey, G.F., "Adoptive Refinement and Non-Linear Fluid Problems", Computer Methods in Applied Mechanics and Engineering, Vol. 17/18, March 1979, pp. 541-560.

[7] Carey, G.F. and Humphrey, D.L., "Mesh Refinement and Iterative Solution Methods for Finite Element Computations", International Journal for Numerical Methods in Engineering, Vol. 6, No. 3, 1973, pp. 345-356.

[8] Collins, R.J., "Bandwidth Reduction by Automatic Renumbering", International Journal for Numerical

Methods in Engineering, Vol. 6, No. 3, 1973, pp. 345-356.

[9] Dafalias, C.P. and Popov, M.N., "A Model of Nonlinearity Hardening Materials for Complex Loading", Acta Mechanica, Vol. 21, No. 3, 1975, pp. 173-192.

[10] Dodds, R.H., Jr., Read, D.T., and Wellman, G.W., "Finite-Element and Experimental Evaluation of th J-integral for Short Cracks", Fracture Mechanics: Fourteenth Symposium - Volume I: Theory and Analysis, ASTM STP 791, J.C. Lewis and G. Sines, Eds., American Society for Testing and Materials, 1983, pp. I-520-I-542.

[11] Duwez, P., "On the Plasticity of Crystals", Physical Review, Vol. 47, 1935, pp. 494-501.

[12] Hill, R., The Mathematical Theory of Plasticity, 1st ed., Oxford University Press, Oxford, England, 1950, pp. 14-45.

[13] Hoffman, O., and Sachs, G., Introduction to the Theory of Plasticity for Engineers, 1st ed., McGraw-Hill Book Company, 1953, pp. 43-54.

[14] Hussain, M.A., Coffin, L.F., and Zaleski, K.A., "Three Dimensional Singular Element," Computers and Structures, Vol. 13, No. 4, 1981, pp. 595-599.

[15] Iranmanesh, Abbas, "A Finite Element Fracture Mechanics Program for Plane Plastic Deformation in Solids," a thesis submitted to University of Oklahoma, Norman, 1982, in partial fulfillment of the requirements for the degree of Master of Science.

[16] Iwan, W.D., "On A Class of Models for the Yielding Behavior of Continuous and Composite Systems," Journal of Applied Mechanics, Vol. 34, Sept. 1967, pp. 612-617.

[17] Johnson, W. and Mellor, P.B., Engineering Plasticity, 2nd ed., Ellis Horwood Limited, 1983, pp. 80-87.

[18] Kalev, I. and Gluek, J., "Finite Element Analysis for Cyclic Plasticity," Journal of the Engineering Mechanics Division, Feb. 1977, pp. 189-201.

[19] Karabin, M.E., Jr. and Swedlow, J.L., "Path

Dependance of J in Three Numerical Examples," Fracture Mechanics, ASTM STP 677, C.W. Smith, Ed., American Society for Testing and Materials, 1979, pp. 600-613.

[20] Kumar, A., "A Finite Element Structural Analysis Computer Program for Fracture Prediction in Three-Dimensional Elasto-Plastic System," a thesis submitted to University of Oklahoma, Norman, 1984, in partial fulfillment of the requirements for the degree of Master of Science.

[21] Levy, S., "3-D Isoparametric Finite Element Program," Report No. 71-C-191, General Electric Technical Information Series, 1971.

[22] Lynn, C.M., "A New J-Integral Approach", Computers and Structures, Vol. 9, No. 5, 1977, pp. 655-659.

[23] Marcal, P.V. and King, I.P., "Elastic-Plastic Analysis of Two-Dimensional Stress Systems by the Finite Element Method," International Journal of Mechanics and Science, Vol. 9, 1967, pp. 143-155.

[24] Miller, R.E., Jr., Backman, B.F., Hansteen, H.B., Lewis, C.M., Samuel, R.A., and Varanasi, S.R., "Recent Advances in Computerized Aerospace Structural Analysis and Design," Computers and Structures, Vol. 7, pp. 315-326.

[25] Mróz, Z., "On the Description of Anisotropic Workhardening," Journal of Mechanics and Physics of Solids, Vol. 15, 1967, pp. 163-175.

[26] Mróz, Z., "An Attempt to Describe the Behavior of Metals Under Cyclic Loads Using a More General Workhardening Model," Acta Mechanica, Vol. 7, 1969, pp. 199-212.

[27] Nadai, A., Theory of Flow and Fracture of Solids, Vol. 1, 2nd ed., New York: McGraw-Hill, 1950, pp. 379-387.

[28] Nayak, G.C. and Zienkiewicz, O.C., "Elasto-Plastic Stress Analysis, A Generalization for Various Constitutive Relations Including Strain Softening," International Journal for Numerical Methods in Engineering, Vol. 5, No. 1, 1972, pp. 113-135.

[29] Prager, W., "The Theory of Plasticity: A Survey of Recent Achievements," James Clayton Lecture,

Proceedings of the Institution of Mechanical Engineers, Vol. 169, 1955, pp. 41-57.

[30] Rolfe, S.T. and Barsom, J.M., Fracture and Fatigue Control in Structures, 1st ed., Prentice-Hall, Inc., New Jersey, , pp.

[31] Shammaa, A.H., "Crack Propagation Using a Moving Finite Element Mesh Refinement Scheme," a thesis submitted to the University of Oklahoma, Norman, 1984, in partial fulfillment of the requirements for the degree of Master of Science.

[32] Yamada, Y., Yoshimura, N., and Sakurai, T., "Plastic Stress-Strain Matrix and Its Application for the Solution of Elastic-Plastic Problems by The Finite Element Method", International Journal of Mechanics and Science, Vol. 10, 1968, pp. 343-354.

[33] Yang, T.Y., Finite Element Structural Analysis, 1st ed., Prentice-Hall, Inc., New Jersey, 1986, pp. 254-265.

[34] Ziegler, H., "A Modification of Prager's Hardening Rule," Quarterly of Applied Mathematics, Vol. 17, No. 1, 1959, pp. 55-65.

[35] Zienkiewicz, O.C., The Finite Element Method, 3rd ed., McGraw-Hill Book Company (UK), 1977, pp. 30-37.

APPENDIX A

Yield Patterns for the Test V-Notched Tension Specimen

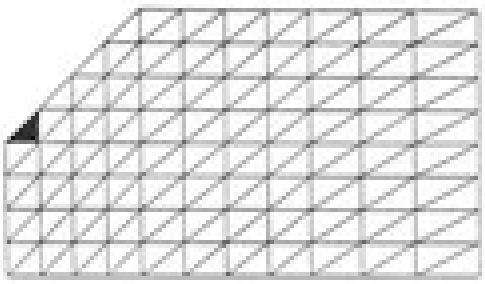

(a) At Initial Yield= 4.6.8 kg.

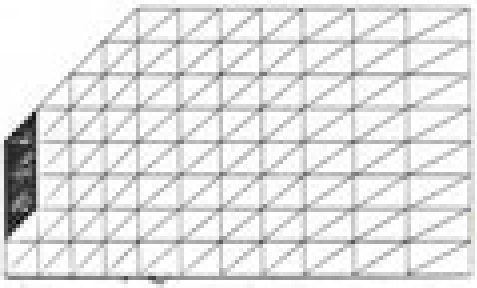

(b) At Load = 718.5 kg.

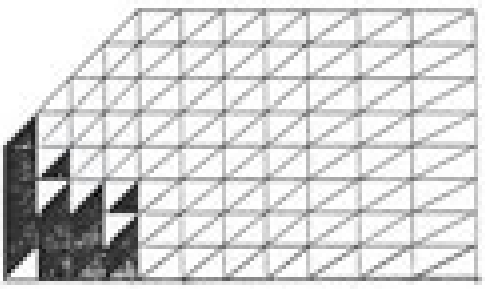

(c) At Load = 764.7 kg.

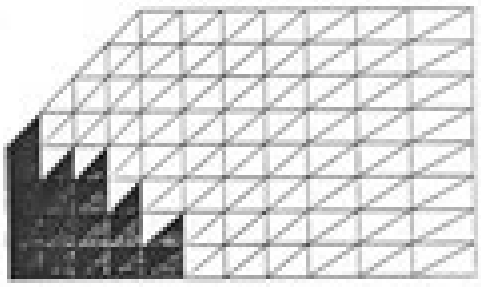

(d) At Load = 771.5 kg.

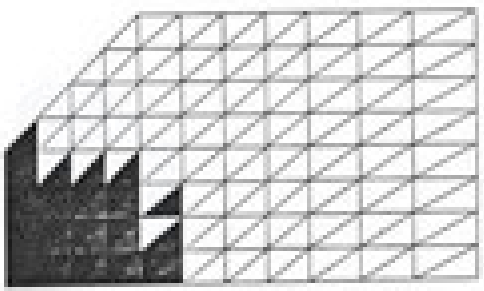

(e) At Load = 773.4 kg.

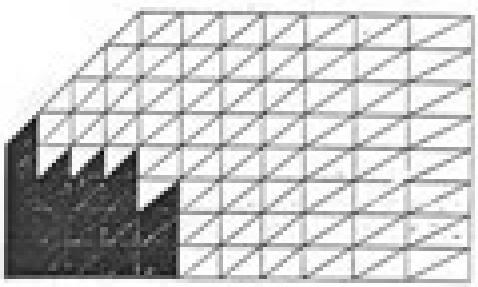

(f) At Failure = 773.9 kg.

Fig. A.1 Yield Patterns For Mesh #1 for the Test V-Notched Tension Specimen

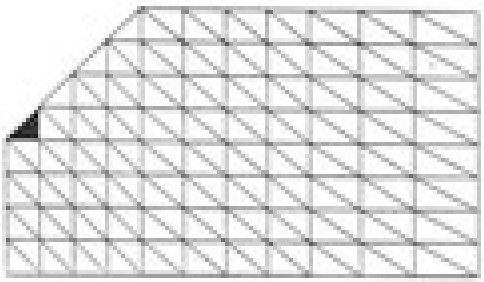

(a) At Initial Yield = 426.7 kg.

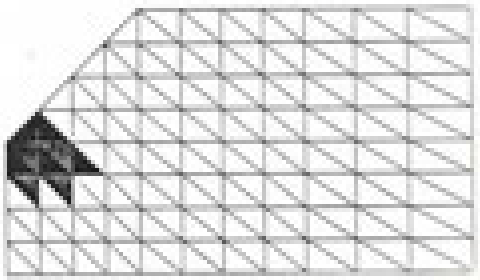

(b) At Load= 728.6 kg.

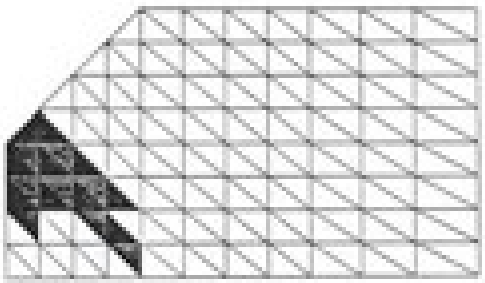

(c) At Load = 759.5 kg.

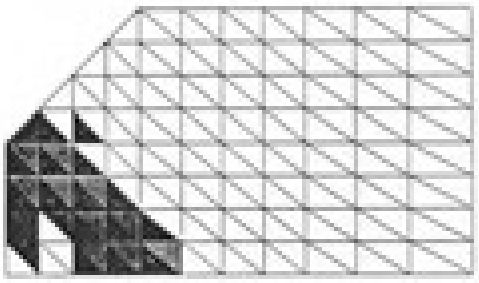

(d) At Load = 763.4 kg.

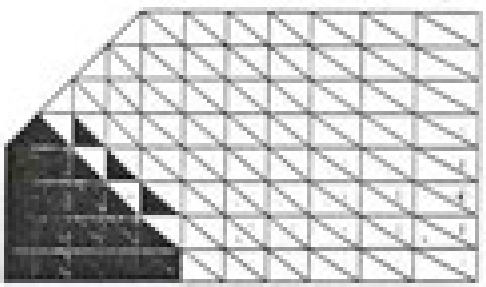

(e) At Load = 768.8 kg.

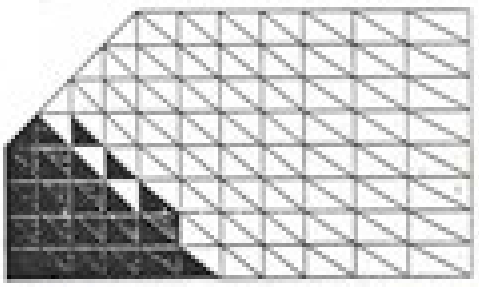

(f) At Failure = 770.9 kg.

Fig. A.2 Yield Patterns For Mesh #2 for the Test V-Notched Tension Specimen

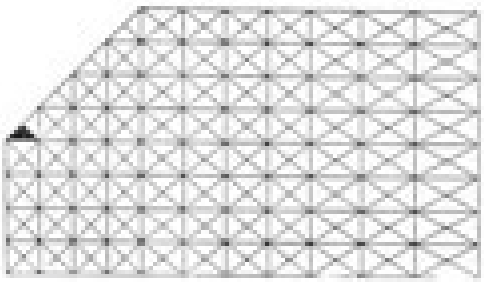

(a) At Initial Yield= 336.6 kg.

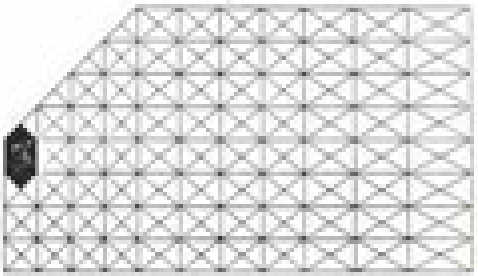

(b) At Load = 604.0 kg.

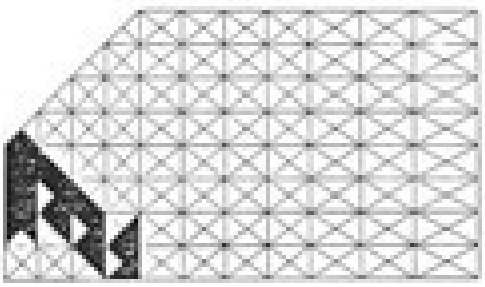

(c) At Load = 718.7 kg.

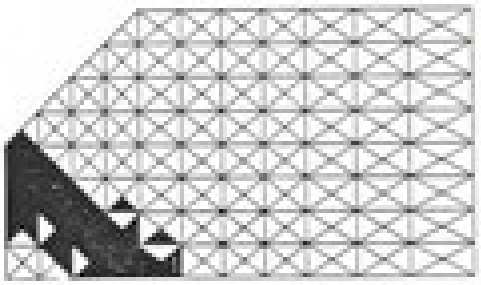

(d) At Load = 728.7 kg.

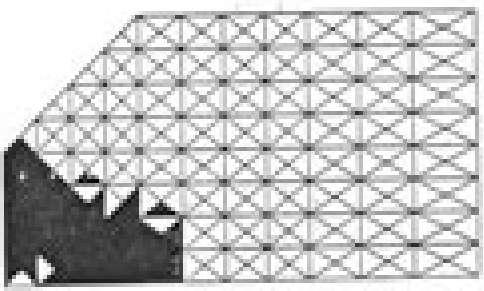

(e) At Load = 735.9 kg.

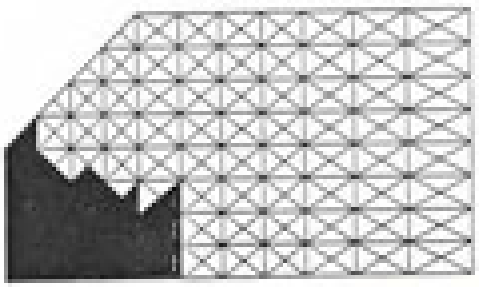

(f) At Failure = 741.5 kg.

Fig. A.3 Yield Patterns For Mesh #3 for the Test V-Notched Tension Specimen

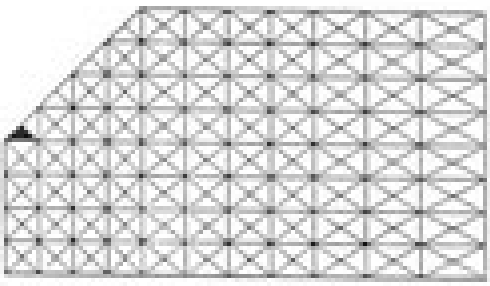

(a) At Initial Yield= 336.6 kg.

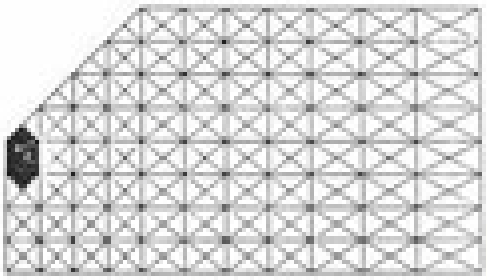

(b) At Load = 604.0 kg.

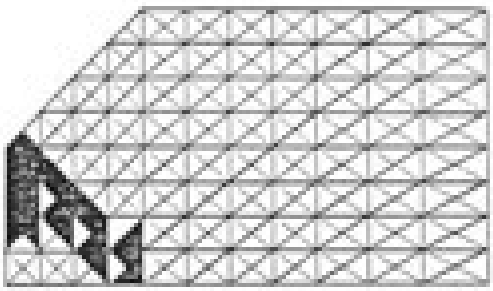

(c) At Load = 718.7 kg.

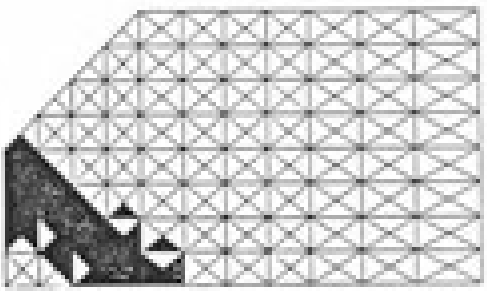

(d) At Load = 728.7 kg.

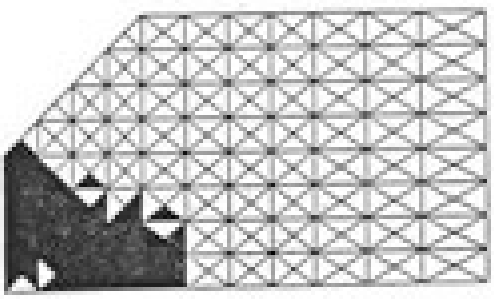

(e) At Load = 735.9 kg.

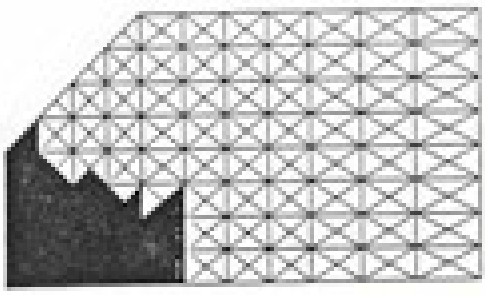

(f) At Failure = 741.5 kg.

Fig. A.3 Yield Patterns For Mesh #3 for the Test V-Notched Tension Specimen

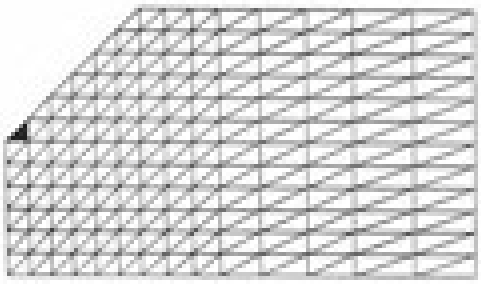

(a) At Initial Yield= 342.7 kg.

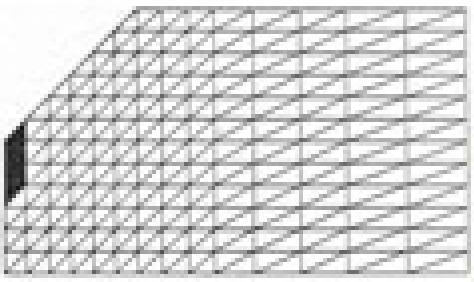

(b) At Load = 629.8 kg.

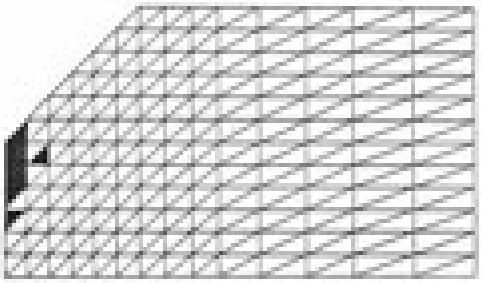

(c) At Load = 686.0 kg.

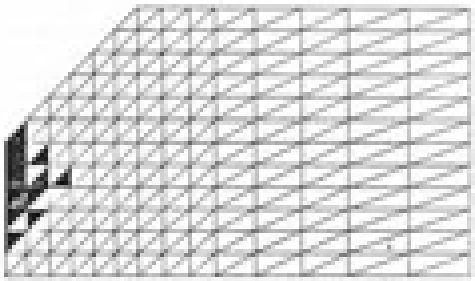

(d) At Load = 721.5 kg.

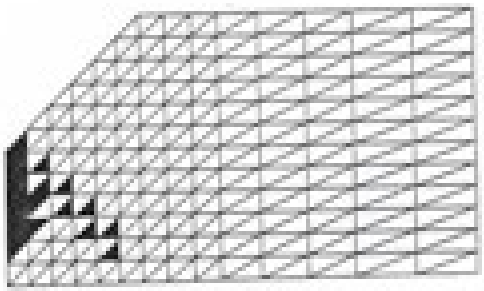

(e) At Load = 731.1 kg.

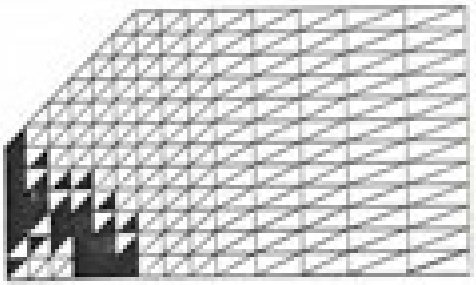

(f) At Load =738.3 kg.

Fig. A.4 Yield Patterns for Mesh #4 for the Test V-notched Tension Specimen

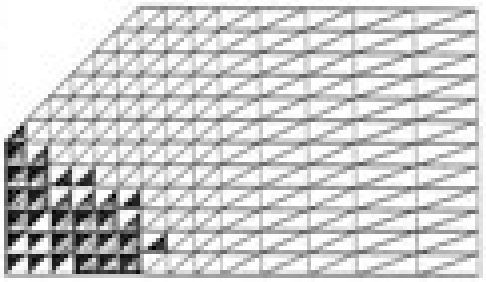

(g) At Load = 740.3 kg.

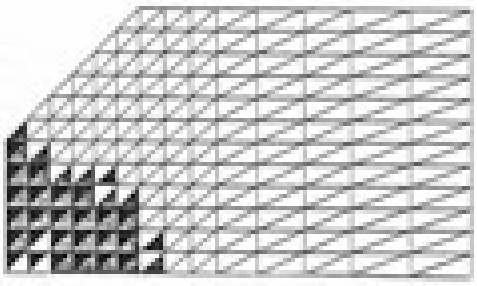

(h) At Load = 743.4 kg.

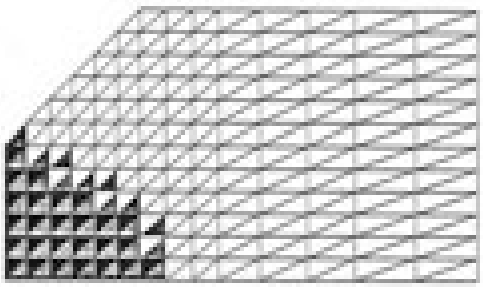

(i) At Load = 744.5 kg.

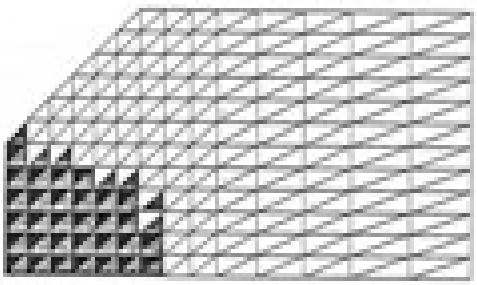

(j) At Load = 746.5 kg.

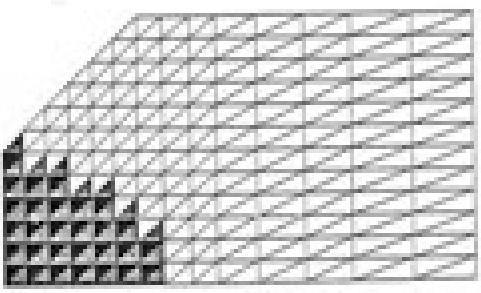

(k) At Load = 748.2 kg.

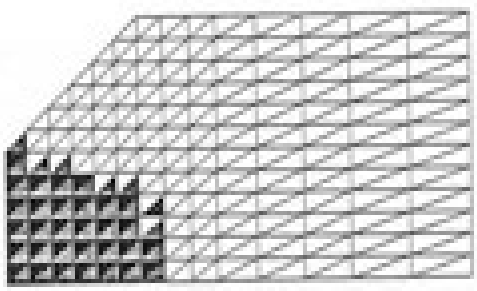

(l) At Failure = 748.4 kg.

Fig. A.4 (Cont'd) Yield Patterns For Mesh #4 for the Test V-Notched Tension Specimen

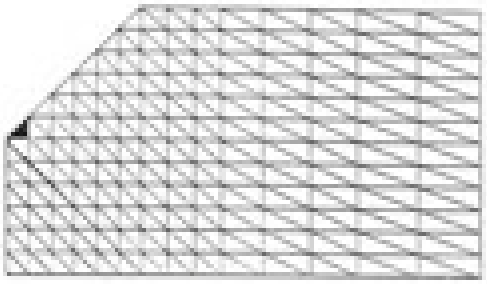

(a) At Initial Yield= 351.7 kg.

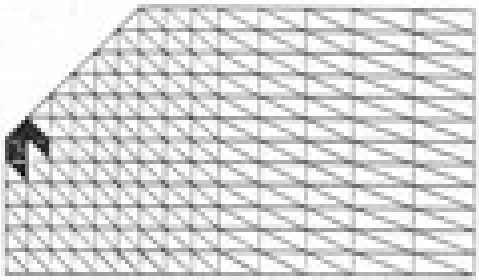

(b) At Load = 579.4 kg.

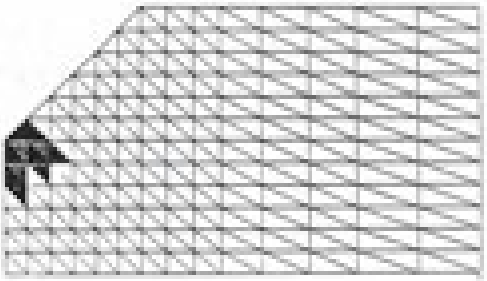

(c) At Load = 638.9 kg.

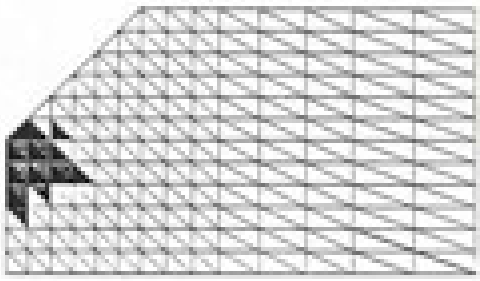

(d) At Load = 709.8 kg.

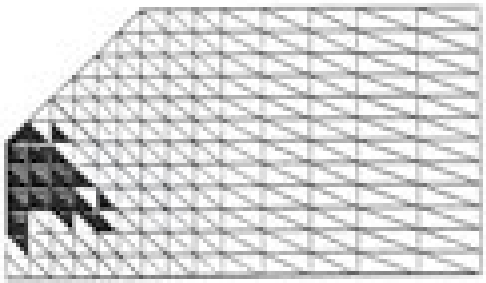

(e) At Load = 729.7 kg.

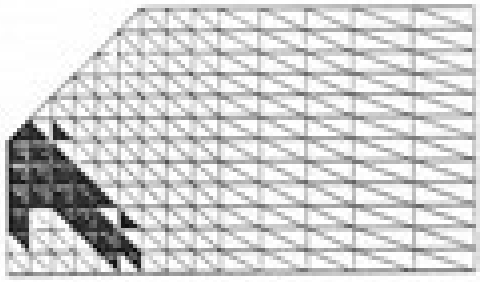

(f) At Load = 731.7 kg.

Fig. A.5 Yield Patterns for Mesh #5 for the Test V-Notched Tension Specimen

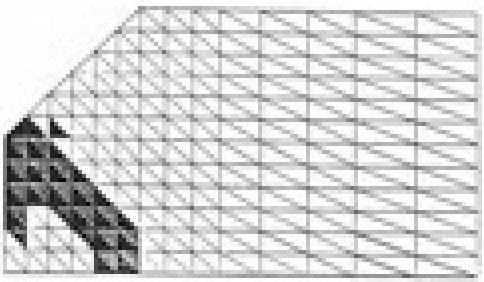

(g) At Load = 733.4 kg.

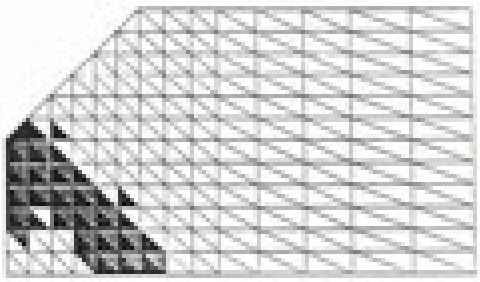

(h) At Load = 736.0 kg.

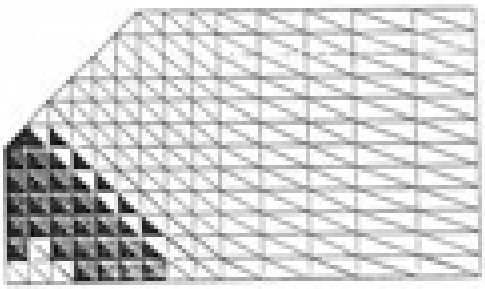

(i) At Load = 740.7 kg.

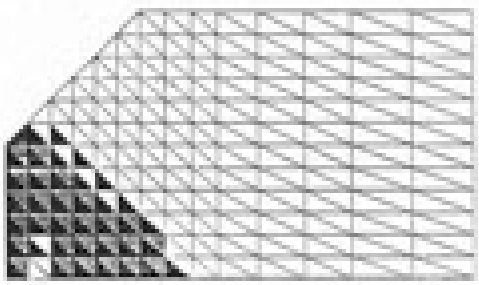

(j) At Load = 742.5 kg.

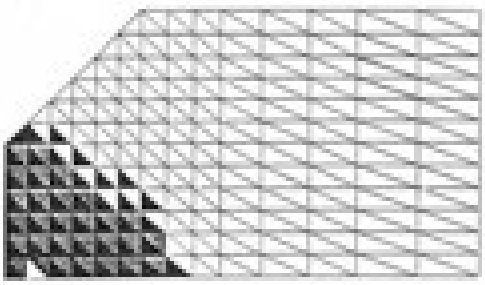

(k) At Load = 744.3 kg.

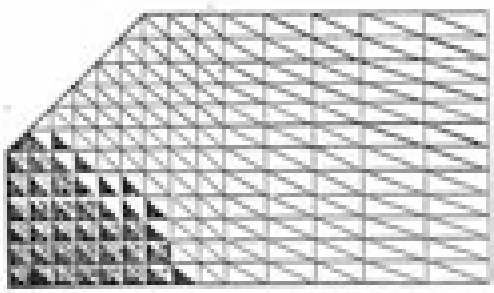

(l) At Failure = 745.0 kg.

Fig. A.5 (Cont'd) Yield Patterns For Mesh #5 for the Test V-Notched Tension Specimen

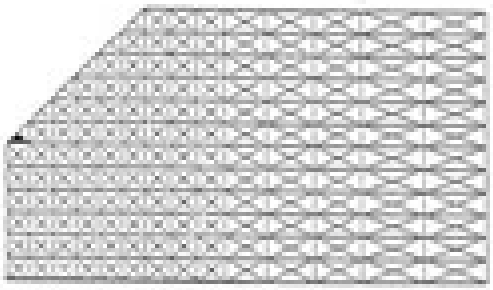

(a) At Initial Yield= 278.5 kg.

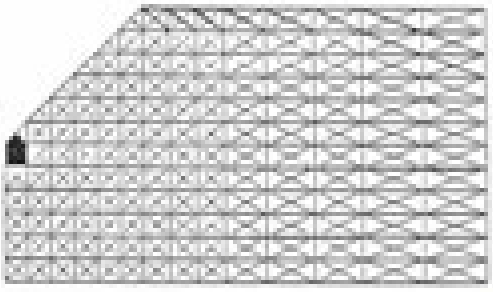

(b) At Load = 511.5 kg.

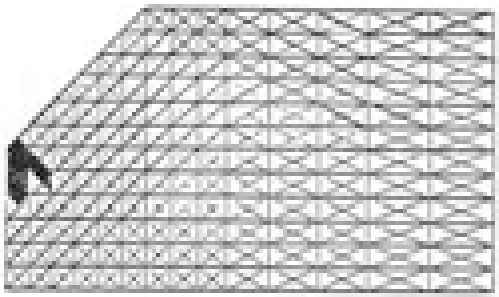

(c) At Load = 611.5 kg.

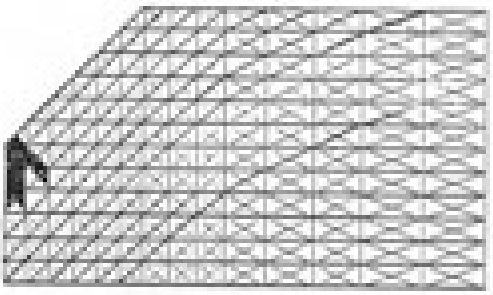

(d) At Load = 637.91 kg.

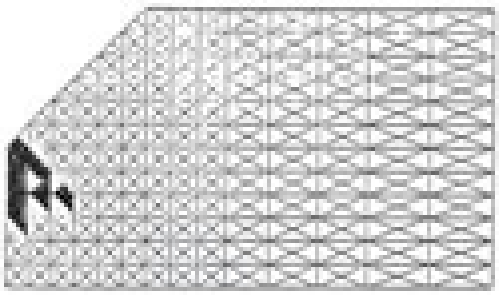

(e) at Load = 669.9 kg.

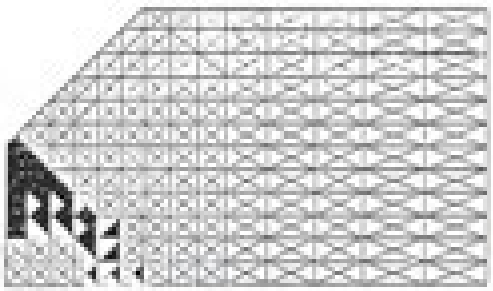

(f) at Load = 700.2 kg.

Fig. A.6 Yield Patterns for Mesh #6 for the Test V-notched Tension Specimen

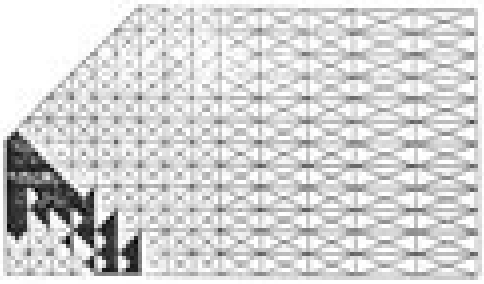

(g) At Load = 707.5 kg.

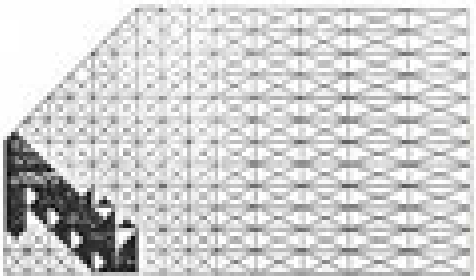

(h) At Load = 709.9 kg.

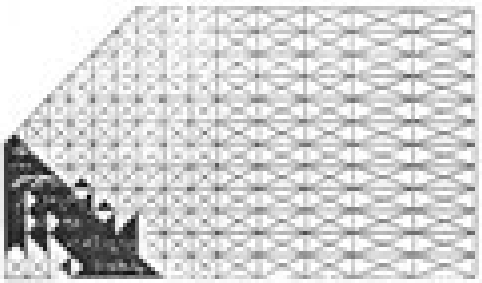

(i) At Load = 714.1 kg.

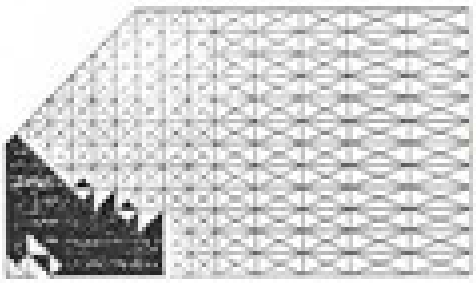

(j) At Load = 720.4 kg.

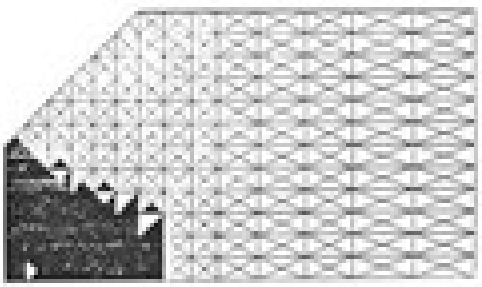

(k) At Load = 722.6 kg.

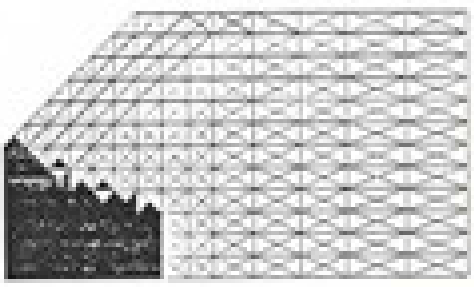

(l) At Failure =724.7 kg.

Fig. A.6 (Cont'd) Yield Patterns For Mesh #6 for the Test V-Notched Tension Specimen

APPENDIX B

Yield Patterns for the Center Pre-Cracked Rectangular Panel Tension Specimen

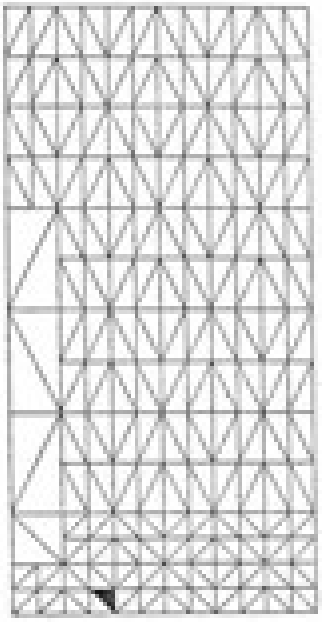

(a) At Initial Yield= 20.7 ksi

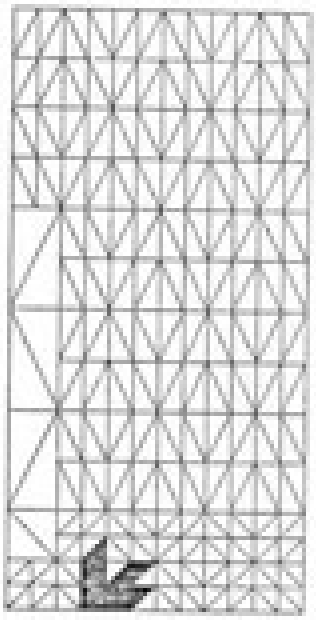

(b) At Load= 28.9 ksi

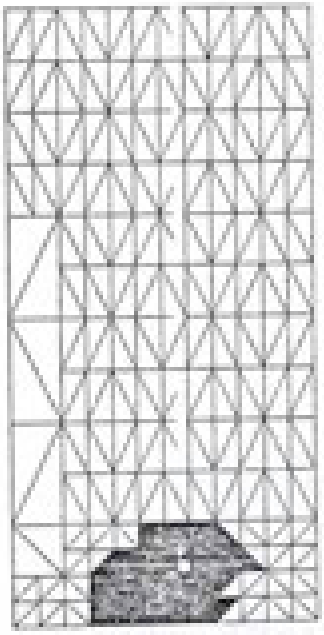

(c) At Load= 34.6 ksi

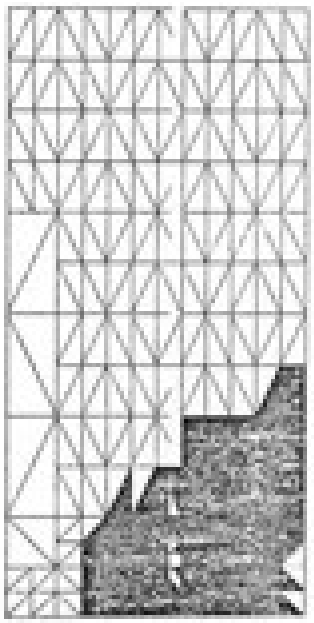

(d) At Load= 37.2 ksi

Fig. B.1 Yield Patterns for Mesh #1 for the Analysis of Center Pre-Cracked Rectangular Panel Tension Specimen

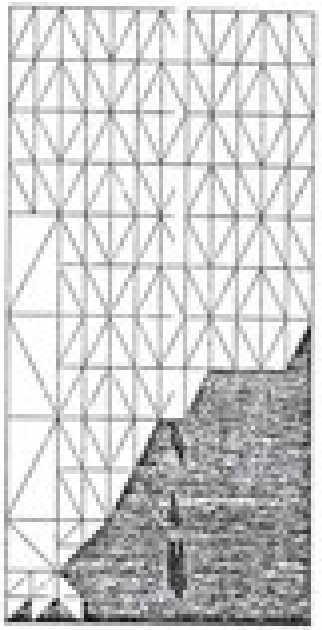

(e) At Load= 38.4 ksi

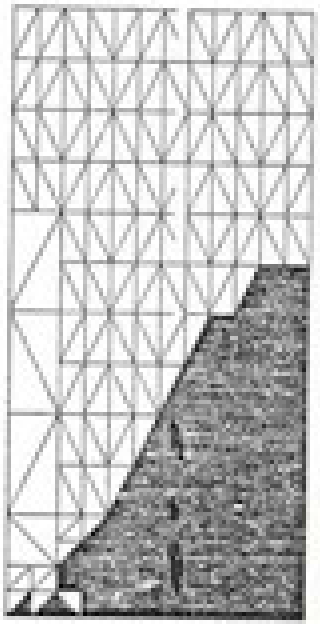

(f) At Load = 40.6 ksi

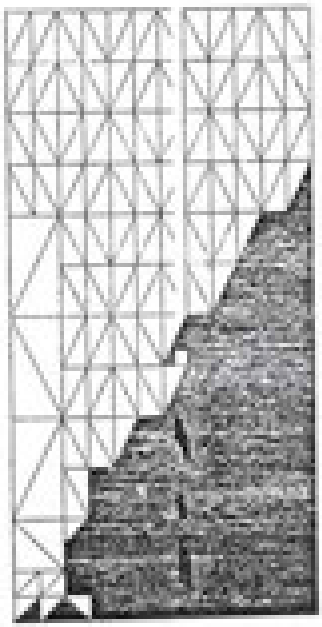

(g) At Load= 42.1 ksi

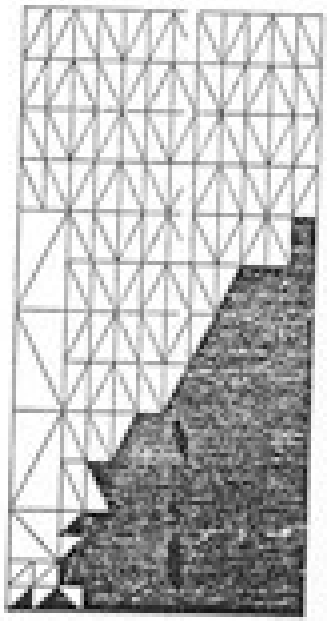

(h) At Ultimate Fracture Failure =43.7 ksi

Fig. B.2 (Cont'd) Yield Patterns For Mesh#1 For The Analysis of Center Pre-Cracked Rectangular Panel Tension Specimen

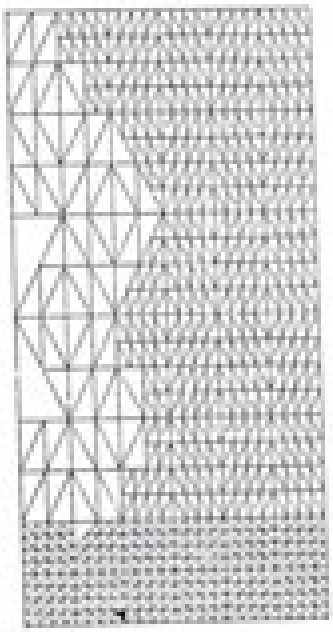

(a) At Initial Yield= 14.2 ksi

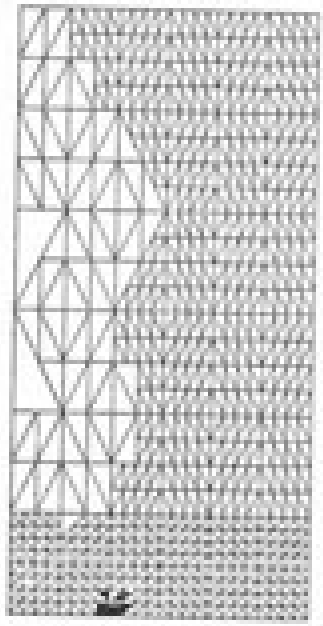

(b) At Load= 21.6 ksi

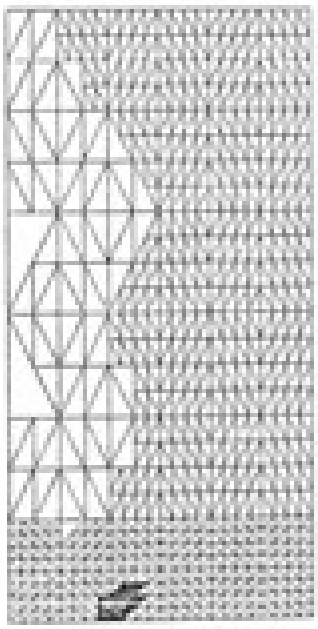

(c) At Load= 25.3 ksi

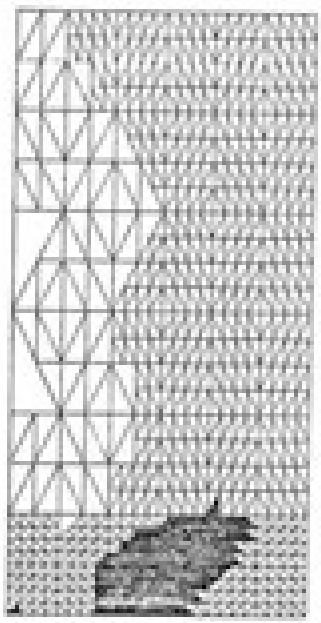

(d) At Load= 33.3 ksi

Fig. B.2 Yield Patterns for Mesh #2 for the Analysis of Center Pre-Cracked Rectangular Panel Tension Specimen

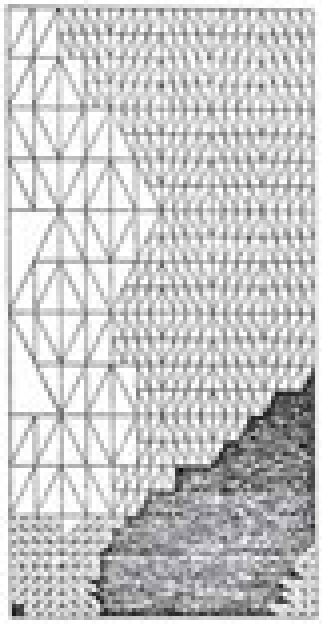

(e) At Load= 35.4 ksi

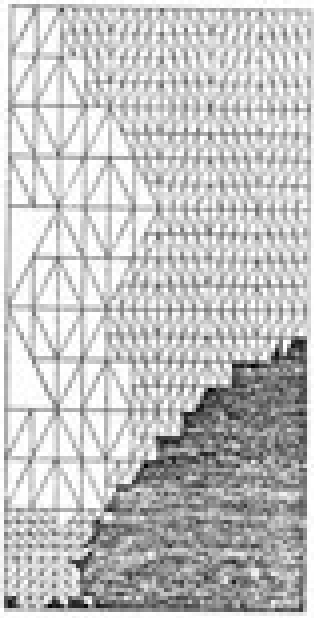

(f) At Load= 37.4 ksi

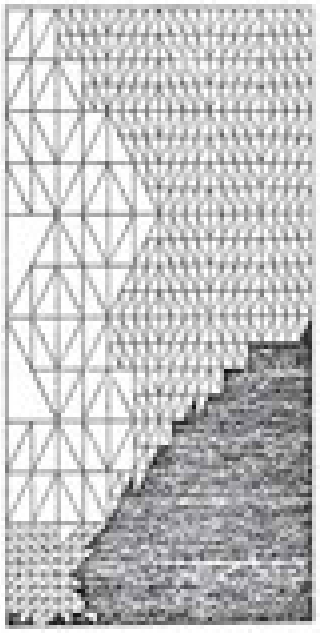

(g) At Load= 38.0 ksi

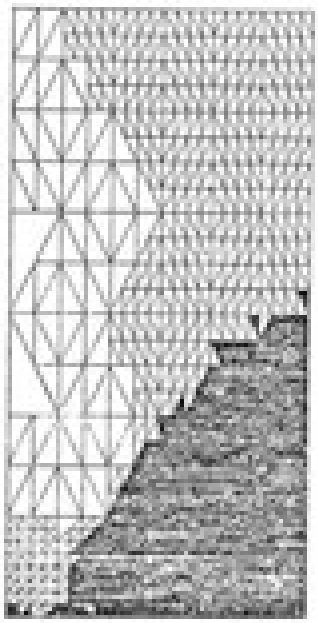

(h) At Ultimate Fracture Failure =39.2 ksi

Fig. B.2 (Cont'd) Yield patterns For Mesh#2 For The Analysis of Center Pre-Cracked Rectangular Panel Tension Specimen

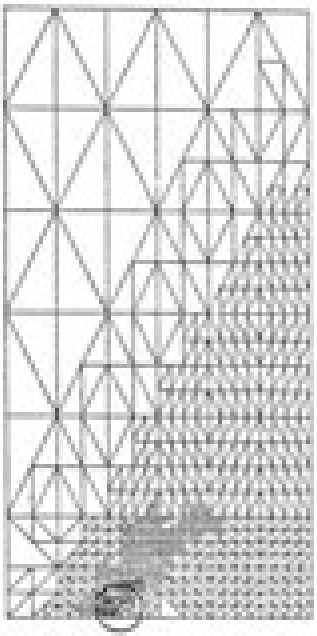

(a) At Initial Yield= 2.9 ksi

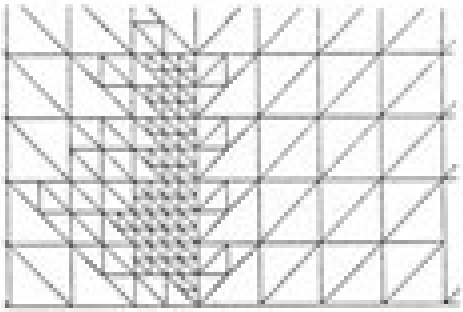

Enlarged View of The Circled Portion of Fig. (a)

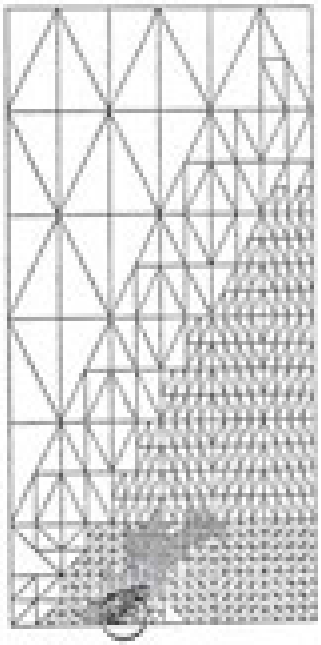

(b) At Load= 17.4 ksi

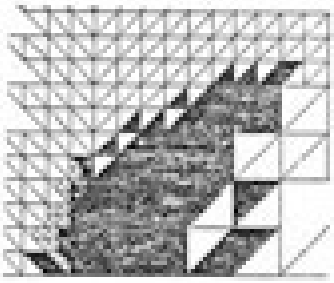

Enlarged View of The Circled Portion of Fig. (b)

Fig. B.3 Yield Patterns for Mesh #3 for the Analysis of Center Pre-Cracked Rectangular Panel Tension Specimen

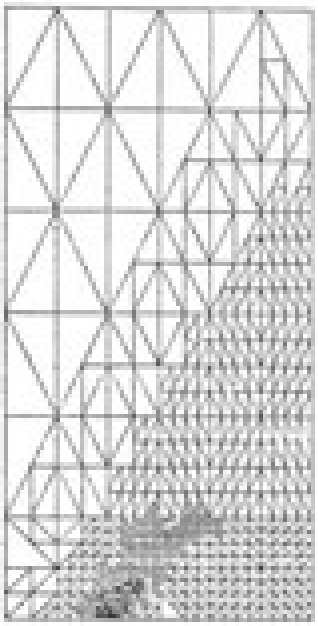

(c) At Load= 20.7 ksi

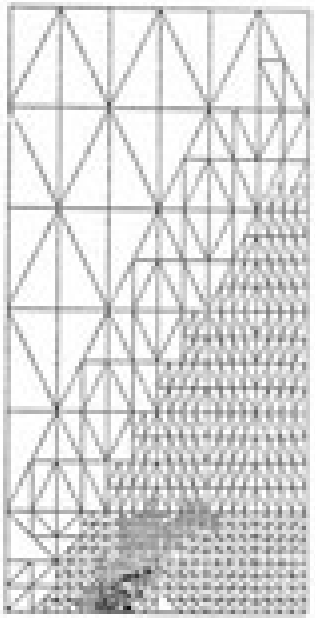

(d) At Load= 25.4 ksi

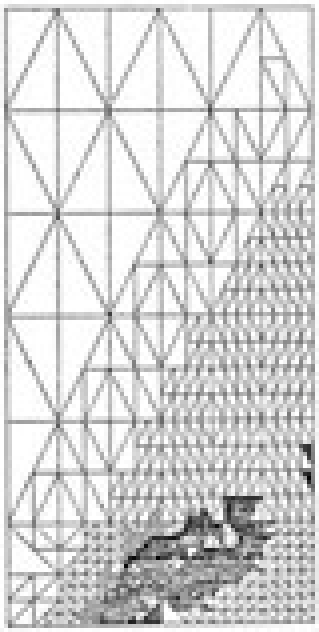

(e) At Load= 32.9 ksi

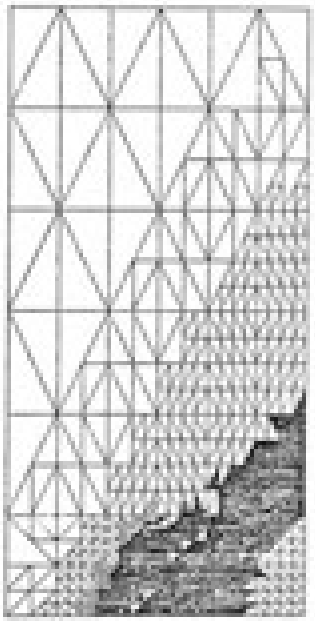

(f) At Load= 33.5 ksi

Fig. B.3 (Cont'd) Yield Patterns for Mesh #3 for the Analysis of Center Pre-Cracked Rectangular Panel Tension Specimen

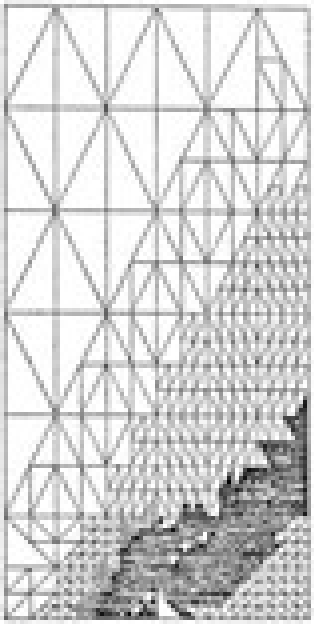

(g) At Load= 33.7 ksi

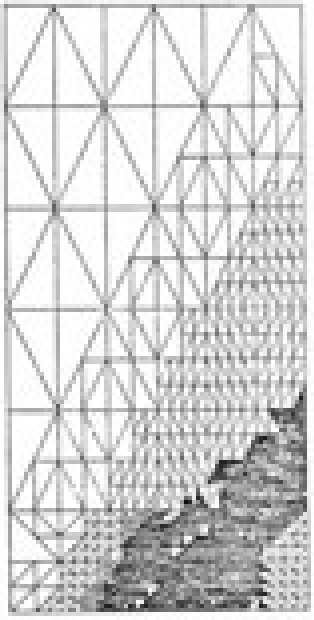

(h) At Ultimate Fracture Failure =33.8 ksi

Fig. B.3 (Cont'd) Yield Patterns For Meshf3 For the Analysis of Center Pre-Cracked Rectangular Panel Tension Specimen

APPENDIX C

Summary of Load and Area Yielded for Each Load Cycle for the Test V-Notched Tension Specimen

Table C.1 Summary of Load and Area Yielded for Each Load Cycle for the Test V-notched Tension Specimen

Mesh # / Cycle #	Load Level (Kg) / Area Yielded (mm^2)							
	1	2	3	4	5	6	7	8
1	416.8 / 12.5	482.6 / 25.0	622.0 / 37.5	633.4 / 62.5	718.0 / 75.0	751.7 / 87.5	755.9 / 150.0	759.2 / 175.0
2	426.7 / 12.5	480.4 / 25.0	536.3 / 37.5	650.7 / 50.0	672.9 / 75.0	691.3 / 87.5	711.2 / 112.5	728.6 / 137.5
3	336.6 / 6.2	412.1 / 12.5	475.1 / 18.7	515.4 / 25.0	598.6 / 31.2	604.0 / 37.5	609.4 / 43.7	635.5 / 50.0
4	342.7 / 5.5	402.2 / 11.1	528.0 / 16.6	539.9 / 22.2	629.8 / 33.2	681.7 / 38.8	686.0 / 60.9	688.9 / 66.5
5	351.7 / 5.5	399.2 / 11.1	448.5 / 16.6	555.6 / 27.7	579.4 / 33.2	617.3 / 38.8	638.9 / 44.3	687.1 / 49.9
6	278.5 / 2.8	343.4 / 5.5	400.3 / 8.3	432.8 / 11.0	511.5 / 13.8	517.4 / 16.6	534.2 / 19.3	550.2 / 22.1

Table C.1 (Cont'd) Summary of Load and Area Yielded for Each Load Cycle for the Test V-notched Tension Specimen

Mesh # / Cycle #	Load Level (kg.) / Area Yielded (mm.^{2})							
	9	10	11	12	13	14	15	16
1	760.5 / 212.5	763.3 / 250.0	764.7 / 287.5	766.7 / 325.0	767.8 / 362.5	770.6 / 375.0	771.5 / 387.5	772.7 / 400.0
2	743.1 / 150.0	747.5 / 187.5	753.3 / 225.0	757.3 / 250.0	758.8 / 287.5	759.5 / 300.0	761.4 / 325.0	762.1 / 350.0
3	651.2 / 56.2	657.4 / 68.7	680.2 / 75.0	689.8 / 81.2	694.2 / 93.7	701.7 / 100.0	705.2 / 118.7	709.2 / 137.5
4	721.5 / 77.6	724.6 / 83.1	731.1 / 110.8	732.8 / 123.9	734.8 / 160.7	736.4 / 193.9	783.3 / 221.6	739.5 / 243.8
5	692.8 / 83.1	703.5 / 94.2	709.8 / 105.3	723.6 / 127.4	725.1 / 138.5	726.2 / 144.0	729.7 / 160.7	730.9 / 193.9
6	561.2 / 24.8	592.4 / 30.4	605.7 / 33.1	610.2 / 35.9	611.5 / 38.6	632.5 / 41.4	637.9 / 44.2	651.8 / 52.4

Table C.1 (Cont'd) Summary of Load and Area Yielded for Each Load Cycle for the Test V-notched Tension Specimen

Mesh # / Cycle #	Load Level (Kg) / Area Yielded (mm^2)							
	17	18	19	20	21	22	23	24
1	773.4 / 425.0	773.9 / 437.5	– / –	– / –	– / –	– / –	– / –	– / –
2	763.4 / 375.0	765.1 / 412.5	766.3 / 425.0	767.6 / 437.5	768.3 / 450.0	768.8 / 462.5	770.9 / 475.0	– / –
3	711.4 / 143.7	713.6 / 150.0	716.2 / 162.5	717.3 / 181.2	718.7 / 193.7	722.0 / 200.0	723.4 / 218.7	725.2 / 243.7
4	740.3 / 265.9	740.9 / 293.6	743.4 / 310.2	744.2 / 337.9	744.5 / 343.5	745.6 / 349.0	746.5 / 360.1	748.2 / 365.6
5	731.7 / 210.5	732.4 / 216.1	733.4 / 232.7	734.9 / 238.2	736.0 / 277.0	737.7 / 304.7	740.7 / 321.3	741.4 / 332.4
6	654.9 / 55.2	665.9 / 57.9	669.9 / 63.5	680.4 / 66.2	682.9 / 69.0	686.5 / 74.5	691.6 / 91.1	694.2 / 99.4

Table C.1 (Cont'd) Summary of Load and Area Yielded for Each Load Cycle for the Test V-notched Tension Specimen

Mesh # / Cycle #	Load Level (kg.) / Area Yielded (mm^2)							
	25	26	27	28	29	30	31	32
1	– / –	– / –	– / –	– / –	– / –	– / –	– / –	– / –
2	– / –	– / –	– / –	– / –	– / –	– / –	– / –	– / –
3	726.6 / 256.2	728.7 / 275.0	730.0 / 293.7	731.8 / 306.2	732.9 / 325.0	733.6 / 343.7	735.9 / 368.7	736.3 / 375.0
4	748.4 / 382.3	– / –	– / –	– / –	– / –	– / –	– / –	– / –
5	742.5 / 365.6	742.9 / 371.2	744.3 / 387.8	745.0 / 398.9	– / –	– / –	– / –	– / –
6	700.2 / 107.6	702.7 / 121.4	704.8 / 132.5	705.8 / 157.3	707.5 / 165.6	709.9 / 184.9	709.9 / 193.2	710.8 / 198.7

Table C.1 (Cont'd) Summary of Load and Area Yielded for Each Load Cycle for the Test V-notched Tension Specimen

Mesh # / Cycle #	Load Level (kg.) / Area Yielded ($mm.^2$)							
	33	34	35	36	37	38	39	40
1	– / –	– / –	– / –	– / –	– / –	– / –	– / –	– / –
2	– / –	– / –	– / –	– / –	– / –	– / –	– / –	– / –
3	736.5 / 381.2	737.8 / 387.5	739.8 / 393.7	741.5 / 412.5	– / –	– / –	– / –	– / –
4	– / –	– / –	– / –	– / –	– / –	– / –	– / –	– / –
5	– / –	– / –	– / –	– / –	– / –	– / –	– / –	– / –
6	711.8 / 207.0	713.2 / 229.1	714.1 / 234.6	715.1 / 242.9	716.1 / 259.4	717.4 / 267.7	718.2 / 273.2	719.2 / 287.0

Table C.1 (Cont'd) Summary of Load and Area Yielded for Each Cycle for the Test V-notched Tension Specimen

Mesh # / Cycle #	Load Level (kg) / Area Yielded (mm.^{2})							
	41	42	43	44	45	46	47	48
1	– / –	– / –	– / –	– / –	– / –	– / –	– / –	– / –
2	– / –	– / –	– / –	– / –	– / –	– / –	– / –	– / –
3	– / –	– / –	– / –	– / –	– / –	– / –	– / –	– / –
4	– / –	– / –	– / –	– / –	– / –	– / –	– / –	– / –
5	– / –	– / –	– / –	– / –	– / –	– / –	– / –	– / –
6	720.4 / 300.8	720.9 / 311.9	721.5 / 317.4	722.1 / 333.9	722.6 / 342.2	723.5 / 347.8	724.7 / 353.3	– / –